



National Library
of Canada

Bibliothèque nationale
du Canada

Canadian Theses Service

Service des thèses canadiennes

Ottawa, Canada
K1A 0N4

NOTICE

The quality of this microform is heavily dependent upon the quality of the original thesis submitted for microfilming. Every effort has been made to ensure the highest quality of reproduction possible.

If pages are missing, contact the university which granted the degree.

Some pages may have indistinct print especially if the original pages were typed with a poor typewriter ribbon or if the university sent us an inferior photocopy.

Previously copyrighted materials (journal articles, published tests, etc.) are not filmed.

Reproduction in full or in part of this microform is governed by the Canadian Copyright Act, R.S.C. 1970, c. C-30.

AVIS

La qualité de cette microforme dépend grandement de la qualité de la thèse soumise au microfilmage. Nous avons tout fait pour assurer une qualité supérieure de reproduction.

S'il manque des pages, veuillez communiquer avec l'université qui a conféré le grade.

La qualité d'impression de certaines pages peut laisser à désirer, surtout si les pages originales ont été dactylographiées à l'aide d'un ruban usé ou si l'université nous a fait parvenir une photocopie de qualité inférieure.

Les documents qui font déjà l'objet d'un droit d'auteur (articles de revue, tests publiés, etc.) ne sont pas microfilmés.

La reproduction, même partielle, de cette microforme est soumise à la Loi canadienne sur le droit d'auteur, SRC 1970, c. C-30.

Preparation and Characterization
of Leached Asbestos Materials

Pius Kipkemboi

A Thesis

in

The Department

of

Chemistry

Presented in Partial Fulfillment of the Requirements
for the Degree of Master of Science at
Concordia University
Montréal, Québec, Canada

March, 1988

© Pius Kipkemboi, 1988

Permission has been granted to the National Library of Canada to microfilm this thesis and to lend or sell copies of the film.

The author (copyright owner) has reserved other publication rights, and neither the thesis nor extensive extracts from it may be printed or otherwise reproduced without his/her written permission.

L'autorisation a été accordée à la Bibliothèque nationale du Canada de microfilmer cette thèse et de prêter ou de vendre des exemplaires du film.

L'auteur (titulaire du droit d'auteur) se réserve les autres droits de publication; ni la thèse ni de longs extraits de celle-ci ne doivent être imprimés ou autrement reproduits sans son autorisation écrite.

ISBN 0-315-41640-8

ABSTRACT

Preparation and Characterization
of Leached Asbestos Materials

Pius Kipkemboi..

In this study, the parameters governing the leaching behaviour of chrysotile fibers in acidic media were investigated. In the presence of strong mineral acids, the main factors which governed the leaching of the chrysotile asbestos fibers were the normality of the acid solution, the temperature and the time. Weak organic acids acted more slowly in the removal of magnesium than mineral acids and their leaching effects were dependent on the acid strength and the pH of the solutions. Oxalic acid and particularly EDTA were effective in the removal of iron impurities; the chelating action of EDTA is suggested to be responsible for faster iron dissolution.

Several physico-chemical techniques were used to characterize the reaction products of the leaching process. The magnesium leaching degree (MLD) was used to follow the gradual physico-chemical modifications during the leaching process. Under mild leaching conditions (MLD 55%), the leached asbestos materials basically retained the fiber

morphology of the parent chrysotile asbestos, and most of the characteristics, such as the degree of crystallinity, the BET surface area, the hydrophobicity and the bulk density of asbestos varied gradually and smoothly with the MLD. Above MLD=55%, acid leaching of chrysotile resulted in a rather rapid morphological degradation which was accompanied by a more rapid loss in crystallinity, a dramatic decrease in bulk density, and a sharp increase in the BET surface area and hydrophobicity. As the MLD approached 100%, a very porous and highly divided residue consisting of some fragments of amorphous silica was obtained.

ACKNOWLEDGEMENTS

I wish to express my sincere gratitude and appreciation to my supervisor, Dr. R. Le Van Mao, for his keen interest, valuable guidance and direction throughout the course of this research and in the preparation of this thesis.

I would like to thank the members of my research committee, Drs. P.H. Bird and G. Dénès, for their cooperation and helpful suggestions.

I am deeply indebted to Dr. P. Lévesque who generously sacrificed some of his time for stimulating discussions and help on some of the theoretical and practical aspects of this research. I am grateful to all fellow members of Catalysis Research Laboratory, particularly Messrs. G. McLaughlin and B. Sjiariel, for their constant technical assistance and moral support. I would like to give special thanks to my colleague, Ms. Vaillancourt, for the wonderful cooperation we had in the execution of this project; I greatly acknowledged the use of her density and degree of crystallinity measurements for leached asbestos materials.

I wish also to express my appreciation to Mr. Walter Yurkiw for his care and diligence in typing this thesis.

Finally, I am grateful to the governments of Kenya and Canada through CIDA for the award of a scholarship and the necessary financial assistance.

TABLE OF CONTENTS

	Page
ABSTRACT	iii
ACKNOWLEDGEMENTS	v
LIST OF TABLES	viii
LIST OF FIGURES	x
1 INTRODUCTION	1
2 CHRYSOTILE ASBESTOS	11
2.1 Chrystal Structure of Chrysotile	11
2.2 Composition of Chrysotile Asbestos	16
2.3 Sources of Asbestos Fibers	20
2.4 Applications of Chrysotile Asbestos	22
3 EXPERIMENTAL APPROACHES AND THEORETICAL PRINCIPLES OF THE CHARACTERIZATION TECHNIQUES ..	25
3.1 Preparation of Leached Asbestos (Alix) Materials	25
3.2 Physico-Chemical Characterization Techniques ..	27
3.2.1. Atomic Absorption Spectrophotometry (AAS) ..	27
3.2.1.1 Theory	28
3.2.1.2 Instrumentation	32
3.2.1.3 Apparatus used	36
3.2.1.4 Sample preparation for elemental analysis ...	37
3.2.2. X-Ray Powder Diffraction	38
3.2.2.1 Theory	38
3.2.2.2 Instrumental apparatus ...	45
3.2.2.3 Experimental procedure ...	45
3.2.3. Infra Red (IR) Spectroscopy	46
3.2.3.1 Sample preparation for IR determination ...	49
3.2.4. Scanning Electron Microscopy (SEM) ..	49
3.2.4.1 Sample preparation for SEM analysis ...	51
3.2.5. Magic Angle Spinning Si-NMR	51

3.2.6.	Specific (BET) Surface Area	54
3.2.6.1	BET Theory	56
3.2.6.2	Experimental set-up	59
3.2.6.3	Experimental technique ...	61
3.2.7.	External Surface Area Determination .	63
3.2.8.	Pore Size Distribution Measurement .	65
3.2.8.1	Experimental procedure	71
3.2.9.	Adsorption of Water and n-hexane. ..	73
3.2.9.1	Experimental apparatus ...	74
3.2.9.2	Experimental procedure ...	76
3.2.10.	Density Measurements	77
4	RESULTS AND DISCUSSIONS	78
4.1	Reactivity and Leaching of Chrysotile with Strong Mineral Acids .	79
4.2	Secondary Leaching of Chrysotile with Weak Organic Acids .	94
4.3	X-Ray Powder Diffraction	102
4.4	IR Spectra	111
4.5	Scanning Electron Microscopy	118
4.6	Solid State NMR Spectra	121
4.7	Specific Surface Area	124
4.8	External Surface Area	129
4.9	Pore Size Distribution	132
4.10	Density	139
4.11	Adsorption of Water and n-hexane	142
5	KINETIC AND THERMODYNAMIC STUDIES OF THE LEACHING PROCESS .	147
6	PROPOSED MECHANISMS FOR THE CHRYSOTILE LEACHING IN THE PRESENCE OF ACIDS .	154
7	CONCLUSIONS AND SUGGESTIONS FOR FUTURE RESEARCH .	156
7.1	Conclusions	156
7.2	Suggestions for Further Research Work	159
8	REFERENCES	162
9	APPENDIX	169

LIST OF TABLES

Page

1.1:	Solubility of asbestos minerals in 25% acid or caustic	3
2.1:	Chemical composition of chrysotile and amphibole asbestos minerals	18
2.2:	World asbestos production in 1978	21
3.1:	Operating conditions for n-hexane and water adsorption of Alix samples	77
4.1:	Effects of HCl concentration on the leaching of chrysotile asbestos at 50 °C and 80 °C	91
4.2:	Effects of H ₂ SO ₄ concentration on the leaching of chrysotile asbestos at 80 °C	82
4.3:	Effects of HCl concentration on the leaching of chrysotile at ambient temperature	83
4.4:	Effects of time on the leaching of chrysotile asbestos with HCl solution at 50 °C and 80 °C	84
4.5:	Effects of time on the leaching of chrysotile asbestos with H ₂ SO ₄ solution at 80 °C	85
4.6:	Second leaching step of an Alix sample with an organic acid at 80 °C as a function of acid normality and pH	96

4.7:	Effects of time on the second leaching step of an Alix sample with an organic acid at 80 °C	97
4.8:	Principal IR absorption peaks for chrysotile asbestos and Alix samples	112
4.9:	Specific surface area of Alix samples	125
4.10:	Computed and experimental surface areas of the chrysotile asbestos	130
4.11:	External surface area of the starting chrysotile asbestos and Alix samples	130
4.12:	Cumulative surface area of the starting chrysotile asbestos and Alix samples from pore size distribution	133
4.13:	Water and n-hexane sorptive capacities of chrysotile asbestos and Alix samples	143
5.1:	Effects of the leaching time of HCl on the MLD at 25 °C	150
5.2:	Effects of the leaching time of HCl on the MLD at 50 °C	151
5.3:	Effects of the leaching time of HCl on the MLD at 80 °C	152
5.4:	The reciprocals of the absolute temperature and the observed initial rate constants	153

LIST OF FIGURES

	Page
1.1: Acid resistance of asbestos minerals	4
1.2: Structure and channel system of ZSM-5 zeolite..	8
2.1: Projection of the crystal structure of chrysotile asbestos perpendicularly to the fiber axis	13
2.2: Idealized representation of fibril packing in chrysotile	14
2.3: Fundamental sheet of chrysotile fibrils	14
2.4: High-resolution electron micrographs of transverse section of chrysotile	14
3.1: Schematic presentation of the concept of atomic absorption spectroscopy	30
3.2: Schematic diagram of a Perkin-Elmer laminar flow burner	35
3.3: Aspiration of sample solution into the nebulizer by venturi action	36
3.4: Representation of a simple cubic crystal structure showing atoms, 2 planes and the interplanar spacings d between the two planes ..	40
3.5: Reflection analogy of X-ray diffraction	43

3.6:	Diffraction of radiation from a crystal	43
3.7:	Nitrogen BET adsorption apparatus	60
3.8:	A t Plot of volume adsorbed versus film thickness	67
3.9:	Cross-section, parallel to the axis of a cylindrical pore of radius r_p showing the "inner core" of radius r_k and the adsorbed film of thickness t	69
3.10:	Vapor adsorption-vaporization apparatus	75
4.1:	Effects of the normality of the mineral acid on the MLD	86
4.2:	Effects of the normality of the HCl solution on the MLD at ambient temperature	87
4.3:	Effects of the leaching time of HCl solution at 50 °C and 80 °C on the MLD	88
4.4:	Effects of the leaching time of H_2SO_4 solution at 80 °C on the MLD	89
4.5:	Effects of the leaching time of HCl solution at ambient temperature on the MLD	90
4.6:	Weight loss of chrysotile in HCl solution <u>vs</u> time	91
4.7:	A plot of MLD of the secondary leaching of Alix with organic acids <u>vs</u> the normality of the acid	98

4.8:	A plot of MLD of the secondary leaching of Alix with organic acids <u>vs</u> the [*] pH of the acid	99
4.9:	A plot of MLD of the secondary leaching of Alix with organic acids <u>vs</u> the leaching time	100
4.10:	X-ray powder patterns of chrysotile asbestos and Alix samples as a function of MLD	103
4.11:	A plot of degree of crystallinity of the Alix samples <u>vs</u> MLD	109
4.12:	IR spectra of chrysotile asbestos and leached asbestos materials as a function of MLD	113
4.13:	IR spectrum of amorphous silica	117
4.14:	SEM micrographs of chrysotile asbestos and leached asbestos materials as a function of MLD	119
4.15:	²⁹ Si MAS NMR spectra of chrysotile and leached asbestos materials as a function of MLD	122
4.16:	A plot of specific surface area of Alix samples <u>vs</u> MLD	127
4.17:	Pore size distribution of chrysotile asbestos and leached asbestos materials	134

4.18: A plot of bulk density of Alix materials vs MLD	140
5.1: A plot of $\ln K$ against $\frac{I}{T}$ for the dissolution of chrysotile in acidic media	149

I INTRODUCTION

Asbestos is the name given to a group of inorganic silicates which occur naturally and have a distinct fibrous crystalline structure (1). They are distinguished from manmade fibrous silicates, such as rockwool and glasswool, by this true crystallinity and by the extreme fineness of the fibers and fibrils. The other key feature of asbestos as compared to non-asbestiform varieties of silicates is the presence of fibers that can be easily separated.

The inorganic nature and the crystalline structure of asbestos is largely responsible for its unique properties which have found a ready and increasing application in modern technology. The asbestos industry is large despite fears about health effects. Consequently, although there will certainly be greater care about the way asbestos is used in the future, it will not disappear. As a material of commercial importance, asbestos commenced its role in technology around 1880, when large-scale mining operations of chrysotile started in Canada and Russia.

Chrysotile asbestos, basically a magnesium silicate, is by far the most abundant kind of asbestos. About 90% of the past and about 95% of the present world production was or is of the chrysotile variety (2). The other types of asbestos are of the fibrous varieties of amphibole minerals. These are mainly ferromagnesium varieties: annimosite, crocidolite, tremolite, actinolite and anthophyllite. The first two are

produced on an industrial scale, and the last has been produced in the past.

It is commonly thought that the asbestos minerals are indestructible; in fact, all of them are susceptible to both chemical and thermal degradation. Chrysotile in particular is attacked by acids, the degree and rate of dissolution being dependent on the temperature, the concentration and type of acid, and also, to some extent, on the sources of the chrysotile. The resistance of asbestos materials to attack by reagents other than acids is generally considered excellent at temperatures up to 100°C, but deteriorates rapidly at higher temperatures. As far back as 1885 the reactivity of chrysotile with acids was recognized, and in 1890 Clark and Schneider found that chrysotile asbestos was the most susceptible to acid attack. Bates and Nagy (3) confirmed this conclusion with electron microscopic studies on acid-treated chrysotile. Electron micrographs of the reaction products showed that chrysotile was very severely etched and had lost its tubular morphology. Badollet (4,5) studied the differential solubility of chrysotile and amphibole fibers in more detail and summarized the information shown in Table 1.1 on the stability of asbestiform materials. Badollet confirmed that chrysotile is almost completely destroyed in strong acidic media, while amphibole fibers are almost untouched under the same conditions. Therefore, in contrast to the sensitivity of chrysotile, the amphibole fibers are much more resistant to

acids. There are, however, significant differences between these fibers. The data in Table 1.1 shows that anthophyllite, crocidolite and tremolite are significantly more resistant to acid attack than annimosite and actinolite. The high solubility of actinolite was attributed to impurities in the sample. Strong alkalis have little influence on all asbestos fibers, in particular on chrysotile, which makes the latter fiber an excellent reinforcing agent in cement.

TABLE 1.1 Solubility of asbestos minerals in 25% acid or caustic.

	Percent loss in weight, refluxing 2 hours				
	HCl	CH ₃ COOH	H ₃ PO ₄	H ₂ SO ₄	NaOH
Chrysotile	55.69	23.42	55.18	55.75	0.99
Crocidolite	4.38	0.91	4.37	3.69	1.35
Amosite	12.84	2.63	11.67	11.35	6.97
Anthophyllite	2.66	0.60	3.16	2.73	1.22
Actinolite	20.31	12.28	20.19	20.38	9.25
Tremolite	4.77	1.99	4.99	4.58	1.80

Hiscock (6) studied the rate of decomposition of asbestos fibers in boiling 4N hydrochloric acid. He found the following order of stability as shown in Figure 1.1:

Tremolite > anthophyllite > crocidolite > actinolite >
annimosite >> chrysotile

After an initial rapid weight loss, the rate of attack decreases radically with tremolite and anthophyllite showing extremely low rates. The acid-resistance curves for asbestos

4

fibers clearly differentiate between chrysotile and the amphibole fibers, although the range of reactivity of the latter fibers to hydrochloric acid is wide.

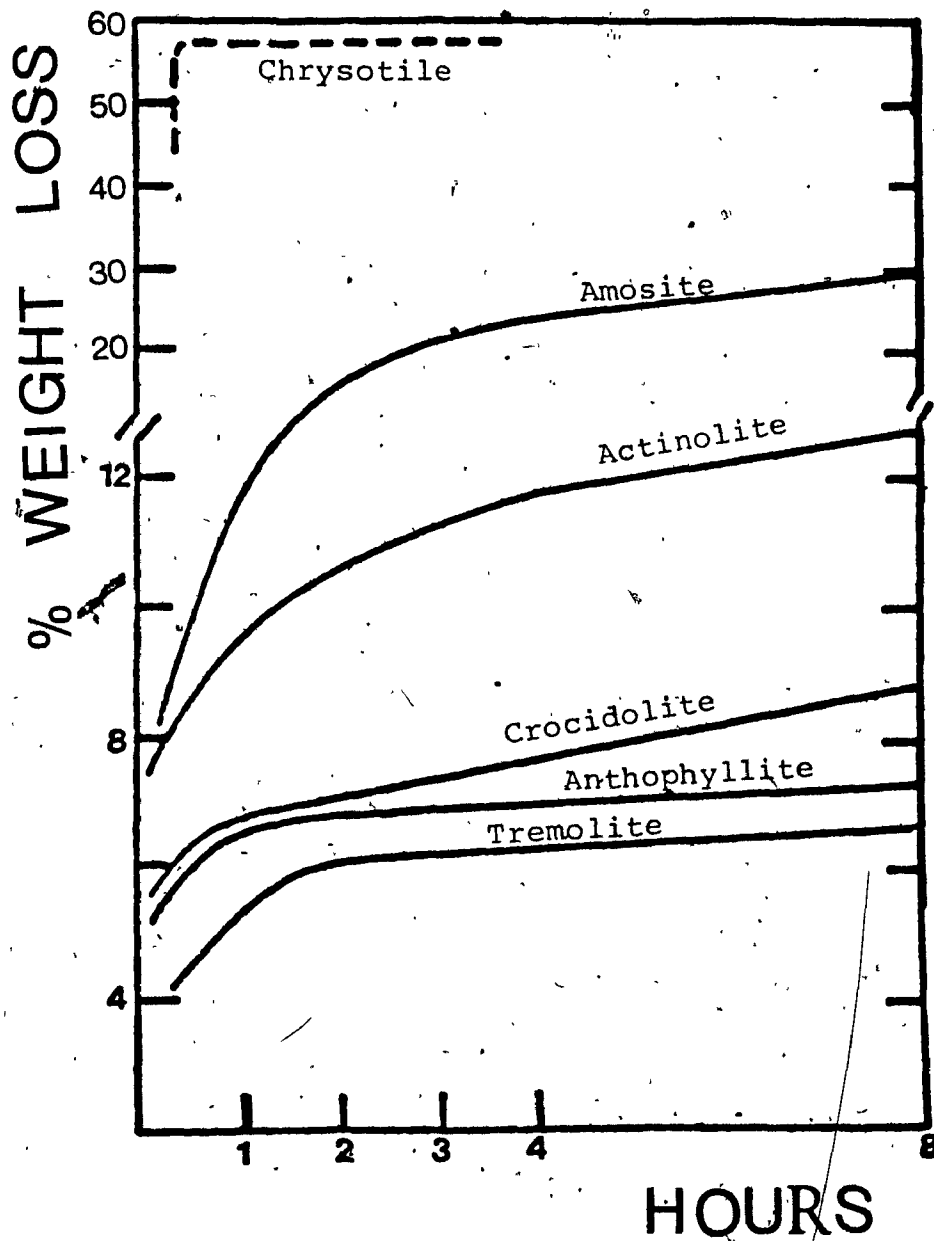
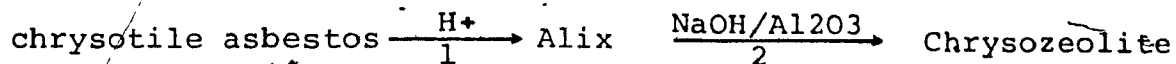


Figure 1.1: Acid resistance of asbestos (4N HCl boiling).

Most of the above-mentioned researchers established that chrysotile is the most rapidly and easily acid decomposed asbestos. In the present work, the reactivity of chrysotile asbestos fibers in acidic media under different leaching conditions was investigated. In order to obtain a better understanding of the leaching behaviour of chrysotile fibers in acid solutions, the resulting reaction products of the acid leaching were characterized with various physico-chemical techniques.

Researchers at Concordia University, led by Le Van Mao (7,8), have developed a new product from chrysotile asbestos that has a lot of potential applications and may boost the asbestos industry. Chrysozeolite, the new material developed, is not toxic. Traditionally, zeolites are prepared from synthetic reagents, namely silica and alumina containing materials. A new route to zeolites has been discovered, using a cheap and abundant natural resource of Quebec, chrysotile asbestos, which, after removal of magnesium, is a convenient source of silica for the synthesis of zeolites and has lost its toxicity.

The non-toxic chrysozeolites are prepared from chrysotile asbestos (7,8) using a two-step procedure. First, some magnesium must be leached out from the parent asbestos fibers using a dilute acidic solution, then zeolitic particles are crystallized from the leached asbestos materials and sodium aluminate under hydrothermal conditions in an alkaline medium, as follows:



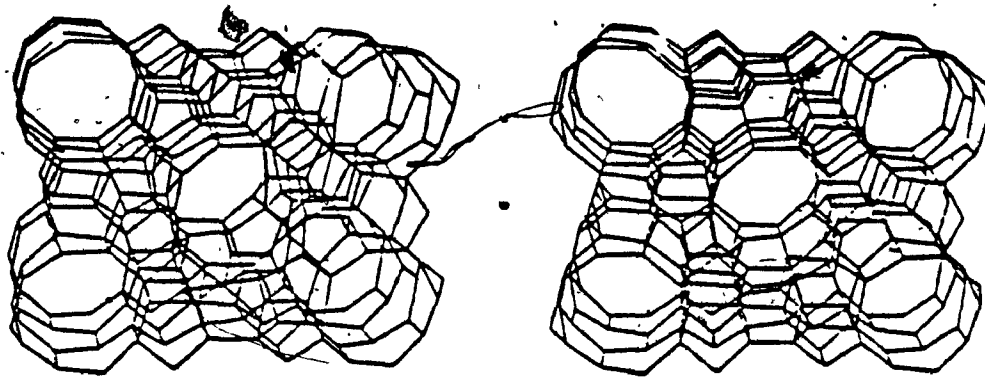
Alix is the name given to the leached chrysotile asbestos materials. The chrysotile fibers contain silica and magnesium oxide as the basic components. By leaching out the magnesium ions, the silica is made available for zeolite synthesis. Thus the highly siliceous residue of acid-leached chrysotile asbestos acts as a source of silica; an aluminum compound is then added and the chrysozeolite is synthesized under strongly alkaline and mild hydrothermal conditions. Submicron zeolite particles are thus formed and embedded in the asbestos remnants (7,8).

The chrysozeolite materials show very interesting catalytic or adsorptive properties. Type-A chrysozeolites display a water retention capacity much higher than the parent A-type zeolites (14). Chrysozeolites having the ZSM-5 zeolite structure, grown in-situ on asbestos fibers, exhibit very interesting catalytic properties in several reactions, such as the conversion of methanol and light alcohols to hydrocarbons, particularly light olefins and liquid hydrocarbons within the gasoline range (7-13). The product selectivities were found to be strongly dependent on the extent of the magnesium leaching process which was determined by the magnesium leaching degree, MLD (7,8). The magnesium still present in the chrysozeolites as well as the porous matrix (asbestos remnants) has been cited as the main causes of such enhanced catalytic and/or sorptive

properties. The use of ZSM zeolite catalyst (15,16) is particularly attractive, as it offers a new and viable route for the direct production of high-grade gasoline from methanol synthesized from coal or natural gas resources. Zeolite-based ZSM-5 catalysts are the key to Mobil's Methanol-to-Gasoline (MTG) process for which a commercial plant is presently in operation in New Zealand (17).

Zeolites are porous, crystalline aluminosilicates composed of AlO_4 and SiO_4 tetrahedra, interconnected through oxygen atoms, forming a three-dimensional framework (18). As catalysts, zeolites are unique in their ability to discriminate between reactant molecules and to control product selectivity, depending on molecular size and shape (18). This phenomenon, "shape-selective catalysis", is a consequence of the well-defined geometry of zeolite pores, channels and cages, which are of molecular dimensions. A diagram of some framework structures of ZSM-5 zeolite is given in Figure (1.2).

The acid leaching prior to the crystallization of the zeolite is an important step because it regulates the magnesium content of the chrysozeolite and the porosity type of the matrix in which zeolitic particles are formed (19). The Magnesium Leaching Degree (MLD) is mainly used as a measure of the progress of acid leaching (7-14). In previous work by Lévesque (20), it was observed that the most interesting MLD values range from 55-60% to 99%. Moreover, the MLD variations within the aforementioned range



ZSM-5

Pnma

8 T₁₋₁₂[1]

viewed along [010]

Secondary building units: complex 5-1

Framework density: 17.9 T/1000 Å³

Channels: { [010] 10 5.4 x 5.6 — [100] 10 5.1 x 5.5 } ...

Fault planes: (100)

Type species: Mobil synthetic zeolite ZSM-5

$\text{Na}_n\text{Al}_n\text{Si}_{96-n}\text{O}_{192} \cdot 16\text{H}_2\text{O}$ with $n < 27$ and typically about 3

orthorhombic, Pnma, $a=20.1$ $b=19.9$ $c=13.4$ Å

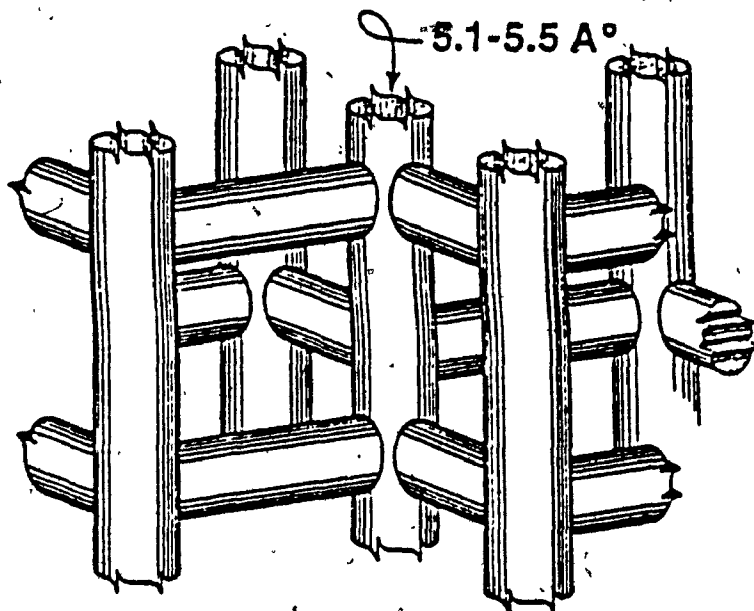


Figure 1.2: Structure and channel system of zeolite ZSM-5.

resulted in significant changes both in catalytic properties and pore size distribution of the chrysozeolites (19,20).

The final objective of this work was to answer the following question: What parameters govern the leaching process and why? In particular, the variations of the magnesium leaching degree (MLD), i.e. the extent of the magnesium removal, upon various acid treatments of chrysotile asbestos fibers were followed. Thus, the acidic properties of the leaching medium as well as its temperature and duration of leaching were studied and extensively correlated to the physico-chemical characteristics of the leached asbestos material. These characteristics were the following: the chemical composition by atomic absorption spectrophotometry (thus providing the MLD and Fe content), the IR absorption spectra, the degree of crystallinity, the morphology through the scanning electron microscopy, the magic-angle-spinning solid state ^{29}Si -NMR spectra, the specific BET surface area, the pore size distribution, and finally the adsorption capacities of the parent chrysotile asbestos fibers and the resulting leached asbestos materials.

The physical and chemical properties of the chrysotile asbestos can be directly related to their crystal structure and chemical composition. In turn, the physical and chemical properties are responsible for the commercial importance of asbestos. Therefore, through this research, some useful information on the physico-chemical properties

of chrysotile asbestos fibers were obtained. Furthermore, with a better knowledge of the physico-chemical behaviour of chrysotile, it would be possible to elaborate a method of analyzing chrysotile asbestos fibers. This method would include the determination of magnesium in the sample and in the products of the acid attack.

The leached chrysotile asbestos material is currently used at Concordia Catalysis Research Laboratory as a source of silica for the synthesis of non-toxic chrysozeolite catalysts. But in order for the synthesis of the chrysozeolite to be successful, a leached asbestos material of MLD in the range of 60-99% has to be used. Through this investigation it was possible to design suitable leaching conditions that could be used as a guiding reference in the preparation of a leached asbestos material with a certain desired MLD value, since the reproducibility of the results obtained was very good.

2 CHRYSOTILE ASBESTOS

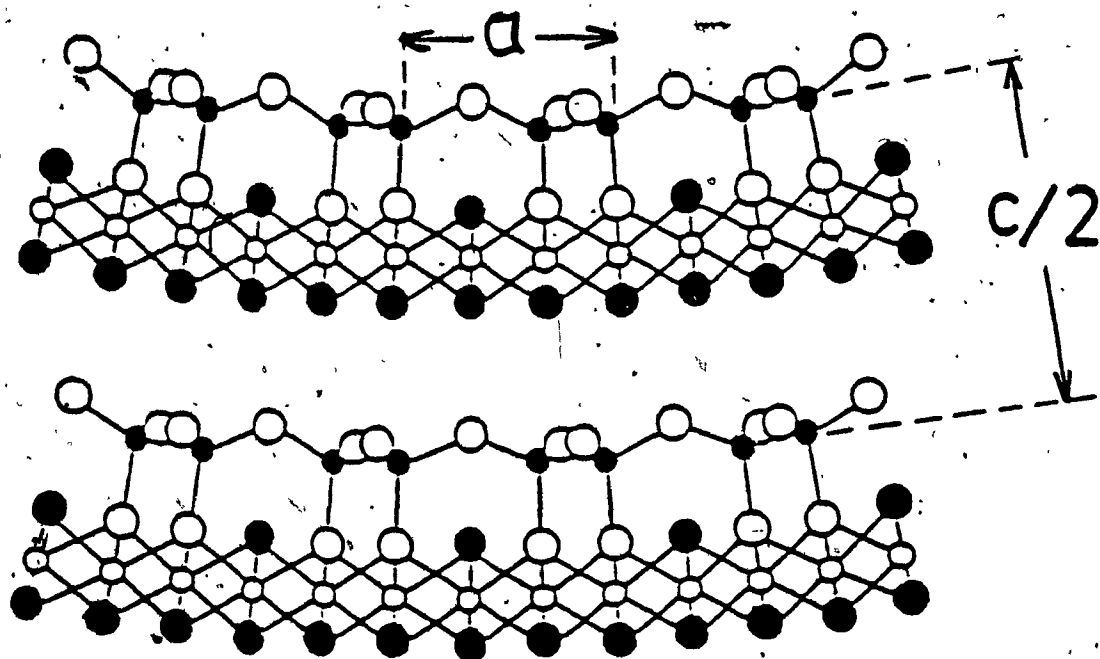
2.1 Crystal Structure of Chrysotile

The crystal structure of chrysotile asbestos was first determined by Bragg (21) and later elucidated by Warren and Herring (22). These investigators determined that the mineral has a layered type structure consisting of parallel sheets of silicon tetrahedra and magnesium octahedra. The basic structure is similar to that of the kaolinite group, with highly hydroxylated magnesium layers alternating with silicate layers. The basis of the structure is an infinite silica sheet $(\text{Si}_2\text{O}_5)_n$ in which all the silica tetrahedra are pointing in the same direction. Attached to one side of this sheet is a brucite $\text{Mg}(\text{OH})_2$ layer in which two out of every three hydroxyls are replaced by the apical oxygens of the silica tetrahedra. A projection of the chrysotile crystal structure normally to the fiber axis is shown in Figure 2.1 (23). In general, although finely fibrous in habit, chrysotile is a sheet silicate. As shown in Figure 2.1, the sheets are composed of alternating layers of SiO_2 tetrahedra bound together by a second layer of linked $\text{MgO}_2(\text{OH})_4$ octahedra through the sharing of oxygen atoms. The composite double layer of laminar structure rolls up to form long hollow tubes (fibrils) like that depicted in Figure 2.2.

In the chrysotile asbestos, the magnesium hydroxide (brucite) layer has slightly larger dimensions than the

silicate (linked SiO_4) layer, i.e. the Mg^{2+} ions are slightly bulkier than the volume normally allowed, as in the case of kaolinite (where the octahedral centers are occupied by Al^{3+}), thereby resulting in the Si component having a smaller repeat dimension than the Mg component and a mismatch between the two is created. The mismatch in the dimensions of the silica and brucite sheets introduces a strain in the structure. The tetrahedra-octahedra sheets are forced to bend in order to relieve the strain and compensate for the larger size of magnesium. Thus the chrysotile structure is curved into a scroll or coil form, with the Mg octahedra on the outside of the curve (Figure 2.3). As a result, the sheets are wound up helicoidally, giving rise to a fibrous crystal shape. The fibrous habit results from the growth pattern of the chrysotile sheet structure.

Ever since the first electron micrographs were published showing the apparent tubular structure of chrysotile, there has been considerable controversy over the morphology of the fibers. The ultimate and complete solution came with the direct evidence from high-resolution electron microscopy (24) that in chrysotile the structural layers are curved to form either scrolls or concentric cylindrical tubes (Figure 2.4). When chrysotile tubes are formed, a particular radius of curvature may be the most stable, and this may impose an upper limit on the diameters of the tubes. In general, curvature of layers has been



● Si

○ O

○ Mg

● OH

Figure 2.1: Projection of the crystal structure of chrysotile asbestos perpendicular to the fiber axis.

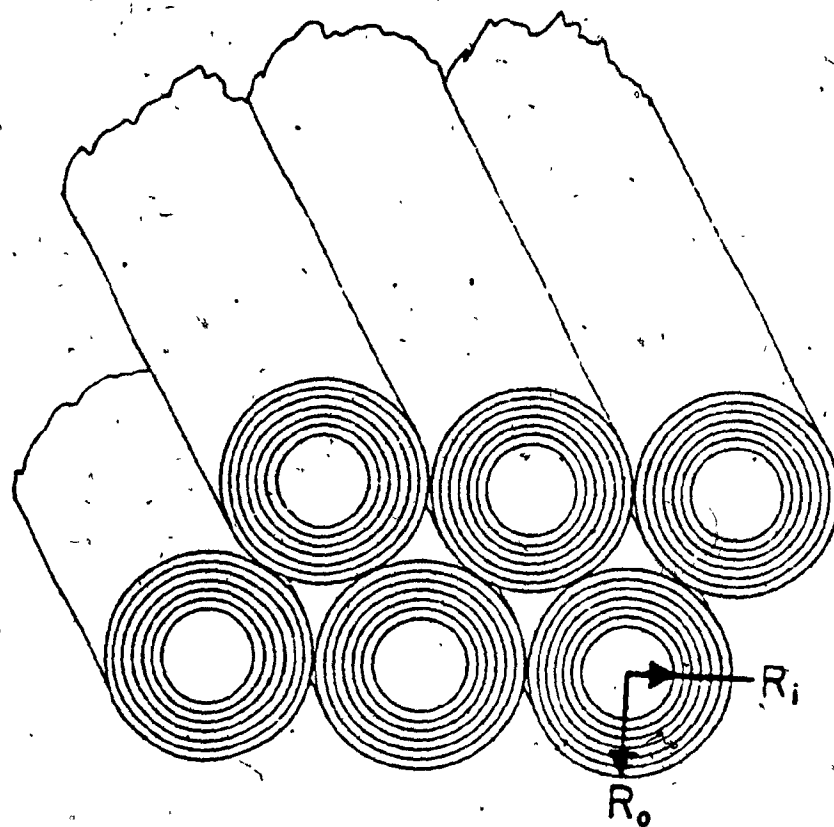


Figure 2.2: Idealized representation of fibril packing in chrysotile.

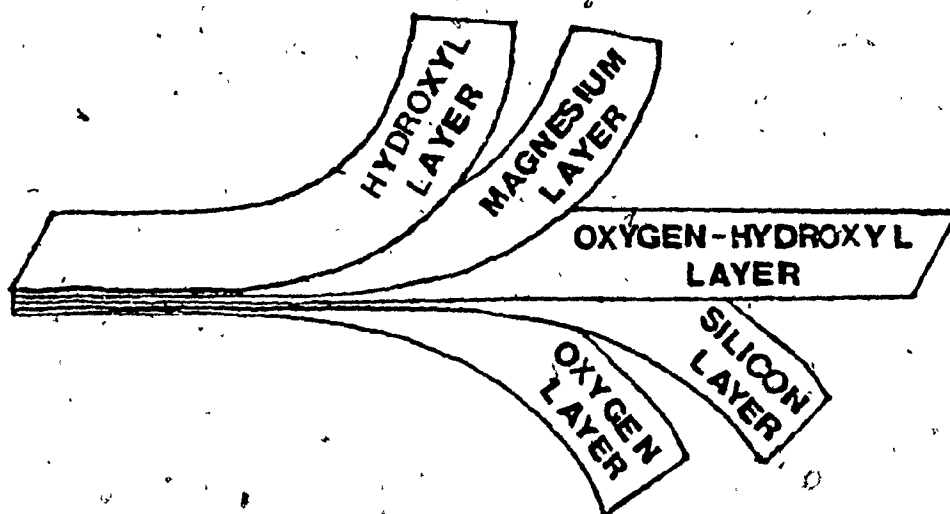


Figure 2.3: Fundamental sheet of chrysotile fibrils.

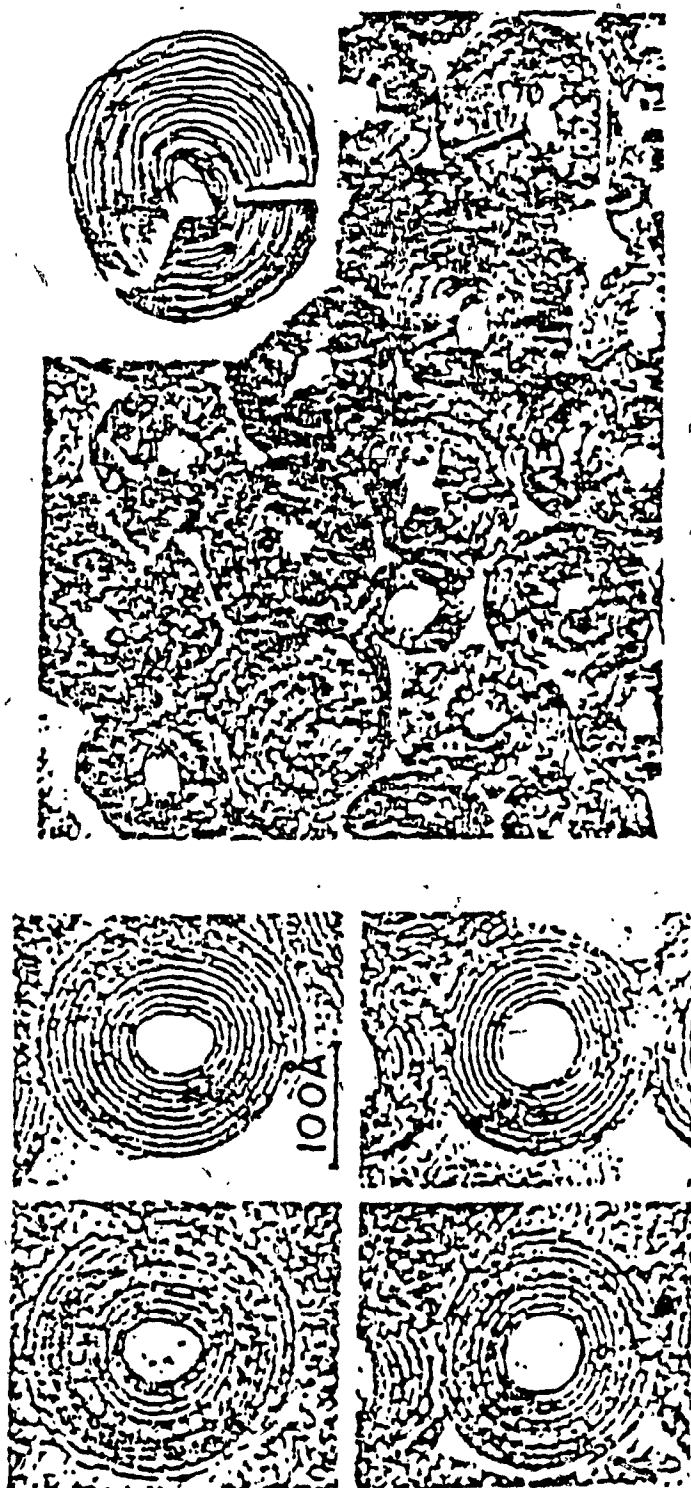


Figure 2.4: High-resolution electron micrographs of
transverse section of chrysotile.

cited as a means for relieving the misfit between two sheets of different sizes, and chrysotile is an excellent example of this structural variation. However, in any given fiber, only one layer will be at the ideal radius of curvature for perfect compensation of the misfit.

As shown in Figures 2.1 and 2.3, the layers are stacked in such a way that the SiO_4 tetrahedra are on the inner side of the fibers and the $\text{Mg}(\text{O},\text{OH})_6$ octahedra on the outer side. It results that the physical, chemical and biological properties of chrysotile asbestos are mostly determined by the magnesium-hydroxyl layers, which are the only parts of the structure in contact with the fiber's environment. Two-thirds of magnesium atoms are hereafter called "skeletal Mg" because they are part of the layered two-dimensional framework, as they are linked to Si via oxygen bridges. The other one-third belongs to brucite-type magnesium hydroxide molecules, which are connected to skeletal magnesium via oxygen bridges; however, because of the absence of linkage to silicon dioxide, they are probably more labile. In addition, the basicity of the hydroxyl groups makes them more susceptible to acid attack in the leaching process, as evidenced by our IR results.

2.2 Composition of Chrysotile Asbestos

Chrysotile asbestos is a hydrous magnesium silicate having the following theoretical composition: $\text{Mg}_3\text{Si}_2\text{O}_5(\text{OH})_4$, also written as $\text{Mg}_3\text{Si}_2\text{O}_7 \cdot 2\text{H}_2\text{O}$. The water content of

chrysotile is usually higher (12-15%) than amphiboles (average 2%); Table 2.1 shows the chemical composition of the chrysotile and the amphibole groups (23). The impurities which are present in chrysotile fibers may be part of the crystal structure or due to associated minerals. The most common impurity is iron. Iron oxides (wustite, FeO ; hematite, Fe_2O_3 ; and magnetite, Fe_3O_4) can amount to 10% in some cases. The content of magnetite may be as high as 4%, while the content of FeO and Fe_2O_3 may reach 6% each; usually the ratio $\text{FeO}/\text{Fe}_2\text{O}_3$ varies between 0.5 and 2.0 (25). The next most common impurity in chrysotile is aluminum. Other impurities, generally found to be associated with chrysotile in lesser amounts than iron and aluminum, are calcium, manganese, sodium and potassium (26).

Since the ions commonly associated with chrysotile vary considerably in size, they can have an effect on the strains which exist in the chrysotile lattice. Ions which are larger than silicon and smaller than magnesium will tend to relieve the strain when substituted in the respective layers. Moderate amounts of aluminum may substitute for silicon and moderate amounts of iron may substitute for magnesium (27). Finally, it is improbable that very large ions, such as the alkali or alkaline earths, can truly be substituted to any significant extent in the brucite layer; and when present in appreciable quantities, may exist as "interlayer" cations between the primary layers.

Among the minerals that exhibit intergrowth with

TABLE 2.1: Chemical composition of chrysotile and amphibole asbestos minerals.

Variety Property	Chrysotile	Crocidolite	Amosite	Antho- phyllite	Tremolite	Acti- nolite
Chemical Composition	$3\text{MgO}2\text{SiO}_2\cdot 2\text{H}_2\text{O}$	$\text{Na}_2\text{OFe}_2\text{O}_3\cdot 3\text{FeO}$ $8\text{SiO}_2\cdot \text{H}_2\text{O}$	$1.5\text{Mg}5.5\text{FeO}$ $8\text{SiO}_2\cdot \text{H}_2\text{O}$	$7\text{MgO}8\text{SiO}_2$ H_2O	$2\text{CaO}5\text{MgO}$ $8\text{SiO}_2\cdot \text{H}_2\text{O}$	$2\text{CaO}4\text{MgOFeO}$ $8\text{SiO}_2\cdot \text{H}_2\text{O}$
Essential Composition	Hydrous silicate of magnesium	Silicate of Na and Fe with some water	Silicate of Fe and Mg; higher iron than antho- phyllite	Mg silicate with iron	Ca and Mg silicate with water	Ca Mg Fe silicate; water
Percentage Chemical Composition						
$\text{SiO}_2, \%$	37 - 44	49 - 53	49 - 53	56 - 58	51 - 62	
$\text{MgO}, \%$	39 - 44	0 - 3	1 - 7	28 - 34	0 - 30	
$\text{FeO}, \%$	0.0 - 6.0	13 - 20	34 - 44	3 - 12	1.5 - 5.0	
$\text{Fe}_2\text{O}_3, \%$	0.1 - 5.0	17 - 20	- - -	- - -	- - -	
$\text{Al}_2\text{O}_3, \%$	0.2 - 1.5	- - -	2 - 9	0.5 - 1.5	1.0 - 4.0	
$\text{H}_2\text{O}, \%$	12.0 - 15.0	2.5 - 4.5	2 - 5	1.0 - 6.0	0 - 5.0	
$\text{CaO}, \%$	Tr, - 5.0	- - -	- - -	- - -	0 - 18	
$\text{Na}_2\text{O}, \%$	- - -	4.0 - 8.5	- - -	- - -	0 - 9	

chrysotiles, those of prime importance are: free brucite and magnetite. These mineral impurities are not dissolved in the chrysotile structure but exist as separate phases, and their concentration is strongly dependent on the mining and processing techniques used. Impurities, amorphous or crystalline, are usually located inside the fibers and between the curved layers of the fibers (23). In general, the contents of magnetite and brucite fall as the degree of disintegration rises, or as the fibers become shorter. The magnetite mineral is the most undesirable impurity, particularly in certain electrical applications. The free brucite phase impurity, which usually exists as a different distinct layer on the external surface of the fibers, should not be confused with the "brucite-type" magnesium hydroxide molecules inserted in the fiber layers between the skeletal Mg atoms. The free brucite impurity can be distinguished from the structural "brucite-type" $\text{Mg}(\text{OH})_2$ by X-ray diffraction (see Fig. 4.10a). High amounts of brucite and magnetite mineral impurities can greatly lower the quality of chrysotile fibers (28).

Since the structural "brucite-type" magnesium hydroxide layer forms the external surface of chrysotile, the fiber possesses strongly basic properties and, therefore, it is not surprising that the fibers behave in some respects as though they were magnesium hydroxide. For example, Pundsack (29) determined that the pH of a suspension of chrysotile in carbon dioxide-free distilled water is 10.33. This compares

to a value of 10.37 for a magnesium hydroxide suspension under the same conditions.

2.3 Sources of Asbestos Fibers

Table 2.2 presents the world production in 1978 ⁽²⁾. Production of asbestos has increased with few changes in the relative standings of the producing countries. The major difference is the great increase in the Russian production which now outranks Canada as the major producer. Russia leads with 46.1% and Canada is second with 28.9% of the world's output. Both countries mine only chrysotile asbestos, and most of it comes from the Ural Mountains of the Soviet Union and Quebec province (near the towns of Thetford Mines and Asbestos). The third leading asbestos producer is the Republic of South Africa (7.1%); the asbestos ore consists of annimosite, crocidolite and chrysotile. These three countries furnished 82.1% of the world's asbestos in 1978. Chrysotile accounts for approximately 95% of commercial asbestos.

With the advent of milling and increased and more varied use of chrysotile asbestos, the need for standardization in the classification of the various grades of fiber marketed by different producers became a major problem. The standardization of the method of grading and classification used by the Quebec producers has achieved world-wide acceptance (30). It permits uniform description and pricing of the product from the longest fiber (crude

TABLE 2.2: World asbestos production in 1978.

FIBER	LOCATION	PRODUCTION, IN THOUSANDS OF (METRIC) TONNES
Chrysotile	North America	
	Canada	1620
	United States	93
	South America	
	Argentina	1
	Brazil	100
	Europe	
	Bulgaria	21
	Italy	162
	Russia (U.S.S.R.)	2582
	Yugoslavia	10
	Africa	
	Zimbabwe	210
	South Africa	118
	Swaziland	48
	Other	1
	Asia	
	China	210
	Cyprus	37
	India	21
	Japan	7
	Korea	7
	Taiwan	1
	Turkey	10
	Oceania	
	Australia	58
World chrysotile total		5317
Crocidolite	South Africa	210
Amosite	South Africa	71

no. 1) to the shortest (Group 7). Chrysotile asbestos is available in more than 50 standard grades to meet specific requirements. Some of the larger asbestos mills produce many of these grades simultaneously by a complex system of continuous crushing, screening and aspiration from the same mill feed material. The classification divides the asbestos into two classes: "crude" and "milled" fiber. The "crude" asbestos consists of hand-selected cross-vein fiber, essentially in its native or unfiberized state, and is normally given final preparation by the ultimate user. The largest fibers are Groups 1 and 2, with fiber lengths of over $\frac{3}{4}$ in. and from three-eighths to $\frac{1}{2}$ in., respectively. The material classed as "milled fiber" is designated under 5 groups (no. 3 to 7), with decreasing fiber length and most of them subdivided into a number of different grades.

2.4 Applications of Chrysotile Asbestos

Asbestos is a fibrous mineral of unique properties. It is used in a multitude of different applications because it can confer superior properties on its products. Asbestos imparts to a great variety of products a combination of properties which cannot be obtained by using other materials. Its strong fibrous form reinforces other media, such as plastics or cement, or controls viscosity of many systems; its inorganic nature is important for resistance to heat and chemical or environmental agents; its fine size contributes filtration efficiency; its abundance and low cost are

significant factors in promoting commercial applications."

On the basis of relative abundance alone, chrysotile will be used wherever possible in preference to other forms of asbestos. The uses of chrysotile asbestos range from asbestos-cement products or floor tiles which consume hundreds of thousands of tons, to specialty filtration applications which may consume only several tons annually. Its use as wall-coatings, drum brake linings, roofing materials and many other outlets has contributed to human safety and convenience. Textile products require a soft, silky and longer grade of chrysotile. In general, although the longer fibers are considered to be of better quality, specific grades of chrysotile have been developed by the asbestos industry for each market.

The widespread use of asbestos has created a health hazard for persons inhaling or ingesting the substance. Therefore, despite the enviable great success for the multiple uses of asbestos products, particularly in the past, the application of asbestos is rapidly dwindling. In some cases, its use has been discontinued and, indeed, the asbestos industry is in trouble with bleak future prospects. The adverse health effects produced by inhalation of asbestos fibers have been extensively documented (31). As a result of these reported toxicity of asbestos and its adverse publicity, it now faces stiff competition from substitute materials which have gradually been making some inroads into the traditional asbestos markets. Accordingly,

asbestos must be considered a useful but hazardous substance, and suitable precautions must be taken when using it. In order to save the asbestos industry, a lot of research is needed to generate new products which are less health hazardous and non-toxic so as to diversify its range of uses.

3 EXPERIMENTAL APPROACHES AND THEORETICAL PRINCIPLES OF THE CHARACTERIZATION TECHNIQUES

3.1 Preparation of Leached Asbestos (Alix) Materials

Chrysotile asbestos fibers (7TF-12 short fiber commercial grade), which were used in the present work, had the following chemical composition (dried oxide basis in % wt): $\text{SiO}_2=41.6$, $\text{MgO}=50.2$, iron oxides=8.0 (as FeO , Fe_2O_3 and Fe_3O_4), $\text{Al}_2\text{O}_3=0.1$ and $\text{Na}_2\text{O}=0.1$. In order to present a standardized oxide composition, water and possible sorbed species were neglected and thus all the oxide contents appear to have values higher than those usually reported. Mineral and organic acids were used as leaching agents. The acidic attack of chrysotile was carried out under conditions of variable temperature, acid concentration and/or time of leaching, but always keeping the ratio of acid solution to chrysotile = 10 (w/w). By varying any of the three variables, that is, the acid concentration, the contact time or the temperature, different amounts of magnesium ions could be leached out of the chrysotile fibers; and hence, a series of leached asbestos materials were generated.

The fibers were first subjected to the magnesium leaching operation with a mineral acid (HCl or H_2SO_4). The general procedure has been fully described (7,8) and basically consists of digesting the fibers with a mineral acid solution by refluxing in a water bath. The concentration of the acid solution was usually varied in the

range of 0.5 to 6.0N at fixed time while the temperature was maintained at 80 °C, 50 °C or about 25 °C (ambient temperature); whereas the duration of leaching was varied from a few minutes to a maximum period of 2 weeks when the temperature and concentration of the solution were kept constant. The digesting acid media were kept well stirred during the entire leaching process to ensure homogeneous interactions between the acids and the fibers. After the leaching operation, the slurry was diluted with sufficient water to allow any solubilized silica to be precipitated in the solid lattice. The resulting suspension was allowed to settle for 12 hours at room temperature, then filtered, washed with distilled water and finally dried at 120 °C for 24 hours. The dry solid was weighed and labelled "ALIX".

Tables 4.1-4.5 report the conditions used for the leaching of chrysotile asbestos in the presence of HCl and H₂SO₄, respectively. Leaching was performed in one or two steps. The one-step process consists of leaching with a mineral acid only as described above.

In the case of a two-step leaching, chrysotile asbestos fibers were first subjected to the Mg leaching action of an HCl solution under mild leaching conditions and then to the secondary leaching with an organic acid, following the same procedure as mentioned before, but the temperature of the acid solution was maintained at 80 °C. Three organic acids were used in the secondary leaching process: acetic acid, oxalic acid and EDTA (ethylene diamine tetraacetic acid).

Tables 4.6 and 4.7 report the conditions used in this two-step leaching process.

3.2 Physico-Chemical Characterization Techniques

The main characterization techniques used in the present work to characterize the samples include atomic absorption spectrophotometry for elemental analysis, scanning electron microscopy (SEM) for morphology, X-ray powder diffraction, IR spectroscopy (some structural information), MAS-Solid State NMR (chemical environment of the Si component), BET measurements (specific surface area), pore size distribution, bulk density and relative affinity index (RAI) measurements.

3.2.1 Atomic Absorption Spectrophotometry (AAS)

Atomic absorption spectrophotometry was used for elemental analysis of Si, Al, Na, Mg and Fe.

The magnesium leaching degree (MLD), which expressed the extent of the leaching process or the dissolution of chrysotile as the percentage of magnesium which had gone into solution during the leaching process, is defined as:

$$\text{MLD}(\%) = \left[\frac{(\text{MgO})_i - (\text{MgO})_f}{(\text{MgO})_i} \right] \times 100$$

where $(\text{MgO})_i$ and $(\text{MgO})_f$ are the initial and the final magnesium contents, respectively (on the dried oxide basis). The magnesium leaching degree (MLD) was a good parameter for following the gradual physico-chemical modifications during

the leaching process.

In this investigation, atomic absorption was an important determination tool in elemental analysis of the leached asbestos materials. Through the determination of Na, Fe, Al, Mg and Si by AAS, it was possible to study the leaching behaviour and decomposition of chrysotile in the presence of an acid as the leaching parameters were varied from mild to medium and finally to drastic conditions.

Atomic absorption spectroscopy is based on the principle that metal atoms absorb radiation at frequencies which are characteristic of a particular metal, the amount of light absorbed being a function of its concentration. AAS is one of the most used analytical tools in the modern analytical laboratory. The wide application of this technique was brought about mainly by the use of the hollow-cathode discharge lamp as a light source and the use of atomizers to provide rapid and efficient atomization of liquid samples. The development of each of these components was vital to the acceptance and development of atomic absorption spectroscopy. Atomic absorption has been used more widely than any other technique for elemental analysis. With current instrumentation, the method, however, is not suitable for qualitative or simultaneous multi-element analysis.

3.2.1.1 Theory

Atomic absorption spectrophotometry is a highly specific means of elemental analysis based on the selective

absorption of line radiation by atomic species in the vapour phase. Quantitative analysis by AAS is based on the measurement of the radiant energy absorbed by free atoms in the gaseous state. The technique owes its high selectivity to the fact that the spectra of gaseous atomic species consist of well-defined narrow lines at wavelengths characteristic of the element involved. In practice, the samples (solution or solid) are vapourized and on further heating the vapour dissociates into free atoms. The atomic vapour is then allowed to absorb radiant energy of a characteristic wavelength. Flames, electrical heating or lasers are commonly used to convert the sample into atomic vapour (32,33). A simple presentation of the process is shown in Figure 3.1.

The sample element of interest usually exists in the ionic state or in a molecular form. They do not exist as free atoms in any common solution. In order to observe AA signals, it is necessary to generate a population of free neutral atoms of the element of interest. The metal atoms are then capable of strongly absorbing radiation at discrete characteristic wavelengths, which coincide with the emission spectra lines of the particular metal. The narrow emission lines which are to be absorbed by the sample are generally provided by a hollow cathode lamp. Thus the theory of atomic absorption concerns the formation of free atoms from the sample and the absorption of radiation by these free atoms which are in an unexcited ground-state level (34,35).

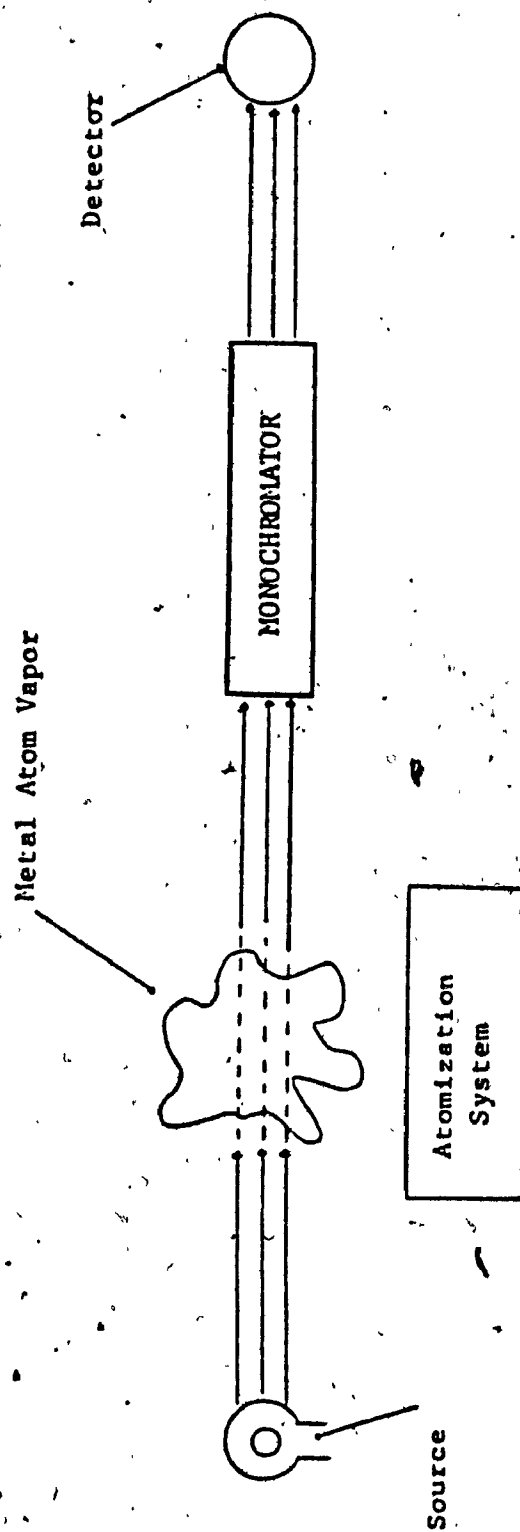


Figure 3.1: Schematic presentation of the concept of atomic absorption spectroscopy.

Since most of the atoms remain in the ground state, absorption is greatest for resonance lines resulting from transitions originating in the ground state. This greatly restricts the number of absorption lines that can be used in atomic absorption. The degree of absorption depends on the population of atoms in the ground state, the ability of those atoms to absorb and the oscillator strength. This factor is an expression of the line intensity and represents the probability that an atom will undergo a transition in unit time.

The degree of absorption is a function of the concentration of the metal in the sample. The absorption follows Beer's Law. That is, the absorbance is directly proportional to the path length in the flame. Both of these variables are difficult to determine, but the path length can be held constant and the concentration of atomic vapour is directly proportional to the concentration of the analyte in the solution being aspirated (36,37).

$$I = I_0 \exp(-KvB) \dots\dots\dots 3.1$$

where: I = transmitted intensity of source beam

I_0 = incident intensity of source beam

Kv = absorption coefficient characterizing the intensity of the absorption line

B = horizontal pathlength of the flame or thermal source.

For the purposes of analytical work, the physical property actually measured is the absorbance, A . We have then:

$$A = \log\left(\frac{I_0}{I}\right) = KcB \log e = 0.4343KcB \quad \dots\dots\dots 3.2$$

The absorbance is directly proportional to the absorption coefficient, K , and this coefficient is then directly proportional to the (number of absorbing atoms and therefore to the concentration of the solution. Plots of absorbance at the specified wavelength against concentration should yield linear relationships.

3.2.1.2 Instrumentation

Instrumentation for atomic absorption spectroscopy has two parts with essentially different functions, the means whereby the population of ground state atoms is produced from the sample, and the optical system. The basic components of AA spectrometers are as follows:

- a) Radiation source to emit the spectral line of the element of interest.
- b) Atomization system (e.g. flame or furnace) to provide sufficient energy for analyte dissociation and vaporization as free atoms.
- c) Monochromator for spectral dispersion and isolation of the spectral line to be measured.
- d) Detector and data-logging device to measure, amplify and display the results.

The most critical component of an atomic absorption spectrophotometer is the source. The hollow cathode lamps have been used almost exclusively as the radiation source for most elements. The hollow cathode lamp emits strong sharp lines of appropriate wavelength characteristic of the desired element. This radiation passes through a flame into which the sample solution is sprayed as a fine mist. Ground state atoms thermally generated by the flame, and which predominate under the experimental conditions, absorb the resonance radiation from the source lamp, reducing the intensity of the incident beam (38).

The monochromator and the slits isolate the desired resonance line from other radiation emitted by the source and allow this radiation to fall on the photomultiplier. The photomultiplier detector converts the light signal into an electrical signal. Because the range of wavelengths detected is determined primarily by the hollow-cathode source, the monochromator and slits serve primarily to minimize the detected background radiation from the flame and to remove extraneous lines emitted by the hollow cathode filler gas. Emitted radiation corresponding in wavelength to the monochromator setting is inevitably present in the flame due to excitation and emission by the analyte atoms. Thermally excited emission by the analyte atoms is discriminated by modulating the source of radiation and using an a.c. amplifier, so that the unmodulated emission

is not detected. The signals generated by the photoelectric detector are amplified by an amplifier tuned to the frequency of modulation. The radiation emitted by the flame is not modulated, and therefore gives no resulting output signal (39).

In order to achieve absorption by atoms, it is necessary to reduce the sample to the free atomic state. The most common atomization device for atomic spectroscopy consists of a nebulizer and a burner (40). The nebulizer is the apparatus which gets the sample solution into combustion flame. The nebulizer converts a sample solution into a fine spray or aerosol, which is then fed into the flame. Figure 3.2 is a diagram of a typical commercial laminar slow burner which was used. The analyte solution is aspirated from the sample container through a capillary tube by suction (venturi action) caused by rapid flow of support gas (oxidant) past the capillary tip (Figure 3.3). The resulting aerosol is then mixed with fuel and flows past a series of baffles that remove all but the finest droplets. The aerosol, oxidant, and fuel are then burnt in a slotted burner.

The use of a flame as the atom cell in analytical atomic absorption is, at present, by far the most widely used method of obtaining a population of free analyte atoms. The flame evaporates the solvent, decomposes and dissociates the molecules into ground state atoms.

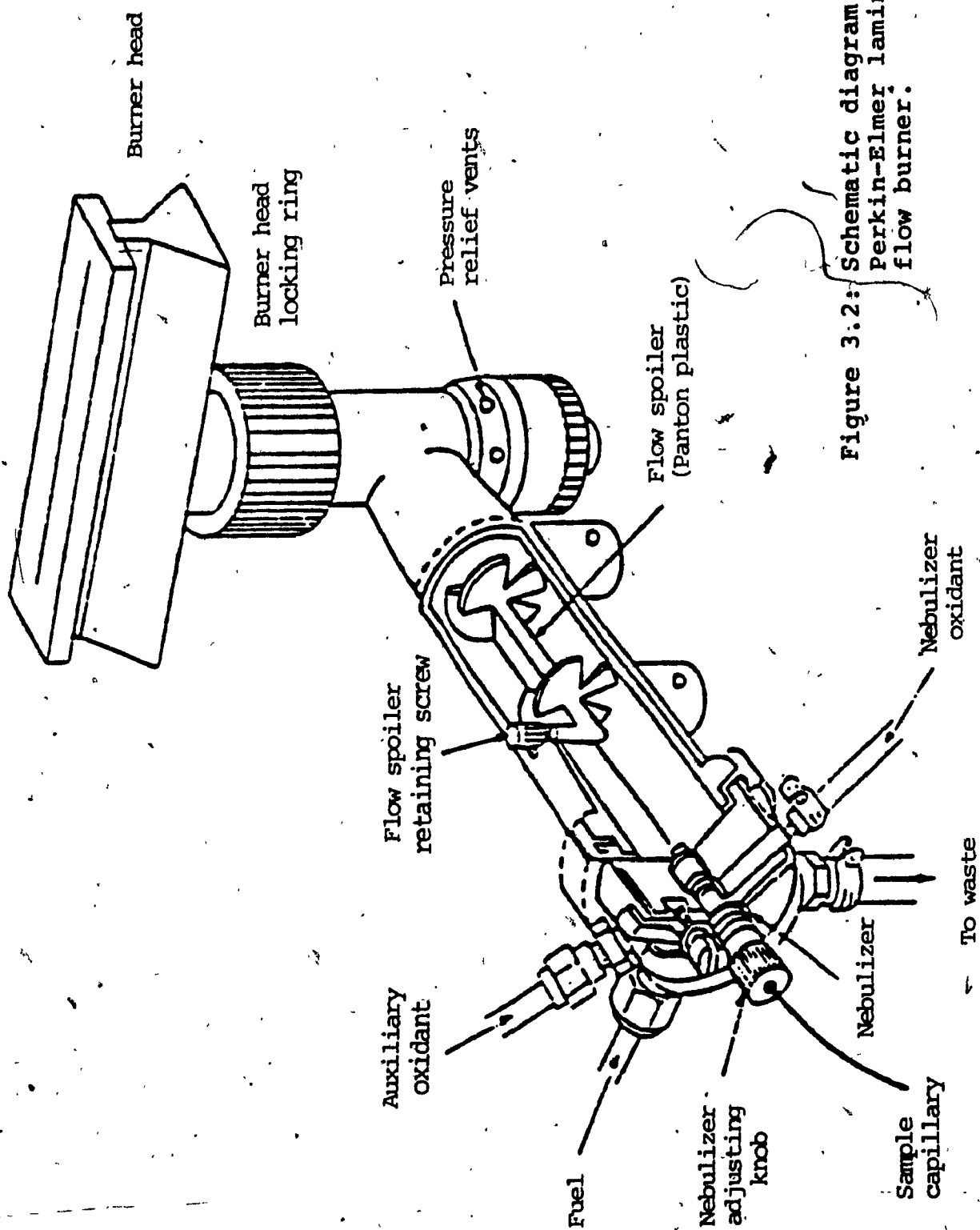


Figure 3:2: Schematic diagram of a Perkin-Elmer laminar flow burner.

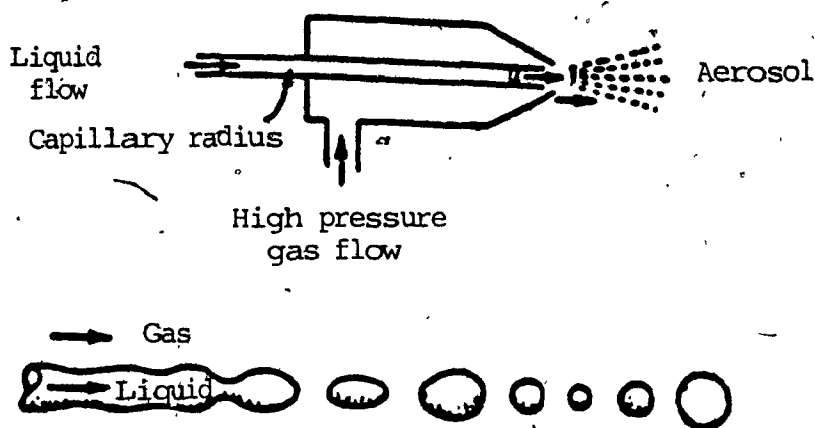


Figure 3.3: Aspiration of sample solution into the nebulizer by venturi action.

3.2.1.3 Apparatus used

A Perkin-Elmer Model 503 atomic absorption spectrophotometer utilizing a double-beam optical system was used and a Perkin-Elmer Model 56 digital recorder. The dispersion optical system included a high quality diffraction grating monochromator.

A laminar flow (premix) burner was used, equipped with two single-slot burner heads, i.e. a 10-cm long and a 5-cm long for air-acetylene and nitrous oxide-acetylene, respectively. The burner heads were held in place by stainless steel cables and a safety pin interlock. A schematic diagram of a typical commercial Perkin-Elmer laminar flow burner that was used is presented in Figure 3.2.

3.2.1.4 Sample preparation for elemental analysis

The sample was accurately weighed (about 0.1 gram) in a platinum crucible, ignited in a furnace at 750 °C for one hour, and reweighed to obtain the dry weight. A fusion mixture of potassium carbonate and lithium tetraborate in ratio 2:1 was added to the Alix material, mixed and ashed in the furnace for another hour. The fusion mixture was then transferred to a 150-ml beaker and digested with a strong mineral acid mixture of hydrochloric acid and sulphuric acid. The beaker was covered with a watch glass to avoid sample loss. The fusion mixture was gently heated on a hot plate until a clear solution was obtained. Hydrogen peroxide (30%) was added and the dissolution mixture was further digested for a few minutes until effervescence had stopped.

The cooled solution was transferred to a 100-ml volumetric flask and diluted to the mark with distilled water. From this stock solution appropriate dilute solutions were prepared particularly for magnesium and iron analysis. Each sample was analysed in a duplicate. Sample concentrations were determined by using the calibration method of flame atomic absorption spectroscopy. Standard solutions were prepared from 1000.0 (\pm 0.2) ppm metal solutions supplied by Fisher Scientific Company, Limited as certified Fisher Standard Stock solutions. The prepared standard solutions were stored in polyethylene bottles.

3.2.2 X-Ray Powder Diffraction

X-ray diffraction (XRD) is a very powerful technique for identification, quantitative analysis, crystallinity and structure determination. The asbestos minerals such as chrysotile each possess distinct crystalline structures, based upon the ordered arrangement of atoms, and are therefore amenable to analysis by XRD. X-ray powder diffraction is particularly a convenient and specific technique for the identification and quantitative determination of asbestos. It is not surprising that analytical procedures using X-ray diffraction for analysis of chrysotile have been described by several authors.

Crable (41), Hayashi (42) and Lange (43) described X-ray powder diffraction diffractometer techniques for the identification and quantitative determination of chrysotile.

In this work, X-ray powder diffraction technique was used to investigate the effect of a mineral acid on the structure, the crystallinity and the diffraction patterns, particularly the intensity of the principal peaks, of chrysotile in the leaching process as a function of leaching time, normality or MLD.

3.2.2.1 Theory

X-ray diffraction analytical techniques can be applied only to solid crystalline materials. The materials include minerals, inorganic compounds and many organic

compounds. The principle of its applicability is based on the fact that crystalline solid materials are composed of atoms or molecules arranged in a regular repetitive three-dimensional array. Crystals have definite morphology which is generally independent of physical size and can be described in terms of certain parameters (44).

The smallest repeating structure of a crystal is termed the unit cell. A crystal type can be defined in terms of the lengths of the sides of its unit cell and the angles between them. The regular repetition of the unit cell gives rise to planes throughout the crystal, and the structure is thus a unique physical characteristic of that particular solid. These planes then form a regular pattern of plane orientations and distances between them, i.e. interplanar spacings (Figure 3.4). The wavelengths of X-rays are the same order of magnitude as the distances between these planes and can be constructively reflected from them. This, then, forms a unique X-ray pattern for each crystalline material and hence this property allows the identification of materials from a knowledge of their unique interplanar spacings.

The most common source of X-rays for analytical work is the X-ray tube. Basically, an X-ray source is a highly evacuated tube in which is mounted a tungsten filament, cathode and a target called the anode. X-rays are produced by bombarding a metal target with high energy

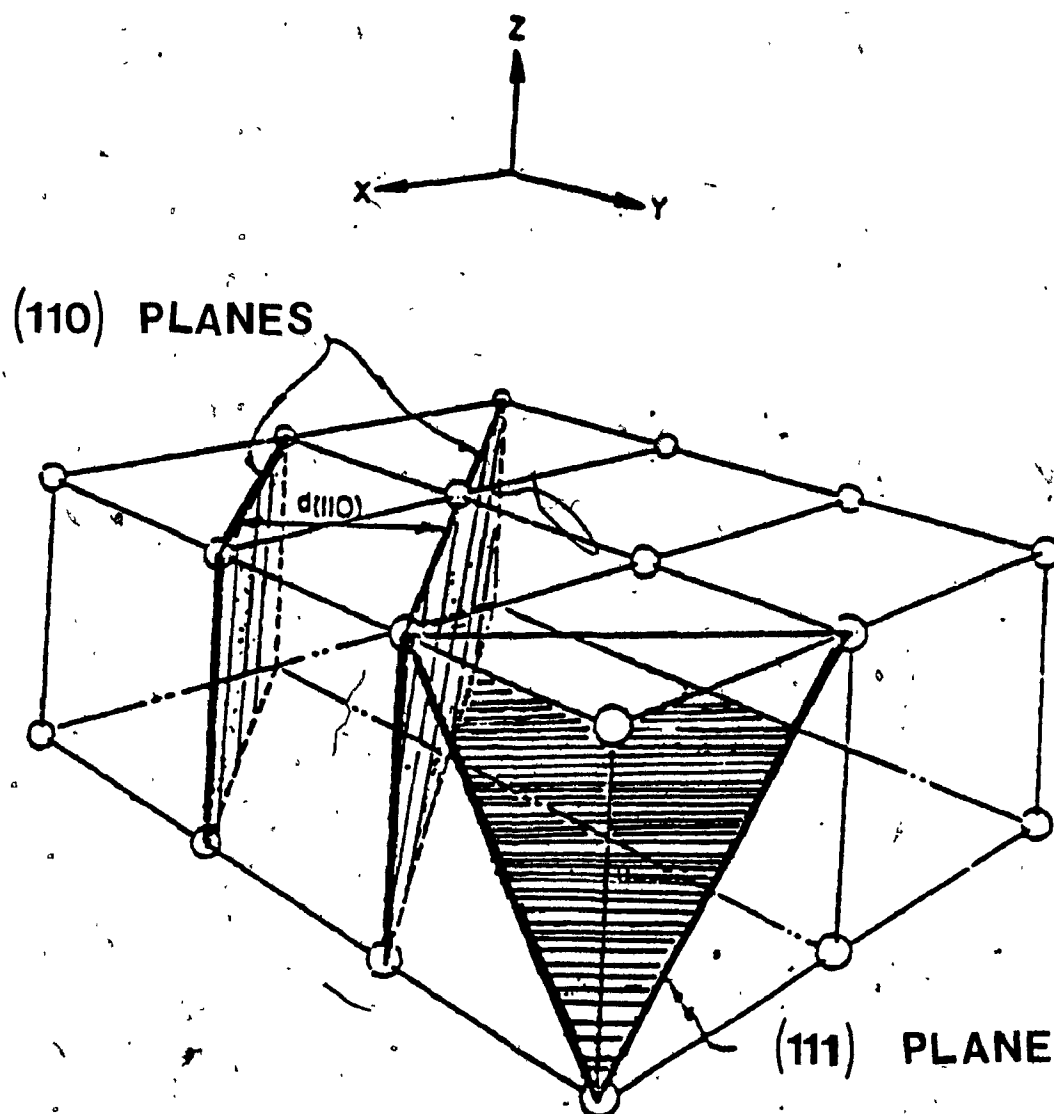


Figure 3.4: Representation of a simple cubic crystal structure showing atoms, 2 planes and the interplanar spacings d between the two planes.

electrons. The source electrons are obtained by thermal emission from the tungsten filament or wire, and are then accelerated towards the target metal (45).

When an X-ray beam encounters an atom of the crystal, each electron in it scatters part of the radiation coherently. The electrons therefore act as secondary sources of X-rays. All of these separate radiation waves can combine either constructively or destructively to give a resultant emitted wave. The amplitude of the emitted wave depends on the number of electrons emitting radiation and their respective phase differences. The phase differences are dependent on the path lengths of the incident and reflected (diffracted) X-rays. Thus a strong diffracted beam (constructive interference) will only occur when the diffracted beams from the many atomic planes are in phase; that is, when the path differences from crystal planes of the X-ray beam are equal to the integral number of wavelengths. The cumulative effect of this scattering from the regularly spaced centers of the crystal is a diffraction of the beam.

An X-ray beam incident on a crystal will be diffracted by the regularly repeating array of scattering centers (the electron clouds surrounding the atomic nuclei) in the crystal. The angle through which the X-ray diffracts depends upon the spacing between the planes of the atoms in the crystal, as demonstrated by the reflection analogies

shown in Figure 3.5 and 3.6, (46). From such an analogy, the Bragg reflection equation was derived as follows:

$$n\lambda = 2d\sin \theta \dots\dots\dots 3.3$$

where n = an integer, expressing the order of diffraction

λ = the X-ray wavelength

d = the interplanar spacing

θ = the angle of diffraction

In order for diffraction to occur from a particular set of atomic planes, they must be properly oriented with respect to the incident X-ray beam, and the diffraction intensity is related to the electron density for that specific arrangement. Diffraction occurs only for a particular angle θ that satisfies Bragg's Law.

Of all the diffraction methods now available (single crystals, powder, etc.), the powder method is the most frequently used for identification. If a monochromatic beam of X-rays strikes a fine homogeneous powder, which actually consists of an enormous number of small crystallites randomly oriented in every possible direction, a diffraction pattern of all possible planes will be obtained and a significant number will be expected to be oriented in such ways as to fulfill the Bragg condition for reflection from every possible interplanar spacing.

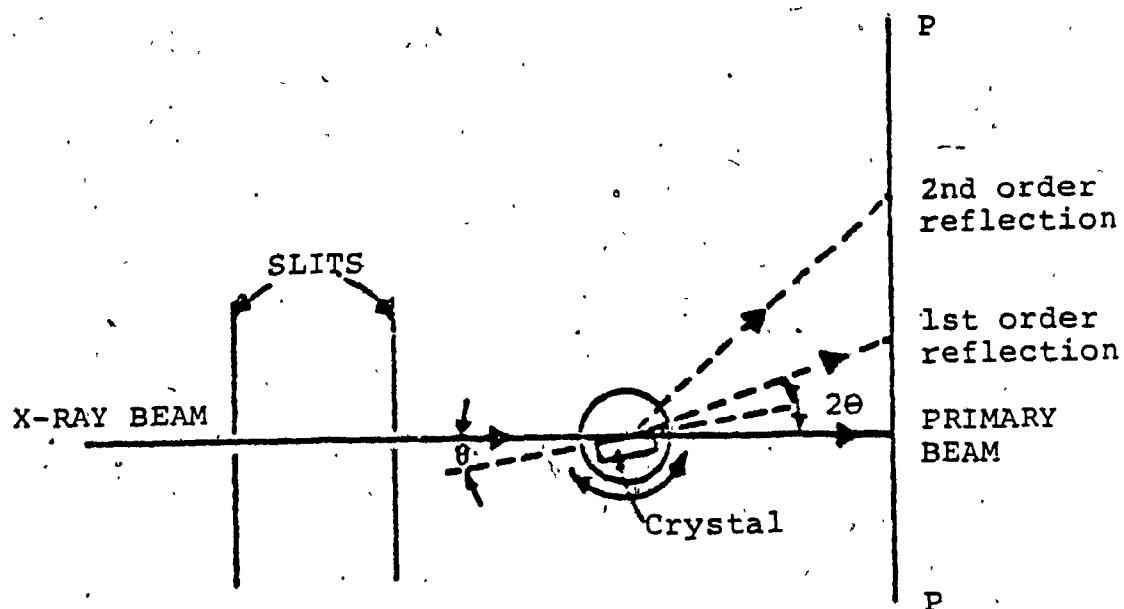
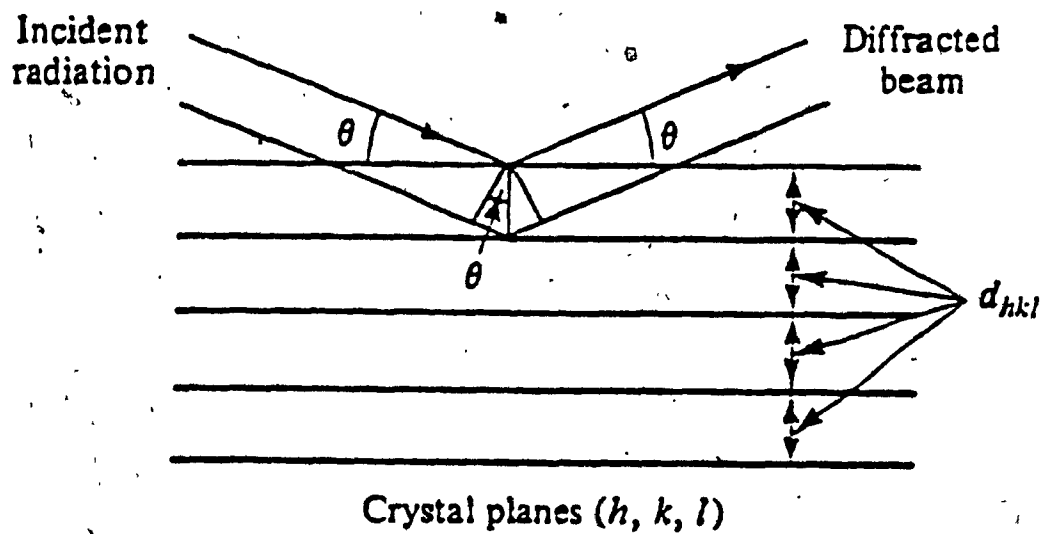


Figure 3.5: Reflection analogy of X-ray diffraction.



$$\text{Bragg condition: } n\lambda = 2d_{hkl} \sin \theta$$

Figure 3.6: Diffraction of radiation from a crystal.

4

The diffraction pattern may be detected either by surrounding the sample with a strip of photographic film or by using a movable detector, such as a scintillation counter, connected to a chart recorder (diffractometer). The diffractometer, which is the most popular device, is essentially a mechanical goniometer where the sample turns at some angle θ and the detector moves at twice that angle to intercept the diffracted beam of X-rays. The objective of an X-ray powder diffraction instrumentation is to measure the intensity of diffracted X-rays with some respect to some reference angle often labelled as theta (θ). This theta is the Bragg angle. Typical data are read out as 2θ versus the intensity of the X-rays; this 2θ can then be converted to d-spacings by the Bragg relation (46).

3.2.2.2 Instrumental apparatus

A Philips PW 1050/25 automated X-ray powder diffractometer was used with a Philips X-ray generator and a scintillation counter. All measurements were obtained using a Philips long fine focus copper X-ray tube. Copper $K\alpha$ monochromatic radiation ($\lambda = 1.54178\text{\AA}$), nickel filtered, was used at 32 Kv and 16 mA.

3.2.2.3 Experimental procedure

The chrysotile asbestos structure was identified by means of its characteristic diffraction pattern (46,47). The Alix sample was dry ground, a well-crystallized internal standard was then incorporated into the sample and thoroughly mixed in a small ball-mill. The mixture was evenly distributed in an adhesive medium on a slide and mounted on a diffractometer. In the diffractometer, the sample was scanned in the region of the chrysotile asbestos and the internal standard peaks and the counts recorded digitally. A slow scanning speed was used over the range $2\theta = 8^\circ - 40^\circ$. Typical diffraction patterns recorded are shown in Figure 4.10.

The degree of crystallinity measurement of the Alix material was designed following the literature method for zeolites (8,48,49). Peak intensities were taken as the number of counts recorded by the digital integration system during a complete scan of the peak at constant

angular velocity. Background correction was applied by subtracting the integral count rate obtained upon scanning the baseline on each side of the peaks. NaCl was used as an internal standard in order to normalize the intensities obtained and to ensure that the measurement did not depend on the sample preparation. By reference to the external standard, the degree of crystallinity in the sample was determined. The degree of crystallinity of the Alix was taken as the ratio of the normalized peak intensity for the Alix to the normalized peak intensity for non-leached chrysotile asbestos, which was used as the external standard for crystallinity, and therefore was assigned a 100% crystallinity. The strongest peak in intensity of chrysotile asbestos was chosen and used for the analysis. The peaks used for intensity measurements are located at $2\theta = 31.76^\circ$ (200) for NaCl, the internal standard, and 12.20° (002) for chrysotile asbestos and Alix materials. The powder diffraction patterns of the Alix materials were recorded by the author while the measurement of the degree of crystallinity was performed by Vaillancourt (50).

3.2.3 Infra Red (IR) Spectroscopy

IR spectroscopy is a technique for measuring the degree to which compounds absorb infrared radiation. Since, with the exception of optical isomers, no two compounds exhibit the same IR absorption spectra, the technique measures a characteristic physical property of

compounds. The information obtained from IR spectroscopic measurements can be used for qualitative and quantitative purposes, the determination of various physical constants, and for the analysis of the structure of compounds (46).

A compound can absorb infrared radiation at certain frequencies used in stretching or bending various bonds within the compound. The transmitted infrared beam not absorbed by the specimen enters the detector of an infrared spectrophotometer and is recorded at specific frequencies. When the transmitted beam is varied across a selected IR region, the IR spectrum of the compound can be recorded. This can be either a transmission or an absorption spectrum. Similar to an X-ray diffraction pattern, an IR spectrum can be also termed a "fingerprint" identification.

Unlike X-ray diffraction, gases and liquids as well as solids can be examined by IR spectroscopy. Each of these sample types has its own requirements for preparation. The major consideration is to ensure that any solvents do not absorb IR radiation in the same regions as the sample material. When solids are analyzed, it is important to reduce the particle size smaller than the IR radiation wavelength. Failure to reduce the sample to this size can result in excessive scattering of the incident radiation beam. Also, with any sample type, it is important to avoid the presence of water as it will absorb strongly. A commonly used method of presenting the solid sample to

the IR spectrophotometer is in the form of a pressed alkali halide (e.g. Potassium bromide) disc (46).

The use of IR spectroscopy for the identification, the quantification assessment and structural studies on asbestos is a relatively recent development favoured mainly because of the low capital cost (51). However, some of the asbestos minerals had their IR spectra recorded for mineralogical purposes several decades ago (52,53). Because of their speed and simplicity, IR techniques are well suited to the routine monitoring of asbestos in an industrial situation where these materials are periodically determined. The chrysotile silicate structures and their various metallic ions produce unique well-defined IR spectra, so that IR spectroscopy can be used to identify and quantify these substances (54). Gadsen et al. (55) used IR spectrophotometry for the quantitative analysis of chrysotile asbestos in airborne samples. The characteristic higher frequency fine band at 3700 cm^{-1} (Figure 4.12a) in the OH-valence oscillation range is used for quantitative determination of chrysotile (55,56).

In this work, the effect of a mineral acid on the IR spectra of chrysotile asbestos and hence its structural changes under various leaching conditions was studied. Thus the decomposition of chrysotile asbestos on leaching with a strong mineral acid (HCl) was followed by determining the IR spectroscopy on leached asbestos

specimens (Alix) prepared at different leaching parameters. The recorded spectra and the observed characteristic frequencies of the reference chrysotile asbestos fibers and their resulting acid reaction products are tabulated.

3.2.3.1 Sample preparation for IR determination

The infrared absorption spectra were obtained using the KBr Pressed-Pellet technique. The properly dried sample was hand-ground in an agate pestle and mortar. The ground specimen was placed in pure dry KBr matrix, and the mixture was thoroughly mixed in a small ball-mill. A typical wafer concentration was 2.5 mg of Alix specimen in 500 mg of KBr. The intimate mixture was then subjected to a high pressure in a hydraulic press to yield a transparent disc.



The IR spectra of Alix samples and parent chrysotile asbestos were recorded on a Perkin-Elmer Model 599B double-beam grating spectrophotometer. The transmittance was usually adjusted to about 70-80% with an attenuator attachment, and then the pellet for each sample was scanned in the range of $4000\text{-}350\text{ cm}^{-1}$. Instrument settings used included a medium scan-speed and a normal slit opening.

3.2.4 Scanning Electron Microscopy (SEM)

In a scanning electron microscope, electrons from an

electron gun source, after acceleration, are first focused by a lens to give a very small spot. The specimen is then scanned by moving the focused spot across it point by point and line by line. This scanning is achieved by the use of scanning coils; and the interaction between the electrons and the solid sample generates low energy secondary electrons. A suitable detector analyzes the secondary electrons ejected from the sample by the incident electrons. The emitted secondary electrons are used to build up an image of the sample surface which can be displayed on an oscilloscope (television tube) screen. The wide magnification range of a SEM makes it most useful for the routine characterization of materials. Non-conducting surfaces usually require coating with a thin layer of electrically conducting material in order to prevent surface charging which would otherwise lead to image distortion (57).

The SEM has a suitable resolution for chrysotile fibers and an image having startling three-dimensional appearance can be obtained. The SEM was used to follow the morphological (particle shape and size) changes of chrysotile asbestos fibers in the leaching process:

Original chrysotile asbestos fibers 
 moderately leached fibers 
 drastically leached fibers. This was carried out by

comparing the SEM micrographs of the Alix samples of widely different MLD values.

3.2.4.1 Sample preparation for SEM analysis

The powdery specimen was mounted on a "stub", a metallic disc about 1 cm in diameter, by sprinkling and pressing the sample specimen onto an adhesive that was firmly attached to the top surface of the stub. The surface of the specimen was coated with an ultra-thin film of gold so as to improve the contrast for the surface features. The sample was then evacuated under very high vacuum and scanned in a scanning electron microscope. The use of a Hitachi S-520 SEM equipped with a polaroid camera permitted the investigation of the morphological changes in the leaching process. The SEM analysis has been done at the Biology Department of Concordia University.

3.2.5 Magic Angle Spinning Si-NMR

The application of conventional NMR to crystalline or amorphous solids leads to broad, featureless spectral bands, which provide little structural information. Recently, however, several new techniques have been developed that overcome this band broadening and make possible the acquisition of high-resolution spectra much like the spectra for liquids. Modern NMR techniques, especially those involving magic-angle spinning (58), are potentially powerful for studying the local structure of silicates and other inorganic solids that have non-zero

nuclear spin nuclides, such as ^{29}Si and ^{27}Al for silicas, aluminas, zeolites and various other aluminosilicates; ^{11}B and ^{29}Si for borosilicates, etc (59). The degree of structural insight achievable with magic angle spinning (MAS) NMR is exceptional, since it probes the immediate environment of a particular nucleus more or less irrespective of whether the sample is crystalline or amorphous. A very important application that has been made of ^{29}Si MAS NMR is the elucidation of the coordination environment of silicon in zeolites. To date, less studied but still promising is the use of ^{27}Al MAS NMR to supplement the information provided by ^{29}Si MAS NMR on aluminosilicates (60).

NMR spectra for solids have in the past not been very useful for structural studies because of line-broadening, which eliminates or obscures the characteristic sharp individual peaks of NMR. Much of this broadening is attributable to two interactions: chemical shift anisotropy and static dipolar interactions, which in liquids average to zero because of the rapid and random motion of molecules. The line broadening represented by chemical shift (shielding) anisotropy is an inhomogeneous broadening associated with the fact that it is a superposition of spectra of randomly oriented individual nuclei. Each of these nuclei has an inherently sharp line for a particular orientation of nuclear environment with

respect to the static field. The net result of the chemical shift anisotropy is that, for highly immobile species, such as those in an amorphous or powdered crystalline solid, the entire range of chemical shift spanned by all possible orientations is present in the spectrum. The chemical shift anisotropy is removed by high-speed mechanical spinning of the rigid sample about an axis making an angle of 54.7° to the direction of the static magnetic field. This technique is known as magic-angle spinning (59,61). In effect, the solid acts like a liquid when spun at the magic angle. Magic-angle spinning can in principle, and sometimes in practice, also be used to eliminate the other important line-broadening interaction, the magnetic dipole-dipole interactions between pairs of nuclear magnetic moments.

The NMR spectra of Alix materials were obtained on a Varian VXR 300 FT-NMR spectrometer operating at 59.592 MHz using superconducting solenoid magnets. A VXR 4000 Model computer system was used for data acquisition and amplifiers for final radio frequency pulse generation. ^{29}Si MAS-NMR spectra were obtained using KEL-F Doty probes (Doty Sc.) with a spinning rate of 4.51 KHz. All ^{29}Si line positions (chemical shifts) were referred to TMS (tetramethylsilane) as zero chemical shift. The MAS-NMR analysis has been done at the University of Montreal.

3.2.6 Specific (BET) Surface Area

The measurement of the total surface area of a solid material requires non-specific physical adsorption. The most useful method is the one developed by Brunauer, Emmett and Teller and is usually called BET method (62). Surface area is a very important textural parameter of a solid and can be used to define the morphology and surface characteristics. The specific surface area is the measure of the accessible surface area per unit mass of solid; this surface is the sum of the internal surface area associated with pores and of the external surface area developed by the outer boundary of the particles (63). In the classical method of determining surface area, an all glass apparatus is used to measure the volume of gas adsorbed on the sample of solid material. Before the specific surface area is determined, it is normal to heat the sample for several hours to remove all physisorbed material, i.e. moisture and other adsorbed vapours, from the surface of the adsorbent. This is best achieved by exposure of the surface to high vacuum, the exact conditions required (temperature and residual pressure) being dependent on the particular gas-solid system. An outgassing period of 2-6 hours is usually sufficient to reduce the residual pressure to $\sim 10^{-4}$ Torr. Nitrogen adsorption at -196°C (the boiling point of liquid nitrogen being used as a means of thermostating the

adsorbent sample) is commonly measured in the routine determination of the surface areas of adsorbents. The use of low temperatures, as opposed to say room temperature, greatly enhances the fairly weak adsorption and under these conditions the measurements become much easier (64).

The surface area of chrysotile asbestos fibers is the most important parameter in all their industrial applications (28). Each process involving asbestos fiber requires a degree of opening or splitting into finer fibers (fiberization), which, within limits, is critical for that purpose. In general, the specific surface area of chrysotile asbestos varies considerably with the physical condition. Furthermore, the specific surface area of chrysotile is directly related to the fineness (the particle size) of the fibers or to the degree of opening. The Quebec long-fiber samples have the smallest surface area, while the commercial grades such as 7TF-12 (one of the most open grades with the shortest fibril lengths), whose powdery appearances are indicative of drastic mechanical treatments, have the largest (65). However, in this investigation, the surface area was necessary to follow the physical and chemical modifications of chrysotile after being subjected to various acid treatment conditions. The chemical opening and decomposition of chrysotile fibers with strong acidic treatments would be expected to yield residue products of higher surface area.

3.2.6.1 BET Theory

The BET treatment is based on a kinetic model of the adsorption process put forward by Langmuir, in which the surface of the solid was regarded as an array of adsorption sites. The BET Theory is based on three assumptions made by Brunauer, Emmett and Teller (62):

- a) A homogeneous surface with equivalent sites for localized adsorption without interactions between molecules adsorbed in the first layer, i.e. all the adsorption sites on the surface are energetically identical.
- b) A multilayer adsorption, i.e. formation of successive layers on the surface with no restriction on the number of layers. Each molecule in the first layer is a possible "site" for adsorption of a molecule in the second layer; each molecule in the second layer is a possible "site" for adsorption of a molecule in the third layer, etc.
- c) That in all layers except the first the heat of adsorption is equal to the molar heat of condensation and the evaporation-condensation conditions are identical, i.e. the model restricts attention to the forces between adsorbent and the adsorbate molecules, the "vertical" interactions, and neglects the forces between an adsorbate

molecule and its neighbours in the same layer,
the "horizontal" interactions.

The physical and mathematical treatment of these hypotheses leads to the following BET equation (64,66):

$$\frac{P}{V(P_0 - P)} = \frac{(C-1)}{V_m C} \frac{P}{P_0} + \frac{1}{V_m C} \dots\dots\dots 3.4$$

where P - equilibrium pressure of the adsorbate.

P_0 - saturated vapour pressure of the adsorbate in the condensed state

V - volume of gas adsorbed at STP

V_m - volume of gas at STP corresponding to the formation of a monolayer coverage

C - a constant varying with the adsorbent-adsorbate interactions. It is related to the differential heat of adsorption E_A and to the heat of liquefaction E_L by the following relation:

$$C = \exp (E_A - E_L) / RT) \dots\dots\dots 3.5$$

where R - ideal gas constant

T - absolute temperature

The graph of $Y = \frac{P}{V(P_0 - P)}$ versus

$\frac{P}{P_0}$ at low pressure ($0.05 < \frac{P}{P_0} < 0.35$)

should give a straight line. From such a BET plot, one can

derive C and V_m . The BET method for calculation of specific surface area A involves two steps: evaluation of the monolayer capacity V_m from the isotherm, and conversion of V_m into A by means of the molecular area a_m . To obtain a reliable value of V_m from the isotherm, it is necessary that the monolayer shall be virtually complete before the build-up of high layers commences; this requirement is met if the BET parameter C is neither too low or too high, in practice it should lie between 50 and 150. It is because nitrogen comes closest to meeting these conditions when adsorbed on an extensive range of solids that it has become the most generally used adsorptive for surface area determination (64). The widely accepted value of $a_m(N_2) = 16.2 \text{ \AA}^2$. The specific surface area, A , of the adsorbent is then given by

$$A = a_m \frac{V_m N}{V} \dots\dots\dots 3.6$$

where N is avogadro constant and a_m is the area occupied by one molecule of adsorbate. For many practical purposes, the BET equation is generally fitted to data over a range of $P/P_0 = 0.05-0.30$, where the model is valid.

In spite of the acknowledged weakness of its theoretical foundations, the Brunauer-Emmett-Teller (BET) method still remains the most widely used procedure for the determination of surface area. The assumptions of the theory are extremely crude, but they are still sufficiently good to contain a number of the important qualitative

features actually observed experimentally. Therefore, despite the apparent shortcomings of the BET model, it gives an extremely useful qualitative assessment and description of the adsorption process. In fact, the BET adsorption method still provides the only means of determining the specific surface of a mass of non-porous powder or a porous solid large enough to constitute a representative sample (64).

3.2.6.2 Experimental set-up

The specific surface area measurements were carried out in a classical multipoint BET volumetric apparatus at liquid nitrogen temperature. The basic apparatus, as shown schematically in Figure 3.7, was a rather simple one constructed in glass. The pumping vacuum system, which consisted of a diffusion oil pump and a mechanical pump, was equipped with throttling valves to prevent sample contamination by pump oil and was able to produce a vacuum of 10^{-4} Torr. Ancillary equipment included heating assemblies, heater control units, Pirani low pressure gauge and adsorption sampling tubes. In this volumetric method, the volume of adsorbed species was determined as a function of the pressure. The gas burette was calibrated. Before the pressure readings were taken it was always necessary to adjust the mercury in the gas burette to some known positions of the gas burette bulbs mark: 6, 5, 4 and

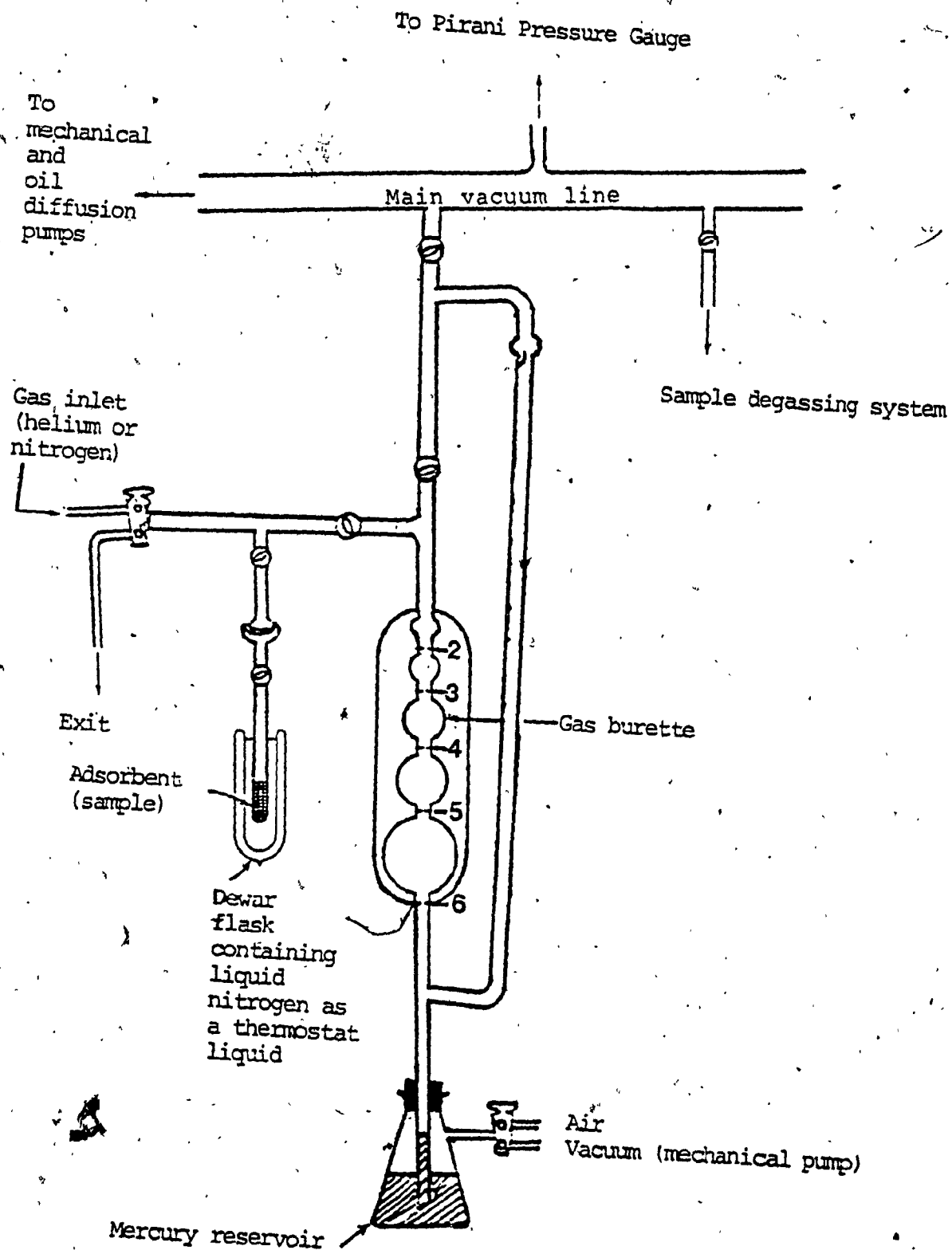


Figure 3.7: Nitrogen BET adsorption apparatus

3, respectively (Figure 3.7), by appropriate use of the mercury reservoir. A mechanical pump was used to adjust the level of mercury in the gas burette. A computer program on an Olivetti PC computer, Model M24, was used for the calculation of the surface areas.

3.2.6.3 Experimental technique

The steps involved in experimental determination of BET nitrogen adsorption included the following:

- a) Weighing of sample and its adsorption sampling tube.
- b) Evacuation of the apparatus until a suitably low pressure of about 10^{-4} Torr was registered on the pressure gauge.
- c) Degassing of sample at elevated temperature of 300°C for 3 hours under the high vacuum. The sampling tube was provided with a porous disc to ensure that the powder samples were not disturbed or displaced and sucked into the vacuum system.
- d) The cooled sampling tube was carefully closed, removed from the vacuum line and quickly weighed so as to obtain the weight of dry degassed sample.
- e) Determination of the "dead space" by introduction of helium from the calibrated gas burette to the sample section by opening the stopcock and raising the mercury to the positions of the gas burette

bulbs marked 6, 5, 4 and 3 before taking the pressure readings.

The change in burette readings gives the effective dead space of the adsorption section since helium adsorption is zero. The dead volume was obtained by helium expansion at room temperature.

- f) Evacuation to remove helium.
- g) The sampling tube was closed and a dose of nitrogen introduced into the gas burette. The mercury was adjusted and the pressure readings taken.
- h) The nitrogen from the gas burette was admitted to the sample section by opening the stopcock and immersing the sampling tube in a dewar flask filled with liquid nitrogen (-196°C). When adsorption was complete, typically after 10-20 minutes as indicated by steady pressure readings, the measurements were taken.
- i) Calculation of adsorption from nitrogen gas introduced less the dead space correction both computed by application of the ideal gas law. The specific surface area of the sample was calculated from the experimental readings by using a computer program (see appendix A).

When the adsorption isotherms were transformed by the BET method, linear plots were obtained. Correlation coefficient (r^2) values exceeded 0.995 in all cases for

which computer tests of best fit were obtained and were typically between 0.999 and 0.9998. The C values of samples, which were all outgassed at 300 °C, calculated from the slopes and intercepts, all exceeded 50 and were less than 300. The BET equation (3.4) can be rewritten as

$$\frac{\frac{P}{P_0}}{V(1-\frac{P}{P_0})} = \frac{C-1}{V_m C} \frac{P}{P_0} \dots\dots\dots 3.7$$

When the slope of a BET plot is measured, errors in the ordinate (P/P_0) caused by errors in measuring either P or P_0 are cancelled by equal errors in the nominator of the abscissa (P/P_0) / $V(1-P/P_0)$, leaving a small residual error caused by the change in $(1-P/P_0)$. However, the main sources of experimental errors were imperfect control of the conditions of outgassing temperature, variation in temperature of the sample during the adsorption, imperfect control of constancy of the level of liquid nitrogen, measurement of the dry degassed weights of samples and incidence of leaks in the apparatus. In general, the method was accurate and reproducible.

3.2.7 External Surface Area Determination

A two-step technique was used to evaluate the external surface area by benzene-pore filling and subsequent nitrogen adsorption. The principle of this technique is that benzene adsorbate is first adsorbed sufficiently until

the internal pore structure is completely filled. The sample is then lowered to a temperature of 77K which freezes the adsorbed benzene, any benzene molecule that may be adsorbed on the external surface is removed by evacuation, and the accessible free external surface is measured by nitrogen adsorption BET method. Niwa et al. (67) have shown that benzene is a more suitable and appropriate adsorbate for this technique than n-hexane or water because it is widely applicable to various kinds of samples. Benzene can be used not only on hydrophobic samples such as ZSM-5 zeolite or silicalite, but also on typical nonhydrophobic samples such as alumina (67). Moreover, during the BET measurement at 77K, benzene remains completely adsorbed and frozen in the internal pores since the sample is kept immersed in liquid nitrogen far below the melting point of benzene (the melting point of benzene is 278K).

The same pre-treatment conditions were applied as in the case of total BET surface area determination. The experimental set-up consisted of nitrogen BET adsorption apparatus, as shown schematically in Figure 3.7, and the vaporization-adsorption system (see Figure 3.10). A vaporization flask, which was fully immersed in an ice bath, was connected to the vacuum system and degassed. About 12 ml of benzene was then introduced into the evacuated flask. The sample section, also evacuated, was

thermostatically maintained at 25 °C. A valve connecting the sample section and the vaporization flask containing benzene was opened. The degassed samples were then left in contact with benzene vapor (saturation vapor pressure of benzene at 25 °C is 28 Torr) for a period of 4 hours. The sample with adsorbed benzene frozen in liquid nitrogen was evacuated for 30 minutes which was ample time for complete removal of benzene vapor from the external surface. Finally, the external surface area was measured by the BET method assuming all the internal pores were completely filled with benzene.

3.2.8 Pore Size Distribution Measurement

The pore size distribution is the distribution of the specific area versus the pore size. It is an important textural parameter for describing the morphology and pore structure of a porous solid. There are several techniques for determining the pore size distribution, the applicability of each depends on the range of the pore size of a solid. Mercury porosimetry has been widely used to measure macropores. The mercury porosimetry technique is based on the determination of mercury volume which penetrates into the solid as a function of the externally applied pressure and the pore size range accessible to this technique varies from a pore radius of about 75Å up to about 75,000Å (63). However, the samples examined

consisted of macropores, mesopores and micropores and therefore it was not possible to apply this technique. The technique based on nitrogen adsorption isotherm can be categorized into two groups: the t-plot analysis method and the classical method. The t-plot analysis method was recently developed by Lippens and deBoer (68). This method is very attractive since, in addition to measuring macropores and mesopores, it gives detailed analysis of micropores. In this method, Langmuir type of adsorption isotherm is established, in which the relative pressure is replaced by "t", the statistical film thickness of the adsorbed gas on the walls of the pores. The method consists of plotting the adsorption isotherm in terms of the volume of gas adsorbed versus t and by extrapolating to the intercept (i.e. $t=0$) the micropore volume can be obtained as illustrated by Figure 3.8. In this method, adsorption has to be performed at very low surface coverage using special microvolumetric apparatus to deliver microquantities of gas to be adsorbed on the surface, which was not possible with our instrument.

The classical method that was adopted in this particular work consists of adsorption of N_2 at saturation under liquid nitrogen and then by applying vacuum, the adsorbed adsorbate is gradually removed. At $\frac{P}{P_0} \rightarrow 1.0$, where P_0 is the saturation pressure, all the pores are completely filled with adsorbed and condensed nitrogen.

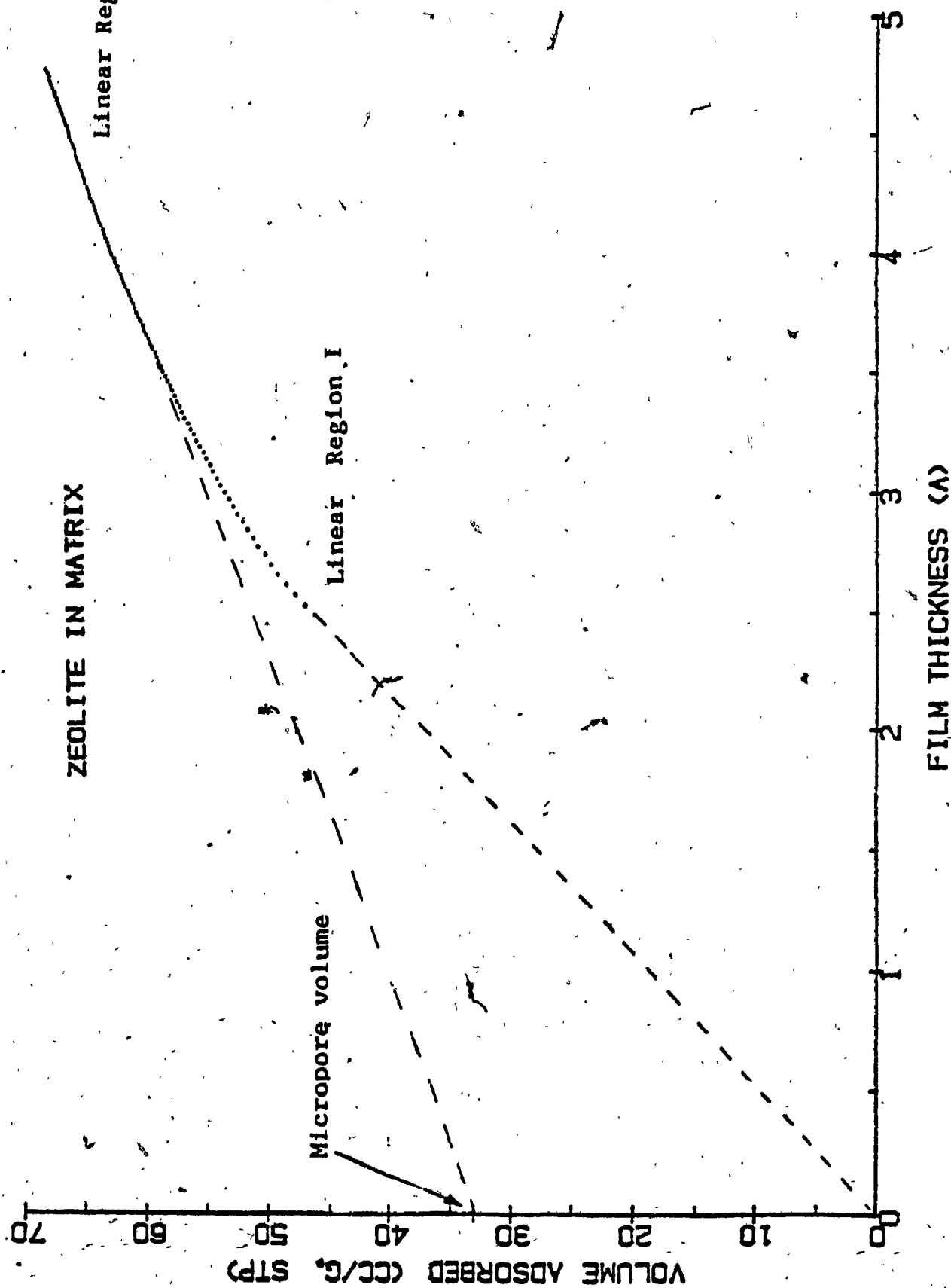


Figure 3.9: A t Plot of volume adsorbed versus film thickness.

Then a desorption isotherm is established by lowering the pressure in small increments; a small amount of nitrogen will first evaporate from the meniscus formed at the ends of the larger pores. Since the vapor pressure of a liquid evaporating from a capillary depends on the radius of the capillary, these data can be plotted as volume desorbed vs. pore radius (69).

The pore size distribution of a mesoporous solid may be calculated from the desorption isotherm of a vapor with the aid of the Kelvin equation (69). The Kelvin equation is

$$\ln \frac{P}{P_0} = - \frac{2 \gamma V}{RT} \cdot \frac{1}{r_K} \dots\dots\dots 3.8$$

where P/P_0 is the relative pressure of vapor in equilibrium with a meniscus having a radius of curvature r_K , and γ and V are the surface tension and molar volume, respectively, of the liquid adsorptive, R and T have their usual meanings. The concept of capillary condensation and its quantitative expression in the Kelvin equation is, indeed, the basis of virtually all the various procedures for the calculation of pore size distribution (70). The Kelvin equation when applied directly to the adsorption branch of the isotherm gives a qualitative picture of pore structure. When capillary condensation occurs during the course of isotherm determination, the pore walls are already covered with an adsorbed film, having thickness t

determined by the value of the relative pressure. Thus capillary condensation occurs not directly in the pore itself but rather in the inner core, as shown in Figure 3.9 (70).



Figure 3.9: Cross-section, parallel to the axis of a cylindrical pore of radius r_p showing the "inner core" of radius r_k and the adsorbed film of thickness t .

Consequently, the Kelvin equation gives values of the core size rather than the pore size. The conversion of an r_k value to a pore size involves recourse to a model of pore shape, and also a knowledge of the angle of contact θ between the capillary condensate and the adsorbed film on the walls; it is assumed, mainly on the grounds of simplicity, that $\theta = 0$ ($\cos\theta = 1$). Several methods which

make use of the Kelvin equation, and in one way or another attempt to correct the Kelvin radius, for the physically adsorbed layers which form the boundary of the evaporating pore have been proposed for the analysis of pore size distribution. However, all these computation methods have one major drawback: they can give an accurate assessment and measurement of the macro and mesopores but not the micropores, therefore the application of these methods are restricted to the desorption isotherms of macroporous and mesoporous solids.

Pore size distributions of leached asbestos materials were computed using a simplified model proposed by Pierce (71), based on the application of the Kelvin equation to nitrogen desorption isotherms. The principal assumptions of the method are as follows:

- a) All pores have cylindrical geometry.
- b) The Kelvin equation is applicable for computing the pore radii from the relative pressures at which desorption occurs.
- c) The film thickness remaining on pore walls after the inner capillary volume is desorbed is the same as on a non-porous surface at the same relative pressure. The Pierce procedure tacitly assumes the film area of a group, the area of the core "walls", to be identical with the area of the pore walls, as desorption progresses.

In the Pierce's method for the calculation of pore size distribution, specific surface area appears as an essential feature of the calculation. Thus by summing the values of pore area, δA_p , for each successive group of pores over the whole pore system, a value of cumulative surface area S_{cum} (equal to $\sum \delta A_p$) is obtained (71). The cumulative surface area represents the total pore area of macro and mesopores and excludes the pore area of micropores since the validity of Pierce's method extends down to a pore radius of 15Å and becomes non-applicable for pores smaller than 15Å.

3.2.8.1 Experimental procedure

Approximately 0.5 g of sample specimens were introduced in long glass tubes and activated by heating in vacuum at 300 °C prior to the adsorption-desorption experiments. In general, the experimental set-up was similar to the one described for surface area, but instead of a gas burette containing gas burette bulbs, a normal 100-ml graduated titration burette was used. Helium gas at room temperature was used to calibrate the dead space. The long glass tube containing the sample was completely immersed in liquid nitrogen and the level of the liquid nitrogen was maintained constant. The evacuated sample was then saturated with nitrogen adsorbate at the temperature of the liquid nitrogen. By lowering then the

total pressure in a gradual and steady way, the partial pressure decreased, the adsorbed gas was progressively desorbed and the residual decreasing volume was recorded as a function of the pressure. The readings of the desorption isotherm generated were converted to STP conditions and transferred to the computer. All pore size distribution measurements were calculated from dry degassed weights of samples. A computer program was used to calculate the pore size distribution and the surface area developed by pores having diameters progressively increasing from 20Å to 300Å. The computer program is given in appendix B. Errors in the measurement of P or P_o can have drastic effects on measurements of pore size distribution, since both P and P_o enter directly into calculation, and therefore in order to minimize such errors, many equilibrium pressure points were measured during the nitrogen desorption experiment. At low relative pressures, desorption equilibrium was rapid and appeared to be complete in less than 30 minutes, but at higher relative pressures, at least one hour was required for equilibrium to be established. A critical potential source of error was the imperfect control of constancy of the level of liquid nitrogen since a small fluctuation in the level was observed to produce some significant change in the equilibrium pressure. In view of the long period of time that was required to perform the nitrogen

desorption experiment, perhaps the most serious error could have resulted from small incidents of leaks in the system. Another main source of error was in the determination of the weight of degassed sample, since the sampling specimen tube used was rather long. Despite these difficulties in the execution of the desorption experiment, the method produced satisfactory and fairly reproducible pore size distributions of leached asbestos materials.

3.2.9 Adsorption of Water and n-hexane

Adsorption capacities of leached asbestos materials were determined by a vapor sorption apparatus (72). Adsorption properties are important since adsorption data obtained with various vapors may give useful information about structure-related factors such as pore channel dimensions, total pore volume and adsorption affinities with respect to various adsorbates.

Traditionally, water adsorbate has been used to determine the adsorption capacity of a porous solid. However, the recently synthesized silica-rich ZSM zeolites and other related materials show water adsorption capacities substantially lower than those of classical zeolites. In addition, the new ZSM type zeolites show a strong hydrophobic character and a higher affinity for some hydrocarbons such as n-hexane and cyclohexane.

Therefore, water is not a good absorptive medium for these materials with so highly hydrophobic surfaces that a repulsion of water molecules from the hydrophobic silica surfaces occurs. Several people including Le Van Mao (72,73) have demonstrated that the volume of n-hexane adsorbed by silica-rich zeolites in comparison to the volume of water adsorbed is very high. Relative affinity index is a very important term derived for the evaluation of the hydrophobic character of inorganic materials (72,73). The relative affinity index (RAI) is defined as the volume ratio of adsorbed n-hexane to adsorbed water, and gives the degree of hydrophobicity of an inorganic material.

3.2.9.1 Experimental apparatus

The experimental set-up consisted of two parts: a chamber for evacuation at high temperatures and a vapour adsorption system (Fig. 3.10). The adsorption system included an adsorption chamber (A) and a vaporization flask (B). A variety of thermostatic baths allowed A and B to be maintained at the desired temperature (25, 23 or 0 °C).

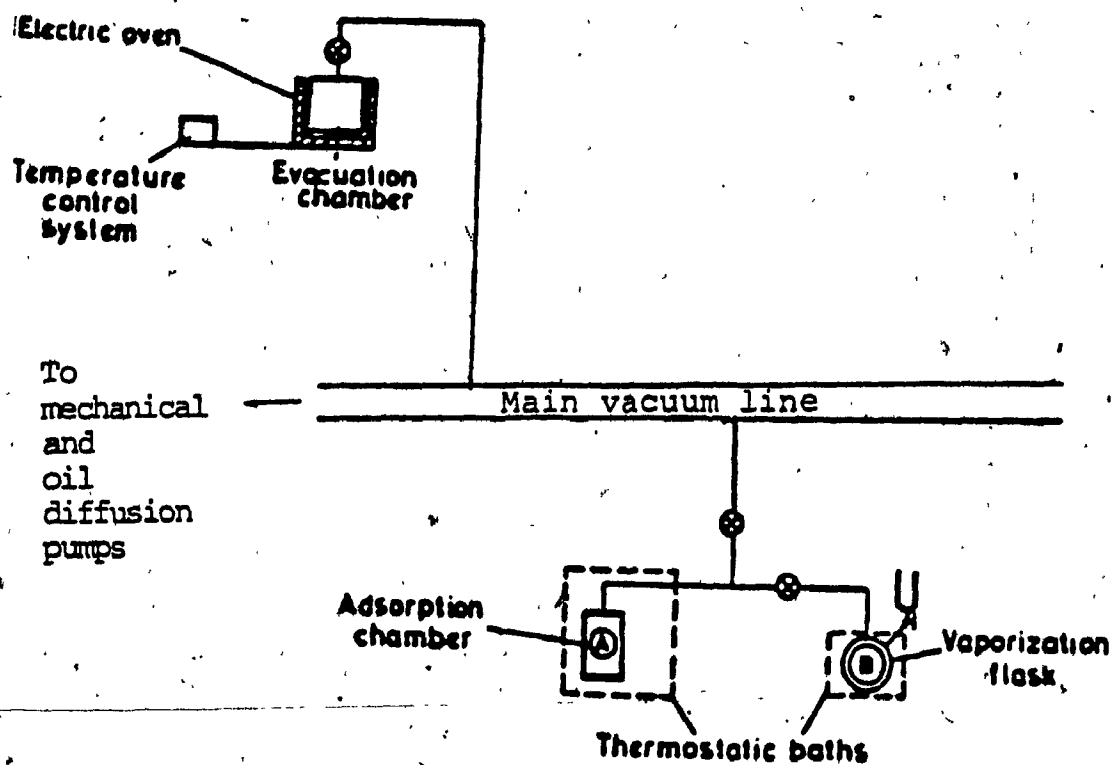


Figure 3.10: Vapor adsorption-vaporization apparatus.

3.2.9.2 Experimental procedure

The adopted gravimetric method has been described by Le Van Mao et al. (72,73). The adsorbates used were water and n-hexane. The evacuated sampling tubes were accurately weighed, then filled with sample specimen (ca. 300 mg). The sampling tubes were then placed into a pyrex chamber and evacuated to 10^{-3} Torr at 300 °C for 3 hours. The cooled specimen tubes were weighed again and placed rapidly into A, where a vacuum of about 10^{-2} Torr was created; the same evacuation procedure was repeated for part B (Figure 3.10). A and B being isolated, they were then placed in the respective thermostatic baths, 15 ml of the liquid was poured into reservoir B. At a temperature of 23 °C (in case of water) or 0 °C (in case of n-hexane), a well-defined vapor pressure was developed (22 Torr with water, 45 Torr with n-hexane). Then, A and B were connected to permit the vapor to expand into zone A. The evacuated samples were then brought into contact with water or n-hexane vapor until an equilibrium was established. The sampling tubes were weighed and the equilibrium adsorption capacity was calculated. The operating conditions are reported in Table 3.1. From the sorption data, it was possible to calculate the affinities of the Alix materials toward organic n-hexane vapor in comparison to water and obtain their relative index values.

TABLE 3.1: Operating conditions for n-hexane and water adsorption of Alix samples.

Adsorbate	Critical diameter (Å)	Vaporization temperature (°C)	Vapor pressure (Torr)	Adsorption temperature (°C)	Time required
n-hexane	4.9	0	45	25	4 hrs
water	2.8	23	22	25	overnight

3.2.2.10 Density measurements

Density measurements were carried out at room temperature by displacement in carbon tetrachloride (Archimedian method). The polycrystalline samples were evacuated on a high vacuum line prior to wetting, and immersed in CCl_4 while still under vacuum, in order to avoid trapping air bubbles between the particles. The density measurements were performed by Vaillancourt (50).

4 RESULTS AND DISCUSSIONS

4.1 Reactivity and Leaching of Chrysotile with Strong Mineral Acids

The acidic attack of chrysotile asbestos was carried out under conditions of variable acid concentration, temperature and/or reaction time, but always keeping the ratio of acid solution to chrysotile equal to 10. Under such conditions of excess acid, the decomposition of chrysotile was found to be strongly dependent on the three intrinsic leaching parameters, namely: acid normality, temperature of solution and duration of leaching. Decomposition of the chrysotile was determined by analysis for magnesium which had gone into the acid solution and called magnesium leaching degree (MLD). Although free brucite and other asbestos impurities could also be solubilized by the acidic reagent, the MLD was essentially related to the magnesium component "chemically" linked to the silicon, or the one "sandwiched" between two "silicon-linked" magnesium atoms.

Tables 4.1-4.5 summarized the conditions used in the leaching process and the results that were obtained. In the presence of a strong mineral acid, such as HCl or H₂SO₄, the leaching process was strongly dependent on the acid normality (Figures 4.1 and 4.2), the time (Figures 4.3, 4.4 and 4.5) and the temperature (Figures 4.1, 4.2, 4.3 and 4.5). However, the nature of the strong mineral acid did not seem to significantly affect the leaching

results (Figures 4.1 and 4.4). This is not surprising as these acids are fully dissociated, therefore, for equal normality, they provide the same amounts of H^+ ions which are the active species, the counter ions being probably fairly inactive. Generally, the MLD increased with the increasing acid normality, temperature and time. The leaching of chrysotile with a strong mineral acid under severe conditions such as high temperature, acid normality and/or for several hours of leaching was found to solubilize almost all the magnesium and non-magnetic iron metallic components, leaving behind a collapsed macrostructure that had chemical composition close to silica gel.

In the continuous leaching of chrysotile there was an initial high release of Mg^{2+} ions, which subsequently reduced to a steady rate after several hours. Referring to Figures 4.3, 4.4, 4.5 and 4.6, the early stages of the acid attack on the chrysotile fibers indicate an extremely rapid reaction, probably due to the removal of the outermost magnesium hydroxide layer and all the other structural magnesium hydroxyls. The very rapid initial reaction of the surface hydroxyls was observed in the X-ray powder diffraction (Figure 4.10) and the IR spectra (Figure 4.12) of the leached asbestos materials. The Figures 4.1, 4.2, 4.3 and 4.4 show that even under very mild conditions such as low to medium acid normality or a few hours of leaching

TABLE 4.1: Effects of HCl concentration on the leaching of chrysotile asbestos.*
 *:Weight of asbestos:100g, volume of the HCl solution:1,000 ml, and leaching time: 4 hours.

Characteristics of the leaching acid solution		ALIX	Weight of ALIX (g)	Chemical composition of the ALIX (wt%, on dried basis)					
Normality N	Temp. (°C)			SiO ₂	Al ₂ O ₃	Na ₂ O	Fe ₂ O ₃	MgO	MLD
0.5	80	076	84.5	48.16	0.10	0.15	8.34	43.25	14.0
1.0	80	077	71.5	54.87	0.23	0.13	7.98	36.79	26.7
1.5	80	067	54.3	68.95	0.12	0.08	8.27	22.58	55.0
1.8	80	068	50.0	81.57	0.12	0.11	6.75	9.86	80.3
2.0	80	078	46.0	83.03	0.24	0.11	5.30	11.32	77.2
2.4	80	061	42.0	91.83	0.25	0.08	3.63	4.21	91.6
3.0	80	072	40.0	95.36	0.29	0.10	1.63	2.62	94.8
4.0	80	073	40.0	97.39	0.31	0.10	0.34	1.86	96.3
5.0	80	074	39.2	97.25	0.60	0.09	0.64	1.42	97.2
6.0	80	075	38.5	98.12	0.50	0.06	0.27	1.05	97.9
1.0	50	093	72.0	54.61	0.14	0.13	8.17	36.95	26.4
2.0	50	094	50.0	79.46	0.20	0.11	4.41	15.82	68.5
2.4	50	095	48.0	82.54	0.10	0.14	4.28	12.94	74.2
3.0	50	096	42.0	92.53	0.25	0.21	5.70	7.90	84.3
4.0	50	097	40.0	89.37	0.29	0.17	2.63	7.54	85.0
5.0	50	098	40.0	92.56	0.31	0.12	0.63	6.38	87.3
6.0	50	099	39.1	94.09	0.35	0.14	0.41	5.83	88.4

TABLE 4.2: Effects of H_2SO_4 concentration on the leaching of chrysotile asbestos. (*)

(*): weight of asbestos : 25 g, Volume of the H_2SO_4 solution:

250 ml, leaching time : 4 hours at 80 °C.

Normality N	ALIX	Weight (g)	Chemical composition of the ALIX (wt %)					
			SiO ₂	Al ₂ O ₃	Na ₂ O	Fe ₂ O ₃	MgO	MLD
0.5	112	20.4	59.80	0.37	0.13	8.39	31.31	37.6
1.0	113	18.0	60.78	0.38	0.15	6.84	31.85	36.6
1.5	114	13.5	74.65	0.41	0.18	4.79	19.97	60.2
2.0	115	12.5	79.06	0.39	0.14	4.51	15.90	68.3
2.5	116	11.5	91.74	0.45	0.15	1.87	5.79	88.5
3.0	117	11.0	95.30	0.50	0.12	2.09	1.99	96.0
4.0	118	10.5	97.82	0.37	0.16	0.91	0.74	98.5
5.0	119	10.0	97.79	0.41	0.15	0.92	0.73	98.6
6.0	120	11.0	97.94	0.43	0.17	0.74	0.72	98.6

TABLE 4.3: Effects of HCl concentration on the leaching of chrysotile asbestos at ambient temperature. (*)

(*): weight of asbestos : 50 g, volume of the HCl solution : 500 ml, leaching time : 2 weeks.

Normality N	ALIX	Weight (g)	Chemical composition of the ALIX (wt %)					
			SiO ₂	Al ₂ O ₃	Na ₂ O	Fe ₂ O ₃	MgO	MLD
0.5	107	38.1	56.24	0.32	0.09	7.78	35.57	29.1
1.0	078	40.3	63.86	0.44	0.16	7.68	28.88	42.5
1.5	108	30.1	74.60	0.43	0.20	7.15	17.02	66.1
2.0	079	28.2	73.07	0.48	0.09	6.68	18.68	62.8
2.4	109	23.0	90.05	0.41	0.11	5.35	4.08	91.9
3.0	081	21.0	90.00	0.41	0.10	4.79	2.71	94.6
4.0	082	20.0	97.32	0.43	0.18	0.71	1.36	97.3
5.0	110	19.1	97.97	0.39	0.12	0.27	1.25	97.5
6.0	111	18.5	98.25	0.39	0.16	0.00	1.20	97.6

TABLE 4.4: Effects of time of operation on the leaching of chrysotile asbestos.*
 *: Weight of asbestos: 100g; volume of the HCl solution: 1,000 ml, and concentrations of the HCl solution: 2.4N.

Leaching time (Hours)	Temp. of Solution (°C)	ALIX	Weight of ALIX (g)	Chemical composition of the ALIX (wt%, on dried basis)					
				SiO ₂	Al ₂ O ₃	Na ₂ O	Fe ₂ O ₃	MgO	MLD
0.5	80	086	51.6	77.02	0.57	0.10	7.57	14.74	70.6
1.0	80	087	49.0	80.19	0.36	0.12	7.11	11.76	76.6
1.5	80	088	44.0	83.35	0.35	0.15	6.55	9.60	80.9
2.0	80	063	43.0	87.93	0.50	0.10	4.04	7.43	85.2
2.5	80	089	42.5	88.73	0.43	0.18	4.22	3.61	92.8
3.0	80	090	42.5	90.97	0.54	0.12	4.84	3.53	93.0
4.0	80	061	42.0	91.83	0.25	0.08	3.63	4.21	91.6
4.5	80	060	42.0	93.69	0.32	0.11	1.89	3.99	92.1
5.0	80	062	41.5	94.57	0.42	0.09	1.38	3.54	93.0
6.0	80	091	41.0	93.91	0.61	0.08	2.97	2.43	95.2
7.0	80	092	39.5	95.33	0.20	0.09	2.23	2.15	95.7
1.0	50	100	62.0	67.39	0.29	0.13	5.33	26.86	46.5
2.0	50	101	52.0	78.09	0.21	0.12	5.79	15.79	68.6
3.0	50	102	48.0	84.51	0.51	0.15	4.77	13.45	73.2
4.0	50	095	48.0	84.99	0.10	0.14	4.28	10.49	79.1
5.0	50	103	46.0	87.13	0.14	0.18	4.07	8.48	83.1
6.0	50	104	44.5	89.69	0.16	0.11	4.12	5.92	88.2
7.0	50	105	40.8	90.37	0.20	0.09	3.51	5.83	91.8

TABLE 4.5 Effects of time on the leaching of chrysotile asbestos.*
 *:Weight of asbestos:50 g, volume of the H₂SO₄:500 ml,
 concentration of the H₂SO₄ solution:2.4 N and temperature of
 the solution: 80 °C.

Leaching time (Hours)	ALIX	Weight of ALIX (g)	Chemical composition of the ALIX (Wt%, on dried basis)					
			SiO ₂	Al ₂ O ₃	Na ₂ O	Fe ₂ O ₃	MgO	MLD
0.5	138	27.2	79.34	0.26	0.10	6.42	13.88	72.4
1.0	139	26.3	80.37	0.29	0.10	5.81	13.43	73.3
1.5	140	25.5	82.18	0.31	0.13	6.15	11.23	77.6
2.0	141	25.1	84.75	0.29	0.11	5.75	9.10	81.8
2.5	142	22.9	88.43	0.36	0.10	3.70	7.41	85.2
3.0	143	22.8	88.39	0.37	0.12	3.88	7.24	85.6
3.5	144	22.6	88.35	0.36	0.11	4.75	6.43	87.2
4.0	145	21.9	88.44	0.41	0.12	4.64	6.39	87.3
5.0	146	20.8	90.78	0.39	0.12	4.32	4.39	91.3
6.0	147	19.9	91.49	0.43	0.13	3.39	4.56	90.9
7.0	148	19.6	92.74	0.45	0.10	3.11	3.60	92.8

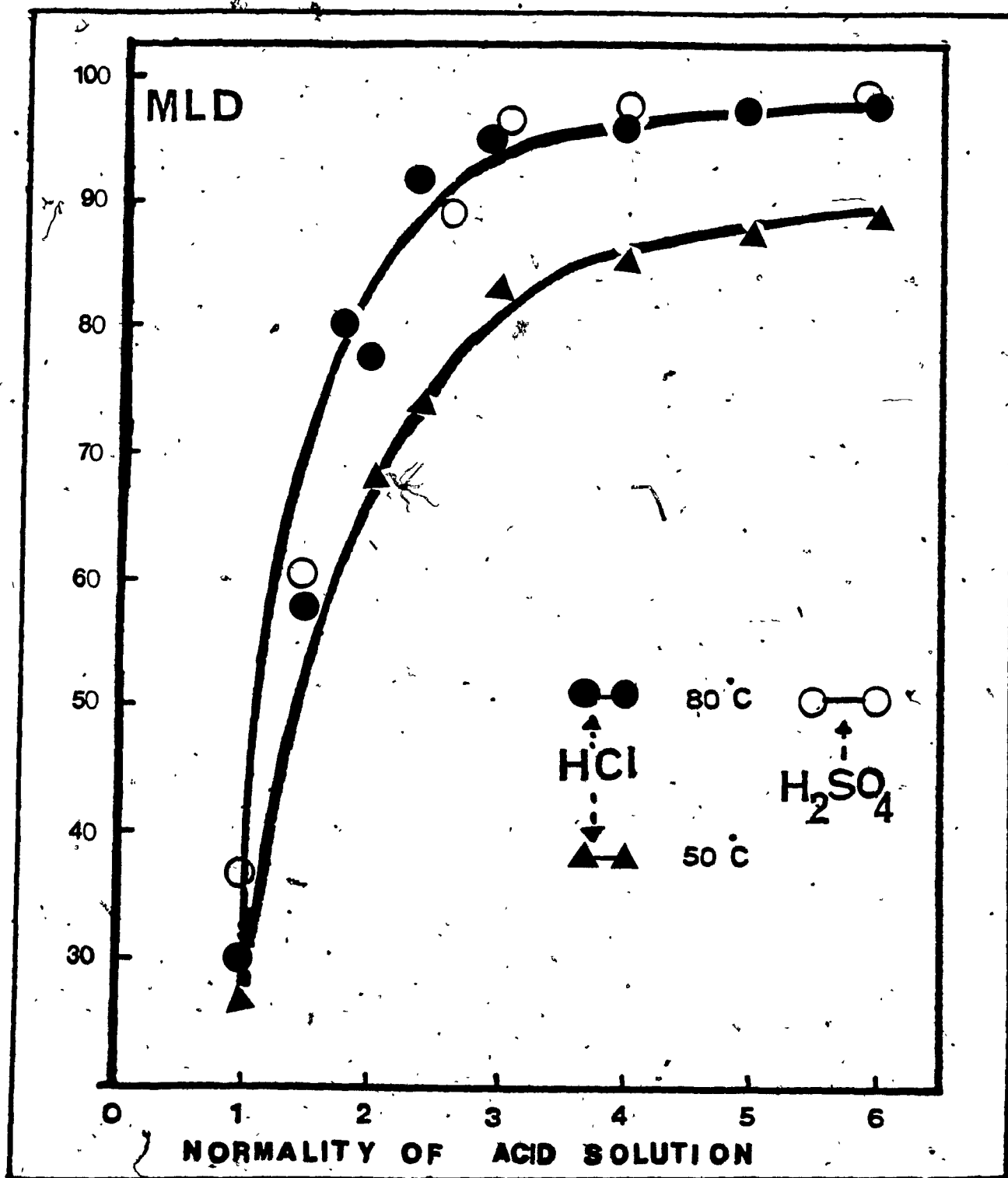


Figure 4.1: Effects of the normality of the mineral acid at 50°C and 80°C on the MLD.

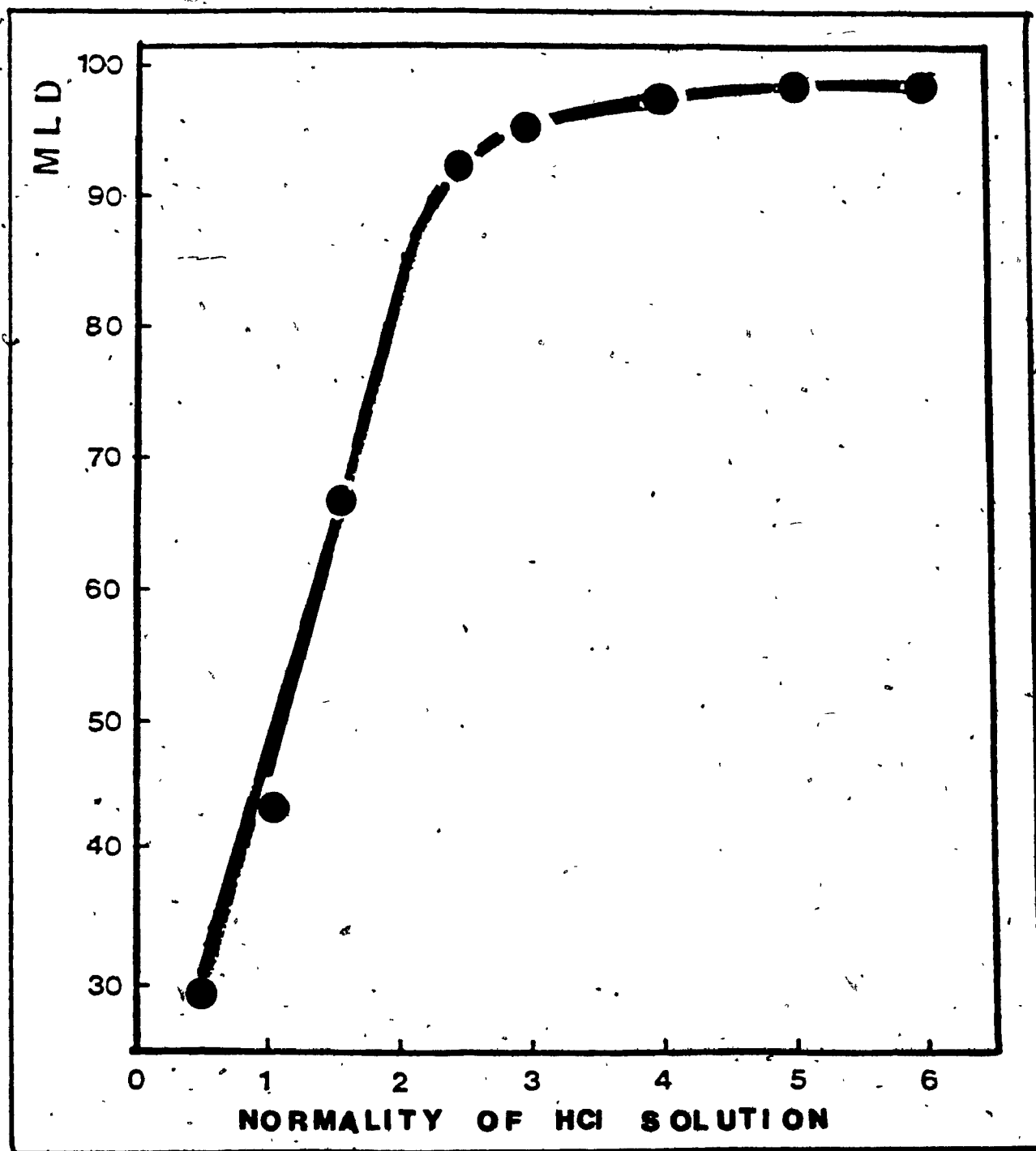


Figure 4.2: Effects of the normality of HCl solution at ambient temperature on the MLD.

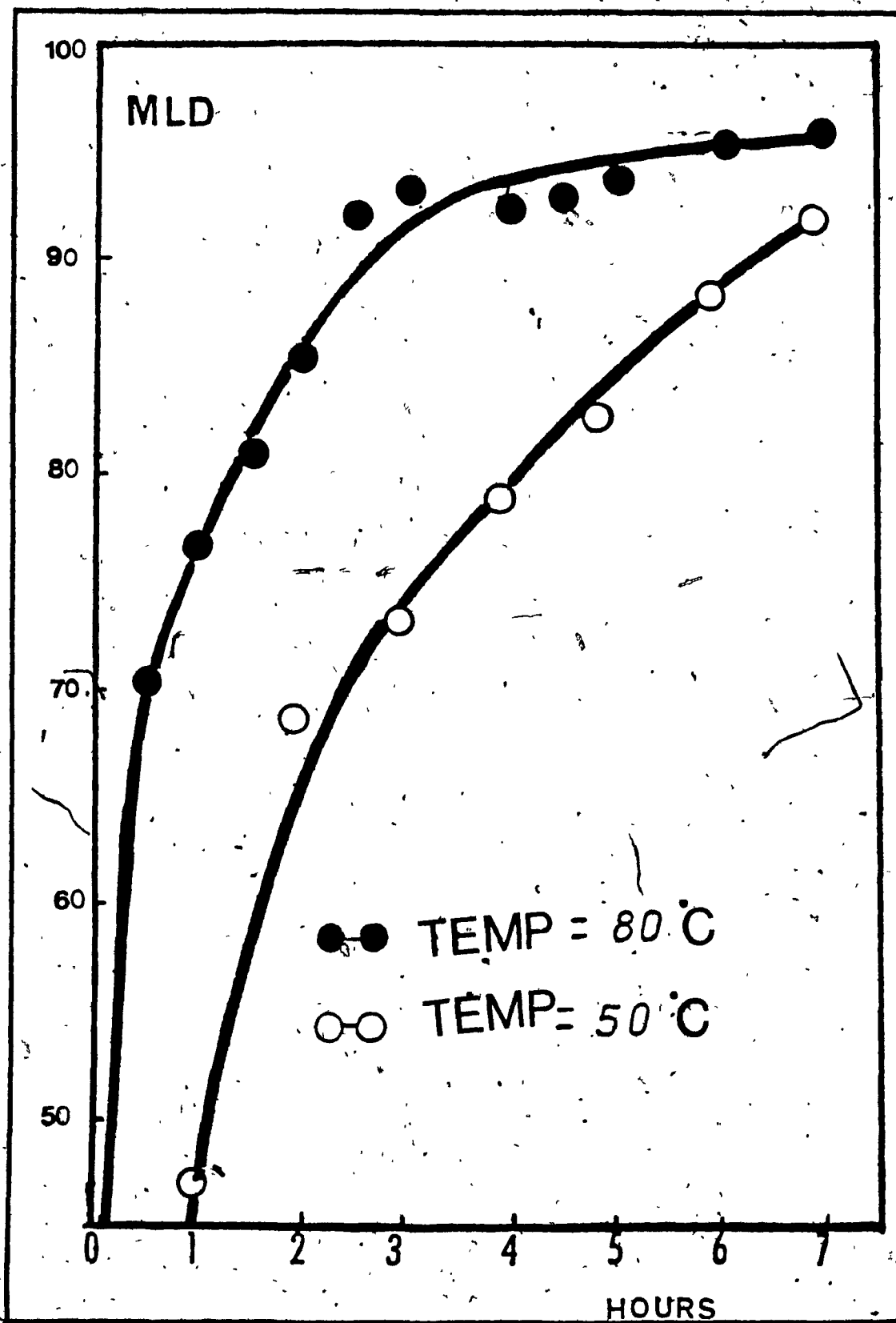


Figure 4.3: Effects of the leaching time of HCl solution at 50°C and 80°C on the MLD.

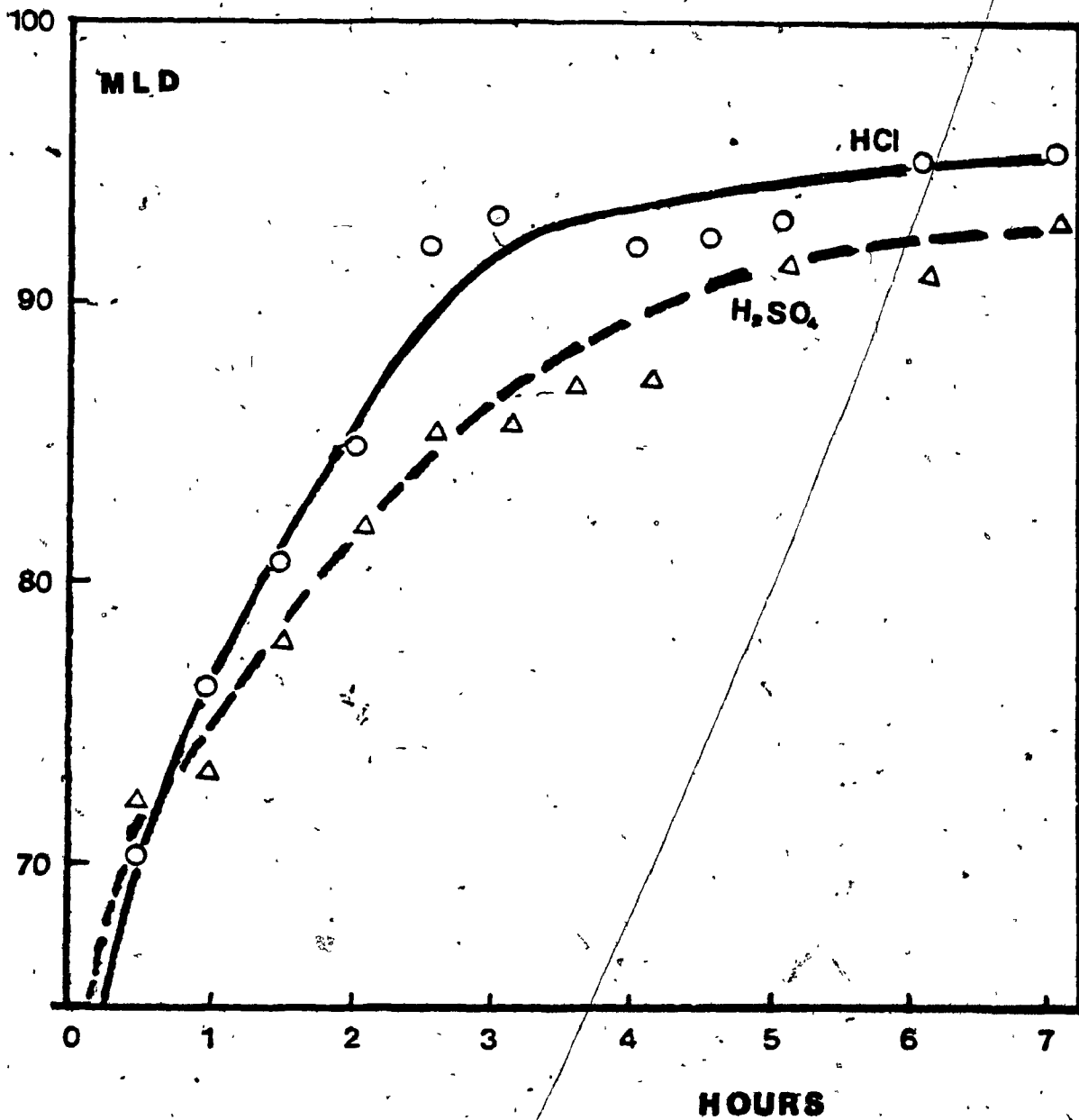


Figure 4.4: Effects of the leaching time of H_2SO_4 solution at $80^\circ C$ on the MLD.

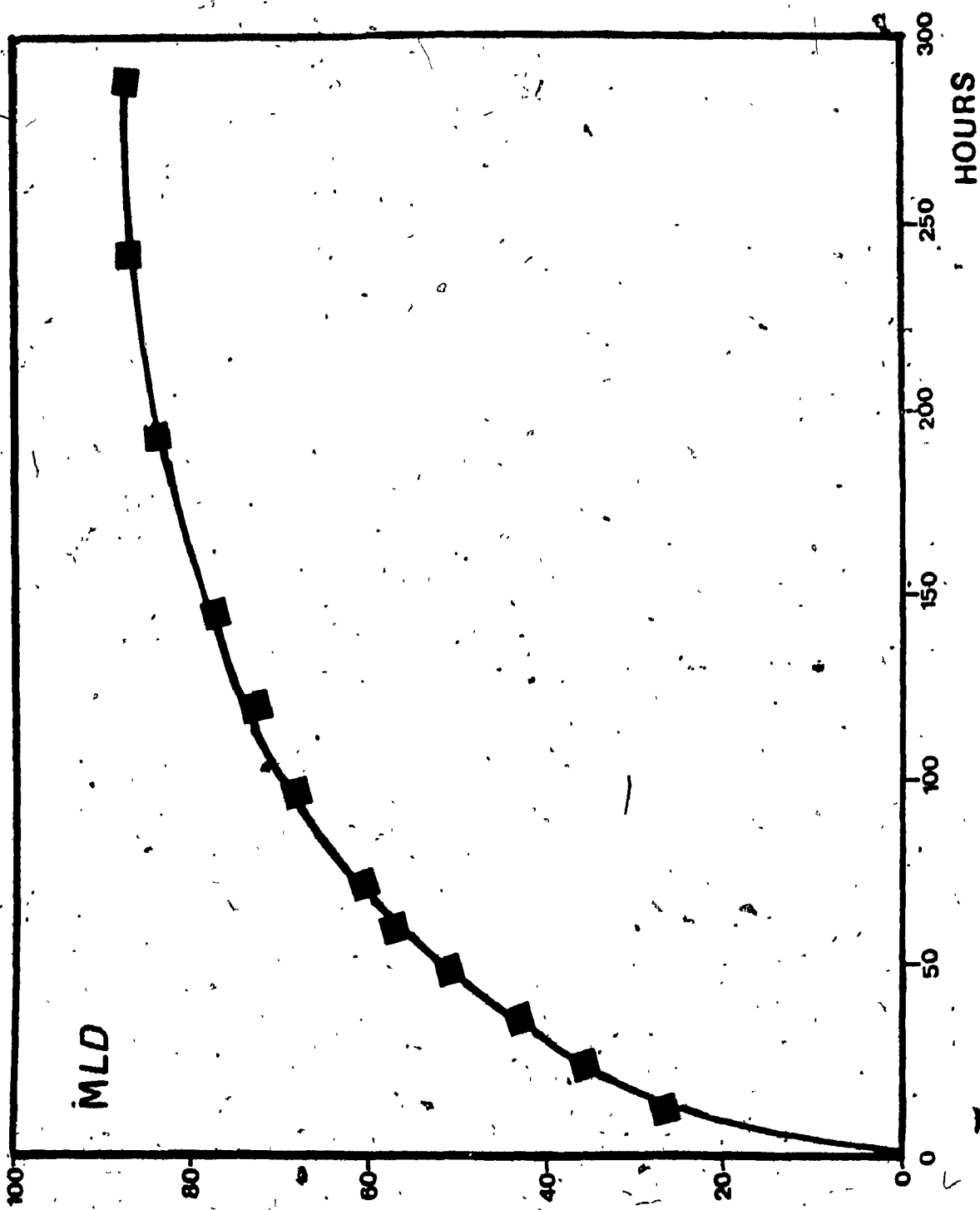


Figure 4.5: Effects of the leaching time of HCL solution at ambient temperature on the MLD.^a

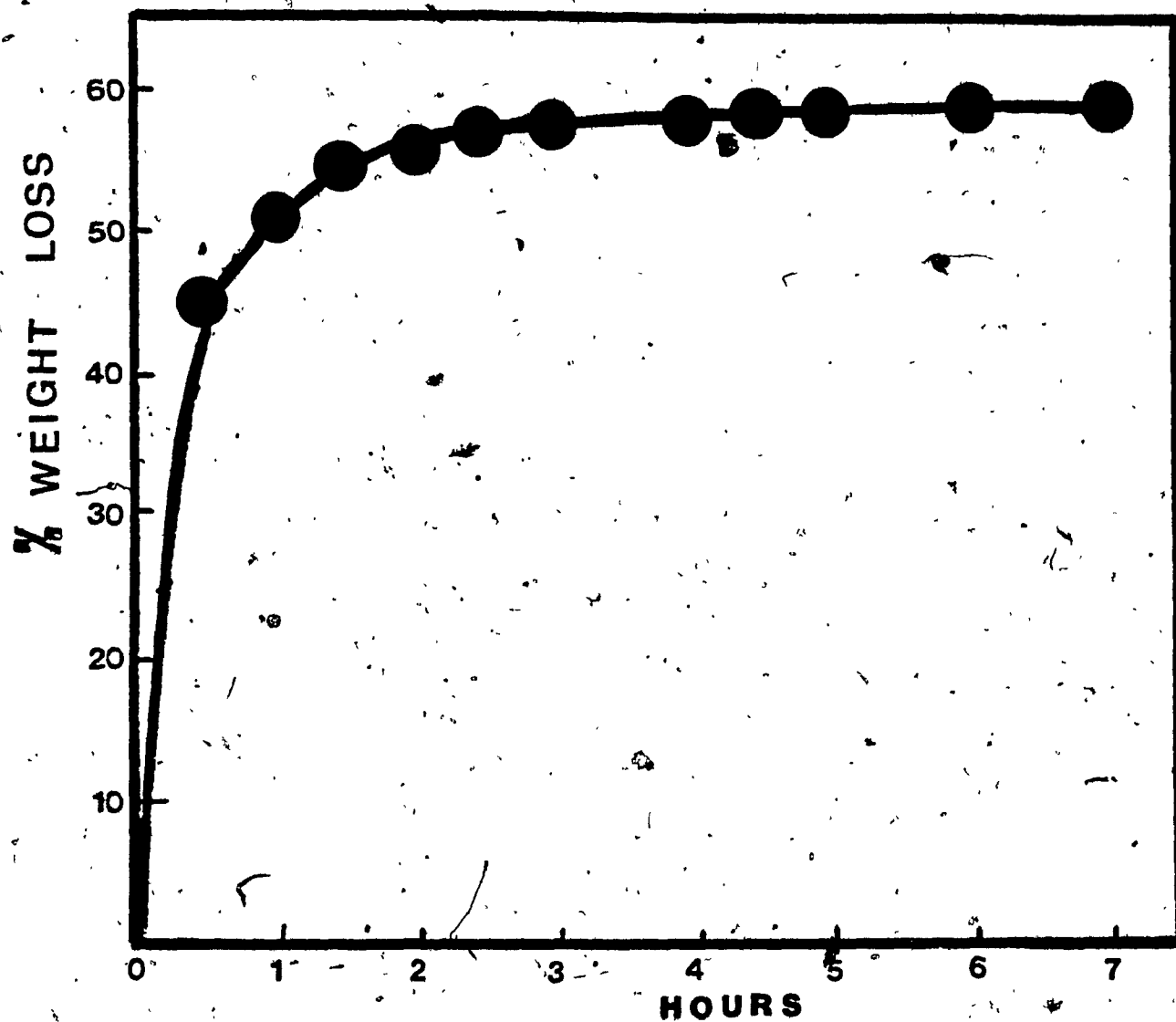


Figure 4.6: Weight loss of chrysotile in HCl solution
vs time.

with an acid concentration of 2.4 N, a strong mineral acid easily removes 60-70% of the Mg^{2+} ions. As the residual magnesium atoms in the chrysotile decreases, it gradually becomes more difficult for these atoms to be leached out and more severe conditions have to be used.

The decomposition of chrysotile is probably diffusion controlled. This conclusion is justifiable because dissolution of the magnesium from the chrysotile structure leaves a residue of silica layer through which both the acid and magnesium ions must diffuse for the decomposition to continue.

The very rapid initial reaction of the surface hydroxyls was also noted by Pundsack et al. (74,75) during a stepwise titration of chrysotile with 0.5 N hydrochloric acid at 100 °C. The titration curve which consists of two parts indicates that all magnesium ions are not identical. According to Pundsack et al., the first part of the curve, indicating extremely rapid decomposition of chrysotile, is related to the reaction with the OH groups, and the second part would correspond to the hydration of silica belonging to the structure of the chrysotile. This is also easily understood if the chrysotile asbestos structure is taken into consideration. Chrysotile, $Mg_3Si_2O_5(OH)_4$, could therefore be considered as a result of two distinct chemical entities, namely $2 Mg(OH)_2$ and $MgSi_2O_5$. In this way, it is possible to explain the results of the

dissolution of magnesium under strongly acidic conditions. The first two-thirds of magnesium are easily leachable, whereas the last third should behave as in a sheet silicate, undergoing dissociation from the structure with more difficulty.

The most surprising result obtained was that for chrysotile fibers suspended in acidic media for two weeks at room temperature. Tables 4.1, 4.2 and 4.3 show that the results obtained at ambient conditions were similar to those performed at 80 °C. The corresponding curves, when MLD was plotted against acid normality, as shown in Figures 4.1 and 4.2, respectively, are also identical. Thus 14 days of leaching chrysotile fibers at room temperature had essentially the same effect as the 4-hour 80 °C refluxing exposure. Figure 4.5 also gives MLD as a function of leaching time at room temperature; the acid concentration was kept constant and was similar to that used in Figures 4.3 and 4.4. The leaching process of chrysotile at ambient conditions is economically very attractive, particularly in an industrial situation, since expensive heating costs are eliminated and the process becomes considerably cheaper. The leaching out of iron atoms from the fiber was similar to magnesium removal (MLD), obeying similar intrinsic leaching parameters. Consequently, in the presence of a strong mineral acid, the iron content of the starting chrysotile asbestos fibers

decreased gradually with increasing acid normality, contact time and temperature of reaction solution. However, the presence of Fe_3O_4 (magnetite), which is basically insoluble in a dilute acid medium, has ruled out the iron component as a parameter for determining the extent of the leaching process.

Figure 4.6 shows that the decomposition of chrysotile can also be followed by determining the weight loss of the chrysotile after an acid treatment. After an initial rapid weight loss (Figure 4.6), the rate of attack decreased radically and in the later stages of the reaction, the rate of weight loss became steady and the curve levels off at about 60%.

4.2 Secondary Leaching of Chrysotile with Weak Organic Acids

Chrysotile possesses such a low resistance to acids that it may be decomposed by a weak organic acid such as concentrated acetic acid. Badollet (4,5) on refluxing chrysotile in 25% acetic acid medium obtained 23% loss in weight due to the dissolution of some magnesium ions.

Since the use of strong mineral acids does not allow a fine tailoring of the MLD of the final product, a two-step leaching process has been adopted. It consists of leaching the parent chrysotile asbestos with a mineral acid under very mild conditions in order to obtain a medium MLD value

of around 50-60% and then refining the leaching with an organic weak acid in order to better control the magnesium removal process. The weak acids used in the secondary leaching process were acetic acid (ACA), oxalic acid (OXA), and ethylenediamine tetraacetic acid (EDTA). The secondary leaching with an organic acid involved three main parameters, which were: acid normality, pH and time of operation (the temperature of the leaching solution was kept constant). The leaching conditions employed and the results obtained are given in Tables 4.6 and 4.7. Figures 4.7 and 4.8 report the MLD values of the Alix obtained in the secondary leaching with ACA, OXA and EDTA versus the acid normality and pH, respectively. Figure 4.9 also reports the MLD values of the Alix obtained in the two-step leaching with ACA and OXA versus the time of operation. As expected, the organic acids being weaker than the mineral acids exhibited moderate leaching effects in the following order of strength:

oxalic acid > acetic acid >> EDTA.

In the presence of a weak organic acid, such as ACA, OXA or EDTA, the MLD and hence the leaching process was dependent on the acid normality (Figure 4.7), the pH (Figure 4.8) and the time (Figure 4.9). Thus OXA, being the strongest acid, as shown by the pH values in Table 4.6, exhibited the best leaching effects, whereas the weakest

TABLE 4.6: Second leaching step with an organic acid. (*)

(*) : Volume of the acid solution : 100 ml, weight of the starting material: 10 g of ALIX with MLD=56.8% in the case of (a) and MLD : 55.0% in the case of (b), leaching time : 4 hours at 80 °C.

Nature of the acid	Characteristics of the acid solution		Chemical composition of final ALIX (wt %)					
	Normality N.	pH	SiO ₂	Al ₂ O ₃	Na ₂ O	Fe ₂ O ₃	MgO	MLD
Acetic acid (a)	0.5	2.65	78.01	0.39	0.11	5.01	16.47	67.2
	1.0	2.50	78.68	0.50	0.15	5.97	14.70	70.7
	2.0	2.25	80.47	0.50	0.20	5.99	12.84	74.4
	3.0	2.00	81.22	0.47	0.17	5.98	12.16	75.8
	4.0	1.95	81.56	0.41	0.16	5.52	12.35	75.4
	5.0	1.90	84.69	0.43	0.12	3.63	11.13	77.8
Oxalic acid (a)	0.5	1.40	79.78	0.41	0.15	2.64	17.02	66.1
	1.0	1.25	82.87	0.39	0.16	2.08	14.50	71.1
	2.0	1.10	83.97	0.42	0.15	1.90	13.56	73.0
	3.0	1.00	86.40	0.42	0.16	1.59	11.43	77.2
	4.0	0.70	87.43	0.41	0.19	1.51	10.46	79.2
	5.0	0.60	86.91	0.38	0.14	2.28	10.29	79.5
EDTA (b)	1.0	2.70	78.80	0.17	0.28	0.92	19.81	60.5
	2.0	2.60	80.02	0.22	0.38	0.67	18.71	62.7
	3.0	2.35	82.73	0.31	0.39	0.80	15.77	68.6
	4.0	2.30	85.03	0.26	0.41	0.56	13.74	72.6
	5.0	2.30	85.74	0.23	0.44	0.69	12.90	74.3
HCl	2.4 (0.5hr)	-	70.96	0.32	0.17	6.85	21.70	56.8(a)
	1.5 (4.0hrs)	-	69.69	0.15	0.10	7.48	22.58	55.0(b)

TABLE 4.7: Effects of time on the second leaching step with an organic acid.*
 *: Volume of the acid solution: 100 ml, weight of the starting material: 10 g
 of ALIX with MLD = 70.6 (see (a) below), concentration of organic acid: 3.5N
 and temperature of solution: 80 °C.

Nature of the acid	Leaching time (Hours)	Chemical composition of the ALIX (Wt%, on dried basis)					
		SiO ₂	Al ₂ O ₃	Na ₂ O	Fe ₂ O ₃	MgO	MLD
Oxalic acid	1.0	87.1	0.43	0.12	2.33	10.03	80.0
	2.5	88.6	0.49	0.15	2.32	8.47	83.1
	4.0	90.3	0.51	0.14	2.34	6.69	86.7
	5.5	91.2	0.45	0.14	2.30	5.95	88.2
	7.0	91.5	0.47	0.13	2.29	5.63	88.8
Acetic acid	1.0	85.2	0.48	0.12	5.47	11.64	76.8
	2.5	85.1	0.50	0.11	4.50	9.79	80.5
	4.0	86.7	0.43	0.13	4.13	8.63	82.8
	5.5	88.0	0.42	0.12	4.47	6.99	86.1
	7.0	89.2	0.44	0.10	4.38	5.97	88.1
HCl (2.4N)	0.5	77.2	0.37	0.10	7.57	14.74	70.6 (a)

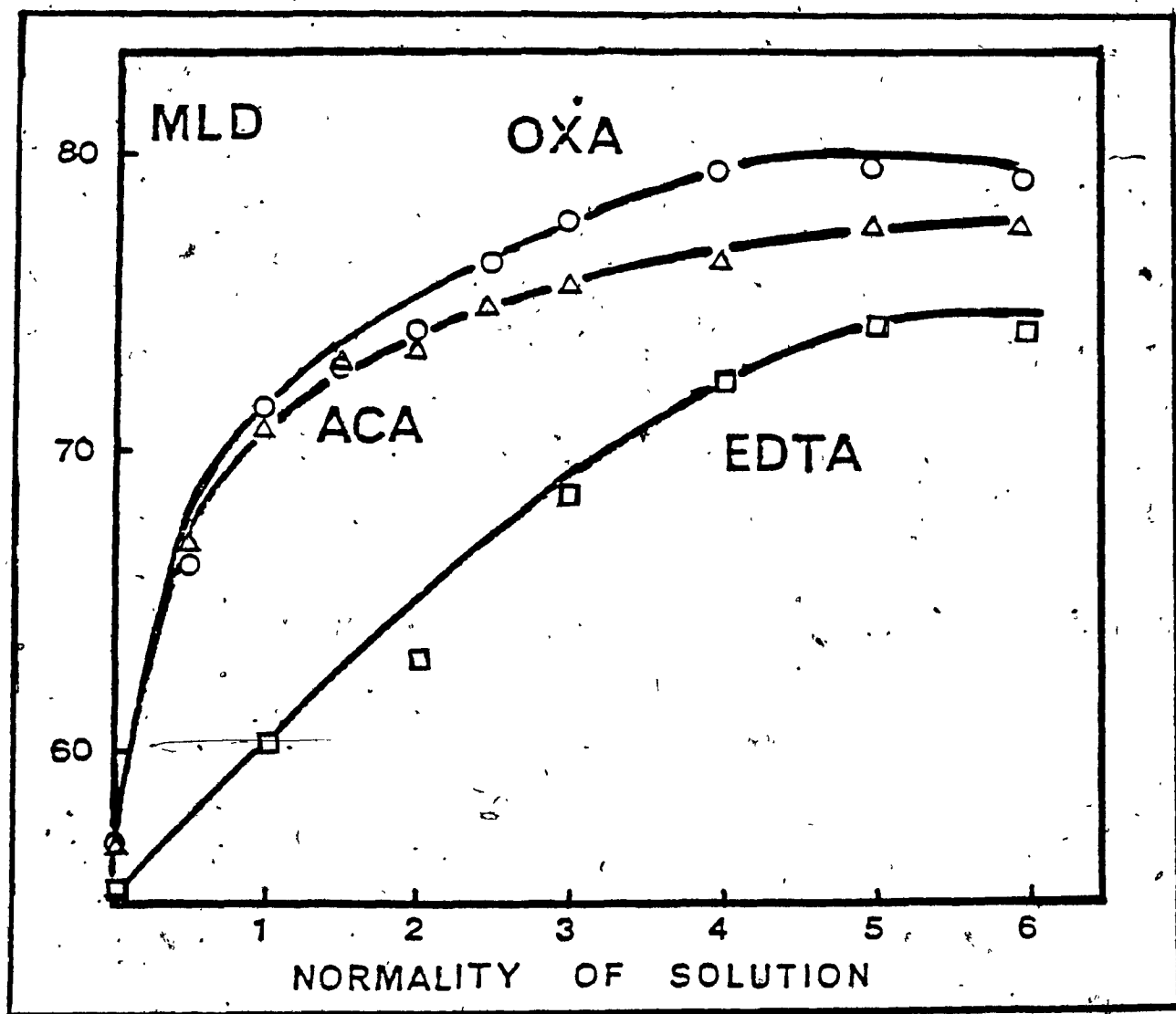


Figure 4.7: A plot of MLD of the secondary leaching of Alix with organic acids vs the normality of the acid.

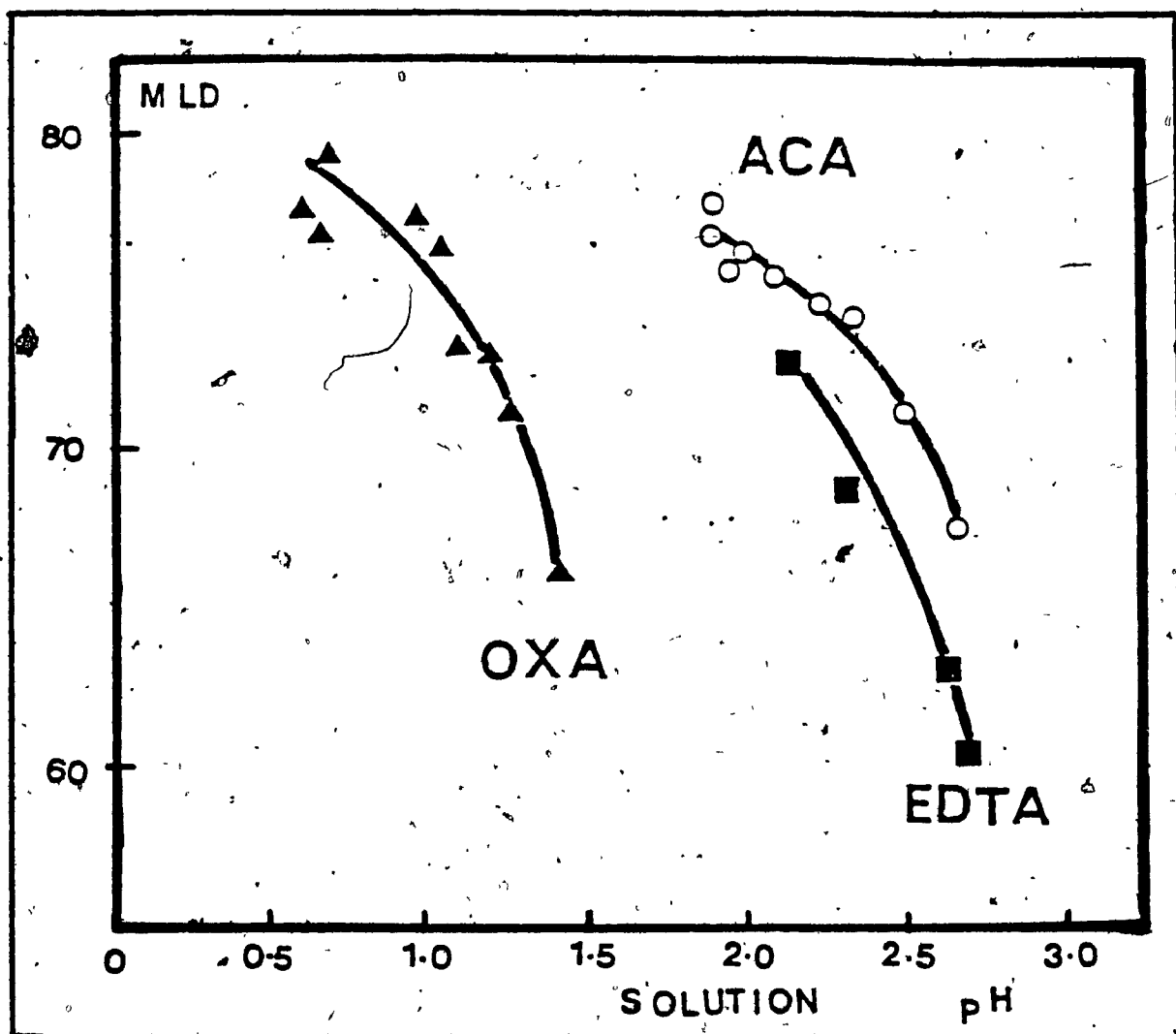


Figure 4.8: A plot of MLD of the secondary leaching of Alix with organic acids vs the pH of the acid.

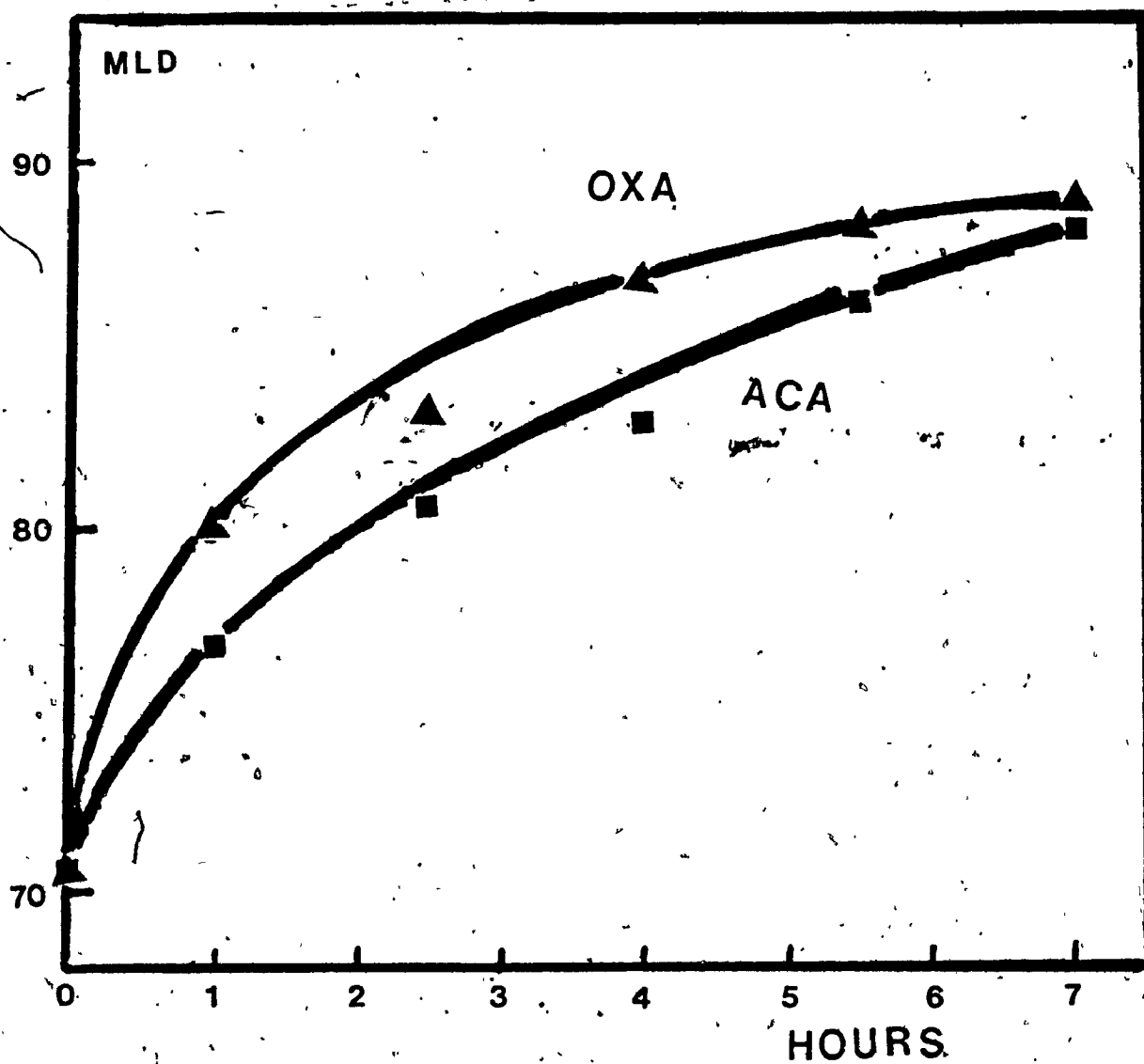


Figure 4.9: A plot of MLD of the secondary leaching of Alix with organic acids vs the leaching time.

acid, EDTA, gave the lowest MLD values for the same acid normalities.

It is important to mention that the amount of iron removed by a strong mineral acid (HCl or H_2SO_4) was very dependent on the leaching parameters such as normality, temperature and reaction time, but uncommon behaviour was observed with weak organic acids. For example, the iron content of the starting Alix samples decreased from about 7.0% to the following values: acetic acid (6.0%), oxalic acid (2.0%) and EDTA (< 1.0%), after the second step leaching (see Table 4.6). Acetic acid exhibited the least iron solubilizing effects. Oxalic acid, because of its higher acid strength, probably removed all the ferrous and ferric ions, leaving out most of the magnetite (Fe_3O_4), which is usually more difficult to be solubilized. The higher removal capacity of the iron impurities by the EDTA was due to its strong chelating properties (76). The iron content in the resulting Alix samples was constant and seemed to be less dependent on the leaching parameters, but was strongly dependent on the nature of the organic acid. Table 4.7 also shows similar pattern in the removal of iron impurity by oxalic acid and acetic acid.

The efficient removal of iron by oxalic acid and EDTA is extremely beneficial, since it is present as an undesirable impurity and can be deleterious to the performance of chrysozeolite as a catalyst when present in

appreciable amounts. The removal of most of the iron impurity by EDTA and oxalic acid yielded more homogeneous leached asbestos materials. It should be noted that one of the ultimate aims of this study was to prepare Alix samples of MLD in the range of 60-85% which could be useful in the synthesis of chrysozeolites. In this respect, the two-step leaching was extremely reproducible and accurate.

4.3 X-Ray Powder Diffraction

The X-ray powder diffraction of the leached asbestos materials was used to study the effect of a strong mineral acid on the crystalline structure of the chrysotile asbestos under different leaching conditions. This was successfully done by following the intensity of the peaks of Alix materials with increasing acid normality or the resulting MLD. In addition, the degree of crystallinity, based on the measurement of the integrated area under the (002) peak of chrysotile, was determined.

Chrysotile asbestos was identified by means of its characteristic pattern of diffraction (46,47). Figure 4.10 gives the X-ray powder patterns of chrysotile asbestos as a function of MLD:

(a). 0%, (b) 14%, (c) 27%, (d) 55%, (e) 77% and (f) 97%.

The X-ray powder pattern of the parent chrysotile asbestos is shown in Figure 4.10a. The powder diffraction pattern

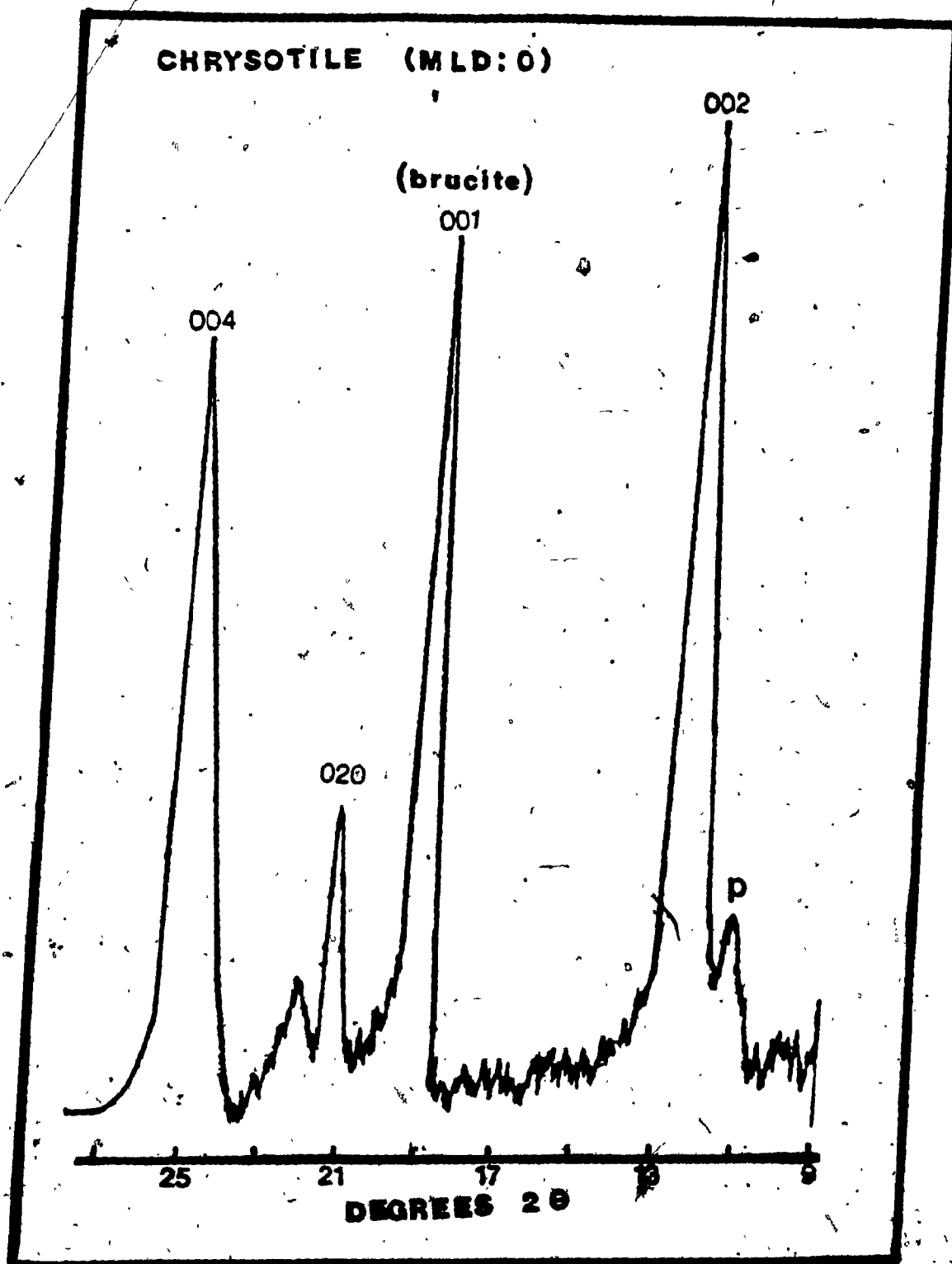


Figure 4.10a: X-ray powder pattern of parent chrysotile asbestos.

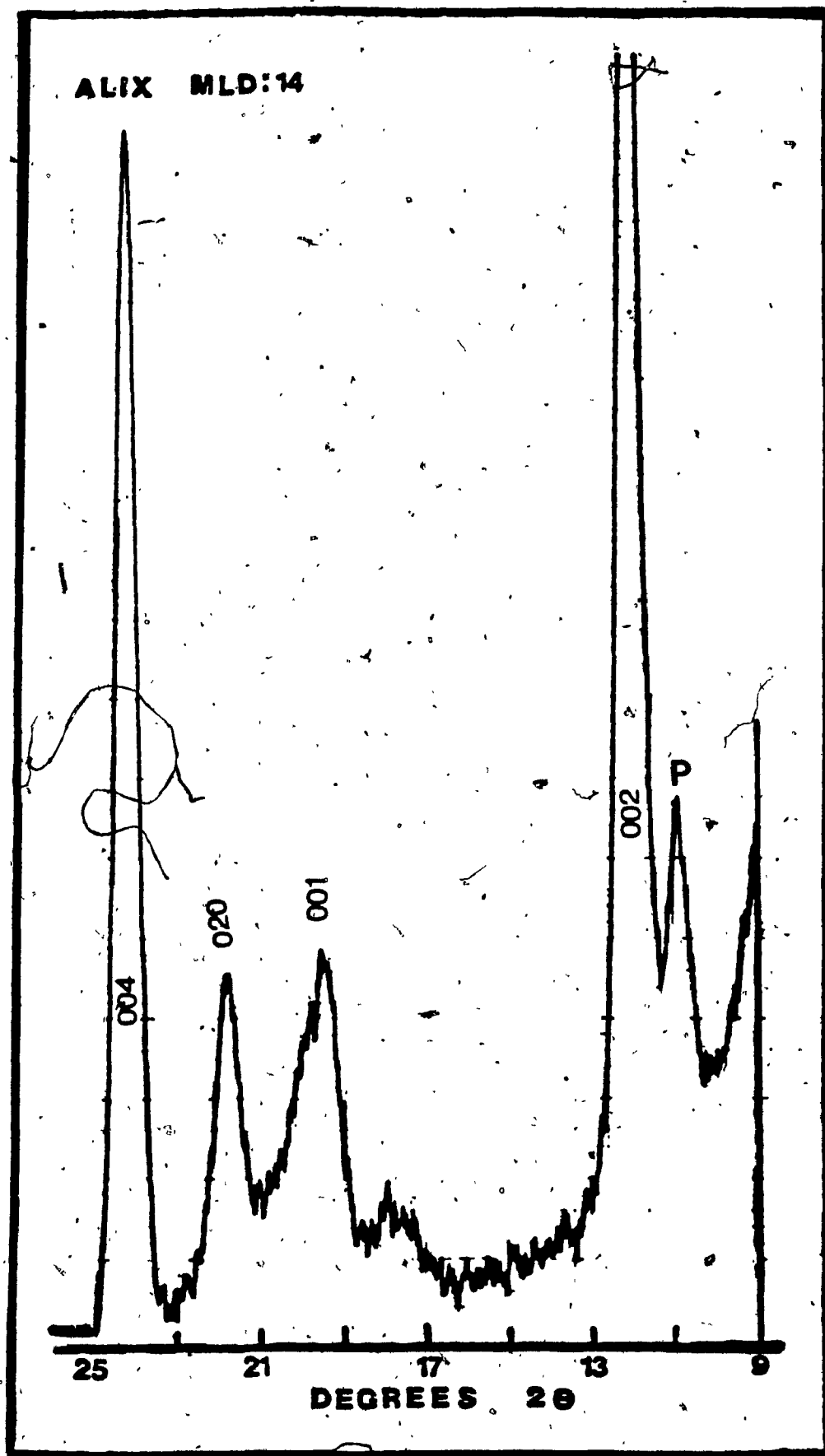


Figure 4.10b: X-ray powder pattern of Alix MLD = 14%.

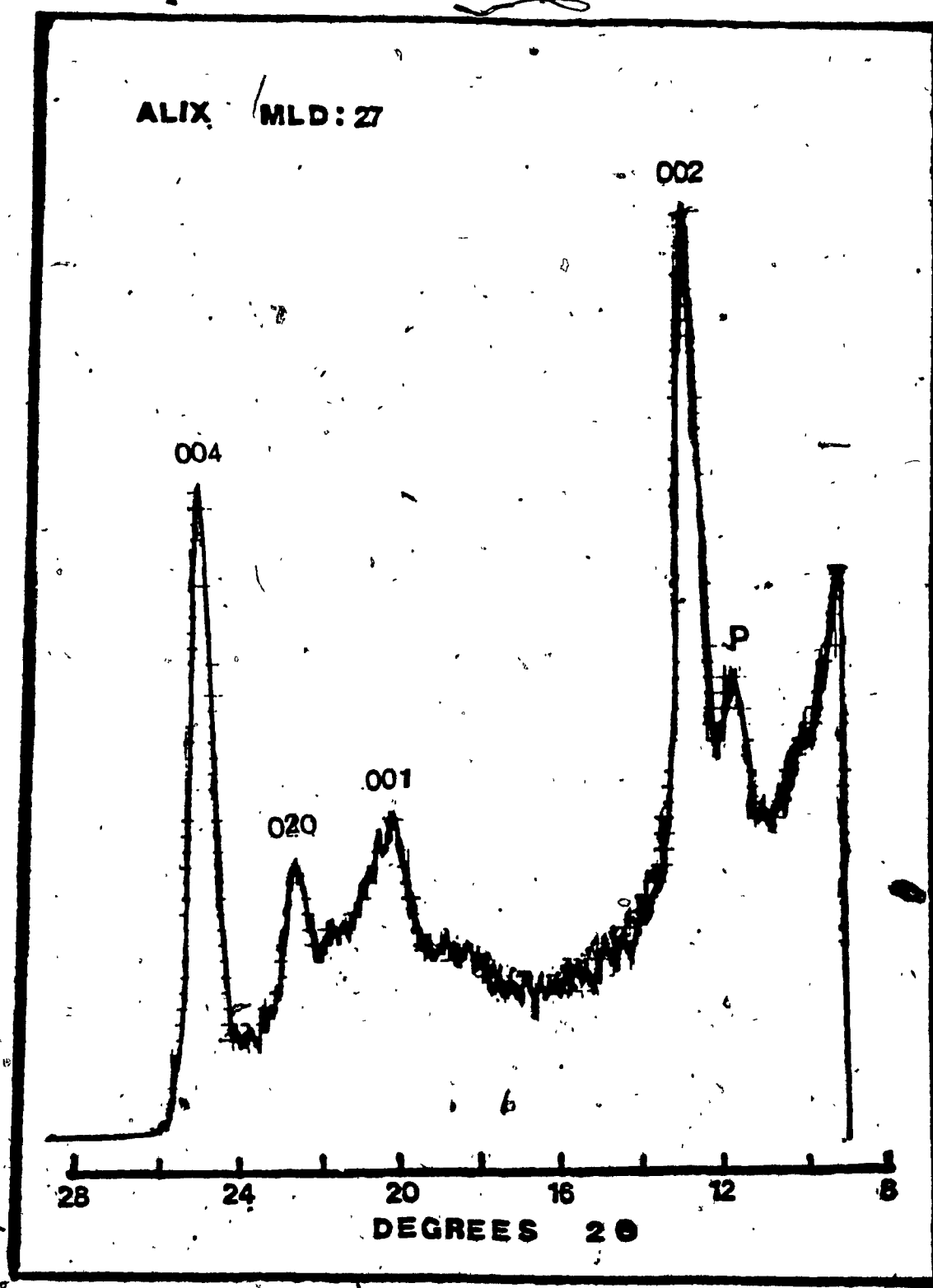


Figure 4.10c: X-ray powder pattern of Alix MLD = 27.

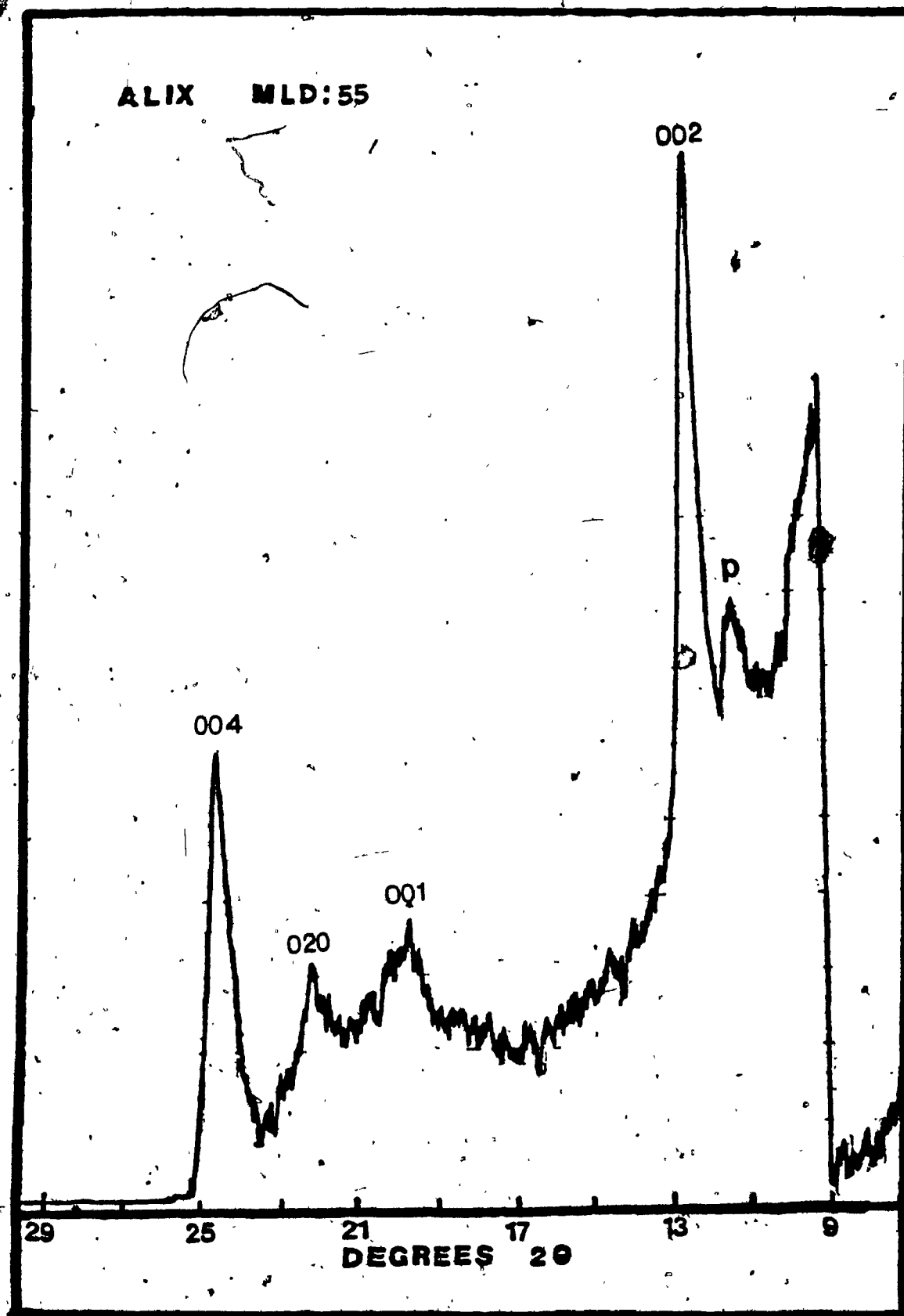


Figure 4.10d: X-ray powder pattern of Alix MLD = 55t.

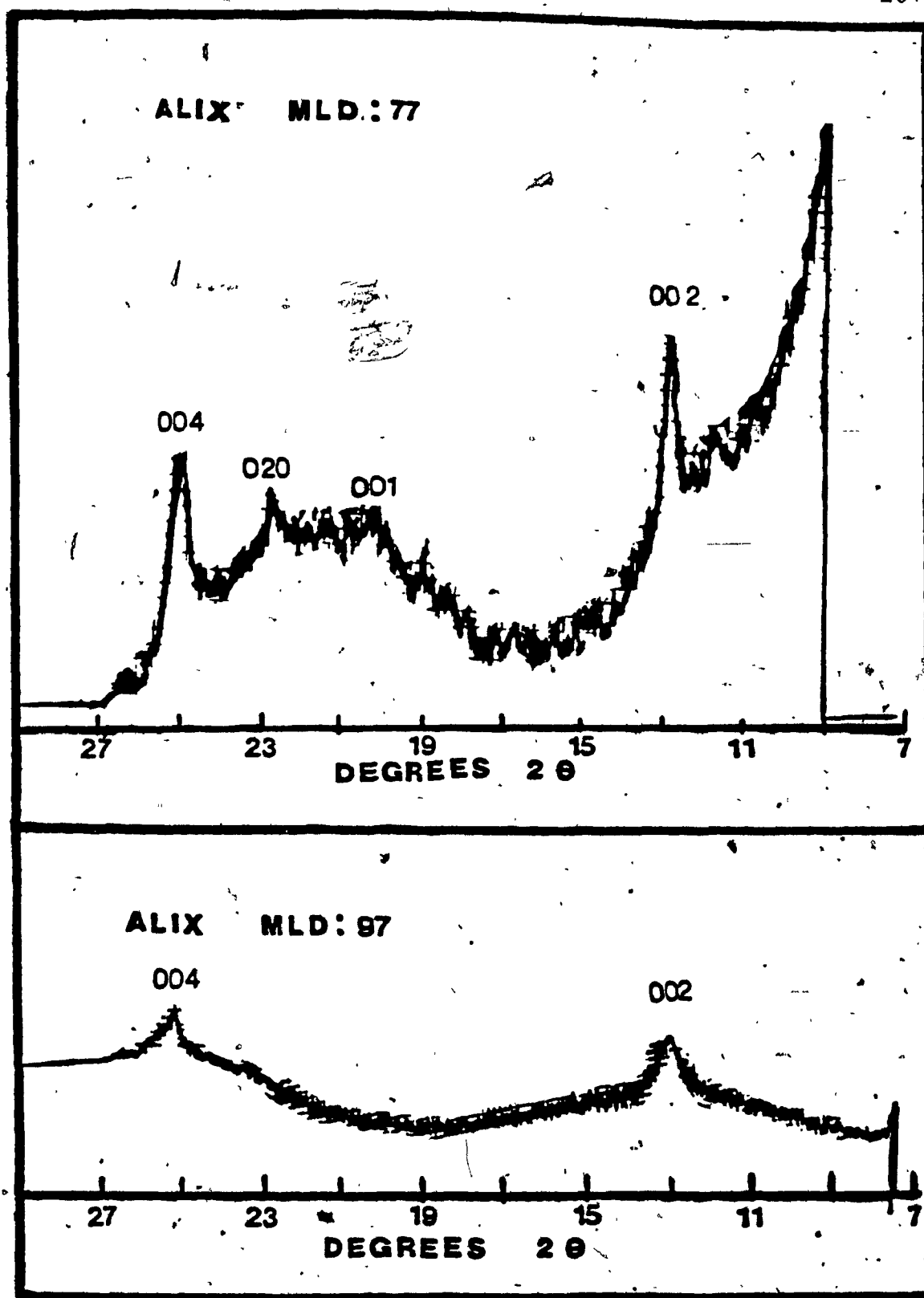


Figure 4.10d and f: X-ray powder patterns of Alix MLD = 77% and MLD = 97%, respectively.

of chrysotile asbestos exhibits four major peaks, three of which are characteristic of the chrysotile asbestos structure, whereas the peak labelled "brucite" is the (001) reflection for free $\text{Mg}(\text{OH})_2$ brucite, usually a common impurity in the fiber (46,47). A weak peak labelled "P" on Figure 4.10a is also present in the literature powder pattern (46,76) but not accounted for; examination of the JCPDS Powder Diffraction File shows that it belongs to pyroaurite, $\text{Mg}_6\text{Fe}_2\text{CO}_3(\text{OH})_{16} \cdot 4\text{H}_2\text{O}$ (006) at $2\theta = 11.40$ (77). The X-ray diffraction scans for some of the leached asbestos fibers that were subjected to very mild acid treatment, i.e. very dilute acid medium and therefore having very low MLD values, showed no change in the intensity of the peaks in spite of the fact that they were more than 15% (w/w) decomposed (Figure 4.6). However, there was a drastic decrease in the intensity of the (001) peak belonging to the brucite impurity (Figure 4.10b). This decomposition represents the immediate dissolution of the surface magnesium hydroxide (brucite), which is easily and rapidly removed by an acid.

The apparent slight increase in the intensity of some of the peaks of leached asbestos materials having very low MLD values (i.e. on leaching the fibers under very mild conditions) as can be observed in the diffraction scans (compare Figure 4.10a and b) and also in the degree of crystallinity being higher than 100% (Figure 4.11), are due

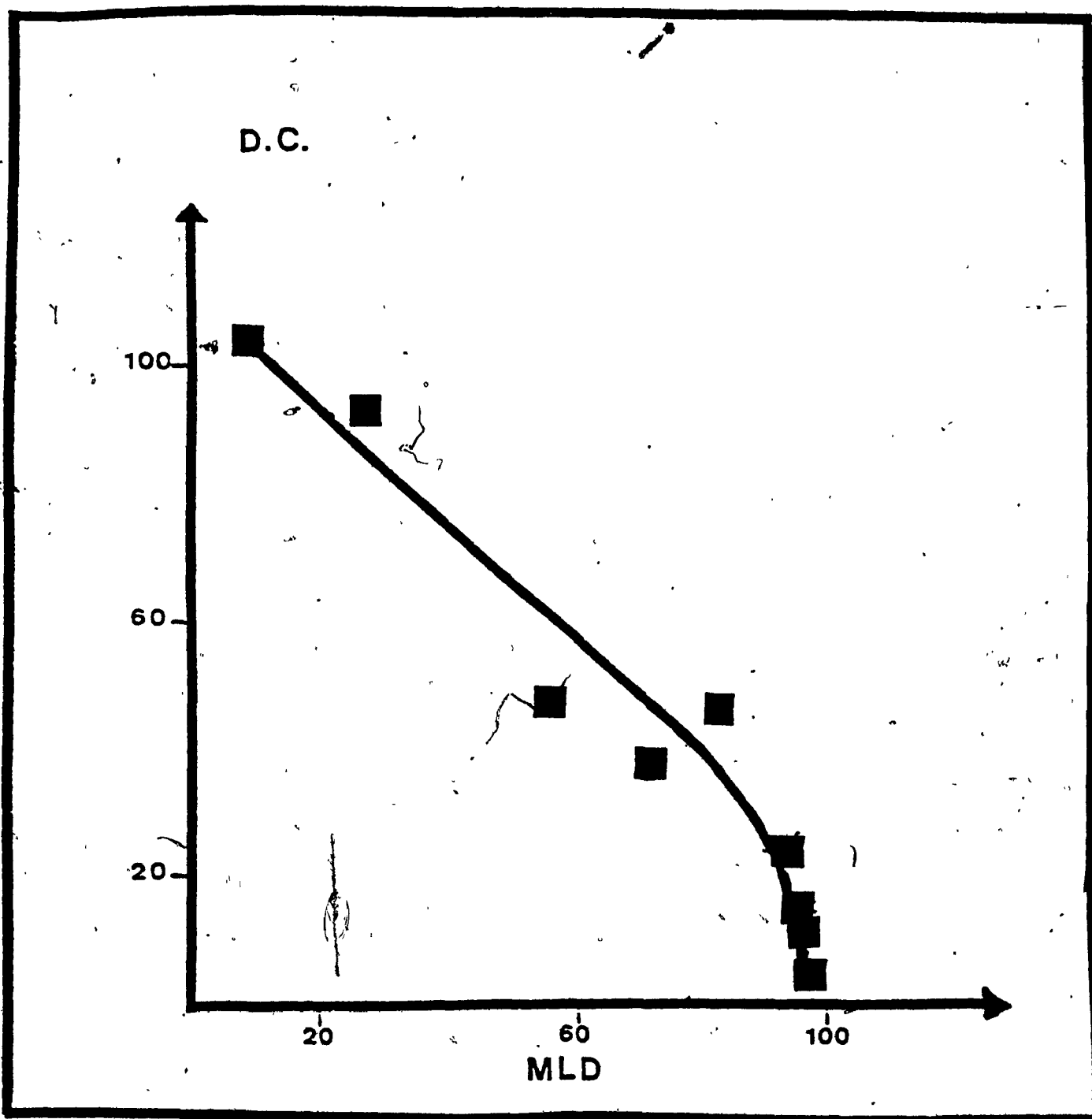


Figure 4.11: A plot of degree of crystallinity of the Alix samples vs MLD.

to the rapid dissolution of brucite impurity, organic matter and some other amorphous impurities normally inherent in chrysotile asbestos (78). These impurities contained in the asbestos do not contribute to the Bragg peaks of chrysotile, but their weight gives an apparent lower degree of crystallinity for unleached asbestos. The dilute acid medium apparently attacks and cleans the surface of the fibrils, leaving an unreacted core which diffracts X-rays the same as or better than the parent chrysotile. The very rapid reaction of the surface magnesium hydroxide layer was also noted by Pundsack et al. (74). Thus under mild acid treatment, the reaction of chrysotile asbestos with an acid is limited to the surface of the fibers, i.e. removal of brucite impurity.

As the leaching conditions were varied from mild to medium and finally to severe, by increasing the acid concentration of the leaching solution, the intensity of the Bragg peaks gradually decreased, showing progressive loss of crystallinity as magnesium was removed (Figure 4.10). The major effect observed on the X-ray powder pattern with increasing MLD was a progressive decrease in the intensity of the chrysotile peaks such that at MLD higher than 98%, no peak was observed. This shows that the crystalline structure of chrysotile is completely destroyed by a strong mineral acid at the appropriate leaching conditions, i.e. when high MLD values are obtained.

Therefore, the resulting Alix material when all the magnesium atoms are removed is amorphous silica. Moreover, heating the Alix for 4 hours at 900 °C showed that it was hydrated, the final formula being $\text{SiO}_2 \cdot (0.5)\text{H}_2\text{O}$ for both HCl and H_2SO_4 leached asbestos products. Furthermore, when the degree of crystallinity was plotted against the decreasing MLD, a linear correlation was obtained up to about 95% MLD at which point it fell abruptly to zero. The degree of crystallinity, which is a measure of the degradation of chrysotile, is shown in Figure 4.11 as a function of MLD. The correlation between the degree of crystallinity and the MLD is in perfect agreement with the hypothesis of the magnesium atoms being originally present in the asbestos fibers framework as "structural" atoms, i.e. directly linked to the structural silicon atoms via oxygen bridges or regularly inserted as magnesium hydroxide between the previously mentioned structural Mg atoms (Figure 2.1).

4.4 IR Spectra

Some acidic chemical properties of chrysotile asbestos were investigated by IR spectroscopy. The principal absorption peaks for the leached asbestos materials and the parent chrysotile asbestos are given in Table 4.8. Figure 4.12 also reports the IR spectra of the chrysotile asbestos and the leached asbestos materials as a function of MLD.

TABLE 4.8 Principal IR absorption peaks for ALIX samples (wave number, cm^{-1})

VIBRATIONS	MLD 0	MLD 12	MLD 55	MLD 80	MLD 92	MLD 98
O-H Stretching	3700 (vs)	3700 (s)	3700 (m)	3700 (w)	3700 (vw)	-
Si-O Stretching	1084 (s)	1085 (s)	1085 (s)	1094 (vs)	1098 (vs)	1098 (vs)
"	1030 (s)	1030 (m)	-	-	-	-
"	965 (s)	965 (s)	960 (m)	968 (w)	968 (w)	960 (vw)
Mg-O Stretching	615 (vs)	617 (s)	618 (m)	620 (m)	613 (vw)	-
Si-O bending	440	440	440	445	448	446

v - very m - medium s - strong w - weak

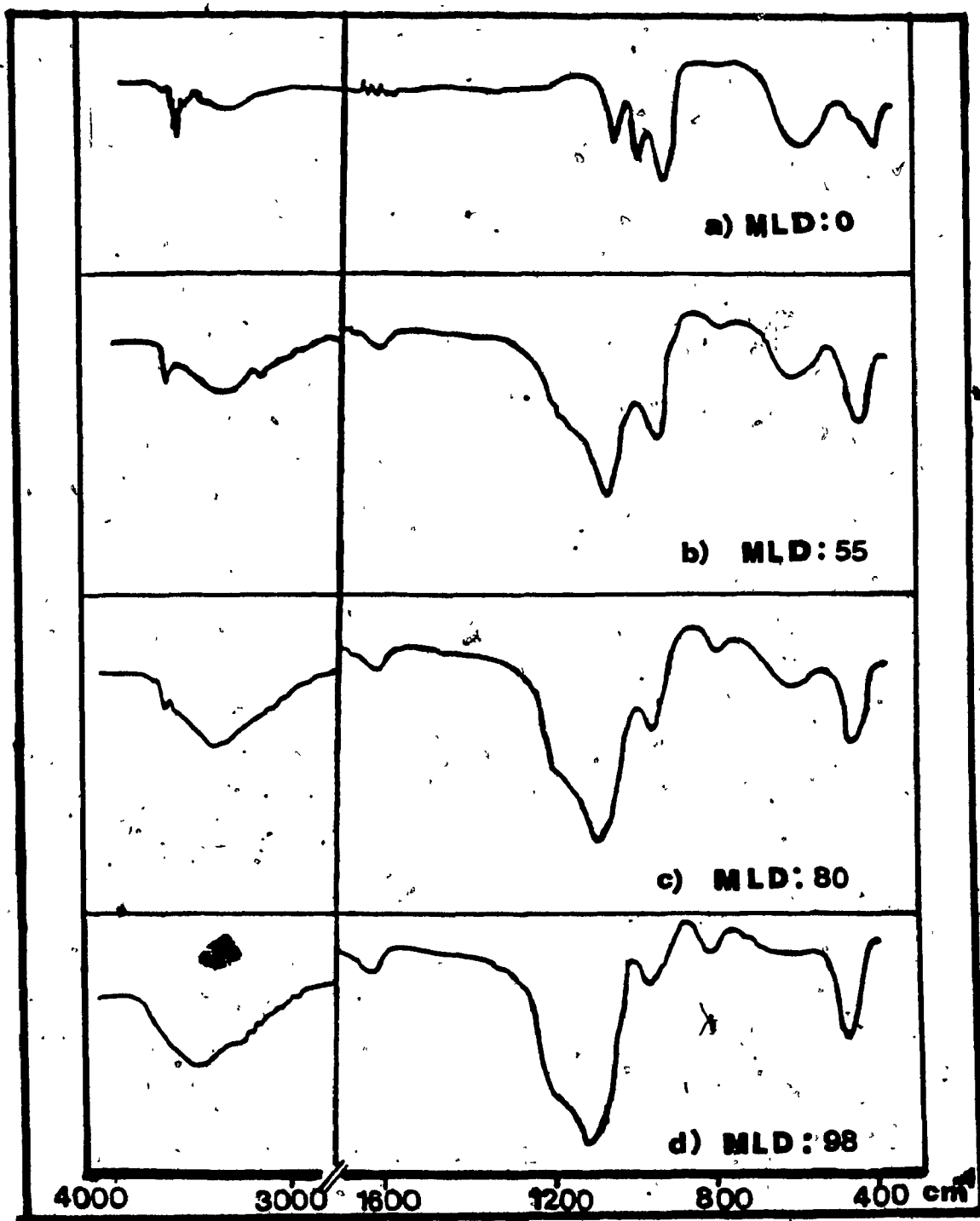


Figure 4.12: IR spectra of chrysotile asbestos and leached asbestos materials as a function of MLD.

Chrysotile asbestos was rapidly decomposed by hydrochloric acid, as indicated by the change in the IR spectra (Figure 4.12) as the leaching conditions were changed gradually from mild to extreme. The spectrum of chrysotile before treatment with hydrochloric acid shows very sharp peaks indicative of a well defined crystal structure. The parent chrysotile asbestos (MLD=0%) exhibits three strong absorptions in the region of 950-1250 cm^{-1} which correspond to the symmetrical stretching vibrations of the Si-O bonds (47). With increasing magnesium leaching, progressive changes are observed, resulting in some overlapping of the peaks so that finally only two peaks are obtained: a very strong absorption peak at about 1094 cm^{-1} and a very weak one at 960 cm^{-1} ; which correspond to the Si-O-Si vibrations as in silicates (47). The particular changes in the Si-O stretching vibrations with increasing magnesium leaching degree occur because the Mg^{2+} ions are directly bonded to the oxygens of the Si-O bonds and the Si-O bond strengths which are not the same for Si-O-Si (high MLD) as for Si-O-Mg (low MLD).

Two I.R. bands, which normally correspond to the O-H stretching vibrations in chrysotile asbestos (46), gave two distinctive peaks in the region 3450-3710 cm^{-1} : a rather broad absorption centered at 3460 cm^{-1} and a strong sharp absorption peak at 3703 cm^{-1} were observed. These

absorption peaks were related to the presence of the external and internal hydroxyl groups in chrysotile (28). The O-H stretching vibration at 3703 cm^{-1} was very sharp and occurred at very high frequency, suggesting that the hydroxyl groups are essentially free and not involved in hydrogen bonding. Since these internal hydroxyl groups correspond to the layers of $\text{Mg}(\text{OH})_2$ sandwiched between the silicate sheets of chrysotile fibers, the rapid disappearance of such hydroxyl groups, as indicated by the sharp decrease in intensity of the peak, even at low values of MLD, means that these structural $\text{Mg}(\text{OH})_2$ entities are easily dissolved in a strong acidic medium. The high frequency band gradually decreases with the magnesium removal; however, it is still observable at MLD as high as 92%; therefore, most but not all of the structural hydroxyl groups are removed at moderate leaching conditions. The broad low frequency band is due to the external hydroxyl groups arising from the samples being hydrated. This band gradually increases in intensity with increasing MLD. As the MLD increases, the leached asbestos material becomes more siliceous and finally, amorphous silica is obtained. The increase in intensity of the low frequency band is due to the contribution from hydroxyl groups of silica (Si-OH vibration), since amorphous silica is easily hydroxylated. The removal of magnesium from chrysotile fibers during the leaching

process can also be observed through the gradual decrease of the Mg-O stretching vibration at 615 cm^{-1} with increasing MLD. The characteristic absorption bands for amorphous silica, which was determined by Kagel (79), are shown in Figure 4.13. Figures 4.12d and 4.13 clearly show that the residue from the dissolution of chrysotile fibers by HCl, whose MLD was 98%, presented the same infrared spectrum as amorphous silica.

The degradation of chrysotile by a strong mineral acid involves the hydrolysis of the fiber to its fundamental unit, silicic acid, with the loss of the magnesium ions as metallic salt. The silicic acid on being dried is dehydrated into an amorphous silica which undergoes slow rehydroxylation. The IR spectroscopy clearly identifies the reaction product of chrysotile after hydrochloric acid treatment under rather severe conditions, i.e. MLD $\geq 98\%$ as amorphous silica. The IR spectra show that the leaching out of magnesium ions from the chrysotile fibers with a strong mineral acid transforms a well-ordered macrostructure into a degraded material, which results in the formation of an isomorphous silica form. The major structural transformation occurs at an MLD higher than 55%, and this is in fair agreement with SEM, X-ray diffraction, density measurements and BET surface area analyses. In general, the present study indicates infrared spectroscopy can provide useful information about structural changes,

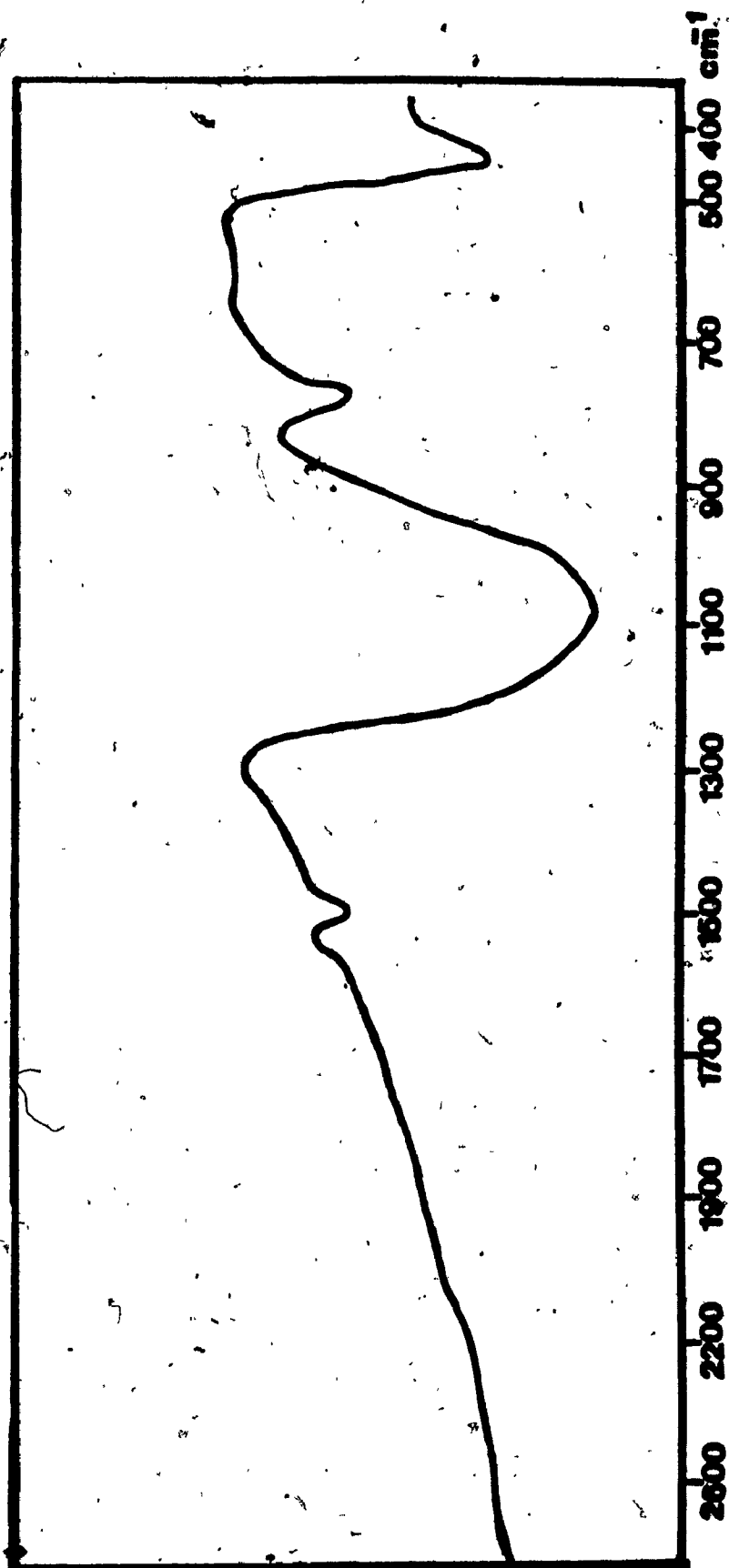


Figure 4.13: IR spectrum of amorphous silica.

particularly acid degradation of chrysotile and other silicate systems.

4.5 Scanning Electron Microscopy

Figure 4.14 shows the general morphology as observed in scanning electron microscopy (SEM) for the chrysotile fibers and the resulting Alix materials at different magnesium leaching degrees (MLD=0, 27, 55, 81, 92 and 98%, respectively). As can be seen from the SEM micrograph, the parent chrysotile has a specific characteristic appearance, exhibiting long, thin and sometimes curved fibrils with cylindrical tubular nature. It clearly appears that under mild leaching conditions leading to low MLD values ($\leq 55\%$), the acid treated asbestos fibers first split into thinner fibrils, but the asbestos fibers keep their original fibrous form without any significant modification of their length. As the leaching of chrysotile fibers progresses further, under medium conditions, many thinner fibers possessing very fragile fibrous morphology are obtained. With more severe leaching conditions, high values of MLD are obtained and the loss of the last Mg (out of three per unit cell) leads to a structural collapse, such that the fibers are strongly fragmented into shorter and smaller pieces. For MLD values equal to or greater than 92%, some larger aggregates appear among the remnants. These are probably amorphous

Figure 4.14: SEM micrographs of chrysotile asbestos and leached asbestos materials as a function of MLD:

(a) 0%, (b) 27%, (c) 55%, (d) 81%,
(e) 92%, and (f) 98%. Magnification = 500.



(a) SEM of MLD = 0%



(b) SEM of MLD = 27%



(c) SEM of MLD = 55x



(d) SEM of MLD = 81x



(e) SEM of MLD = 92x



(f) SEM of MLD = 98x

SiO_2 , as evidenced by elemental analysis (Tables 4.1-4.3), complete disappearance of chrysotile X-ray diffraction pattern, i.e. no Bragg peaks observed and IR spectra. The structural collapse of the severely leached fibers results in a large amount of SiO_2 being liberated. The sequence of fiber modifications during the leaching process can be summarized as follows:

original fibers \longrightarrow (dissolution of impurities and mild leaching) \longrightarrow splitting of fibers into thinner fibrils with practically no change in morphology (MLD=55%) \longrightarrow fiber degradation (fragile fibrous morphology) \longrightarrow (MLD=92%) \longrightarrow presence of silica aggregates.

The SEM micrographs show that when the MLD is at least 98% the final residue of the chrysotile leaching has lost its characteristic tubular and fibrillar morphology.

4.6 Solid State NMR Spectra

IR spectra provided useful information on the Mg-O and Si-O bonds. In order to gain further information on the silicon environment, magic-angle spinning (MAS) NMR spectra of ^{29}Si were recorded for Alix materials as a function of MLD (Figure 4.15). Due to the presence of a significant amount of ferromagnetic impurities in the asbestos fibers, mainly Fe_3O_4 , MAS NMR spectra of the

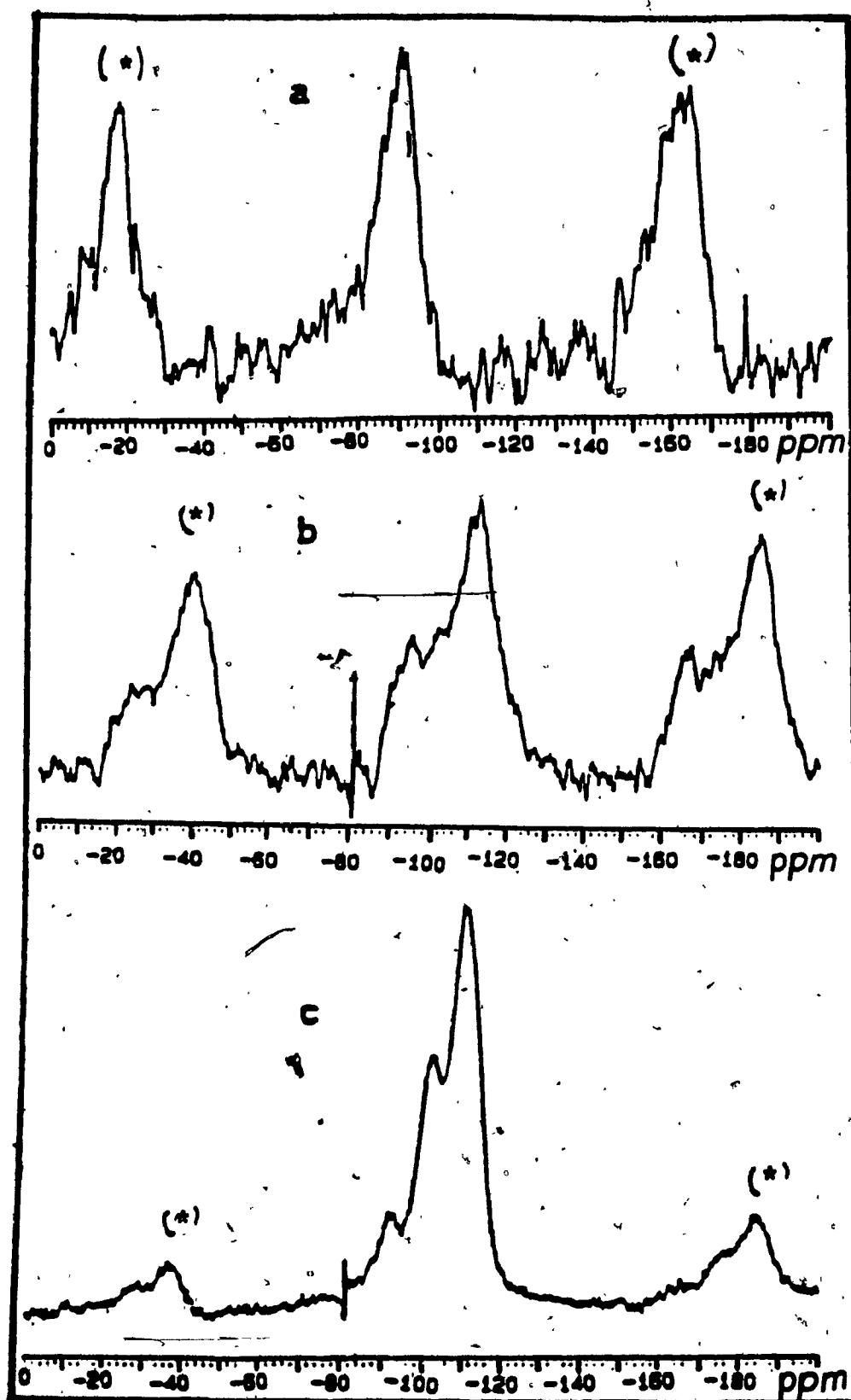


Figure 4.15: ^{29}Si MAS NMR spectra of chrysotile asbestos as a function of MLD: (a) 0%, (b) 63%, and (c) 95%. Peaks marked (*) are spinning side bands.

parent chrysotile asbestos were rather difficult to interpret (Figure 4.15a). However, the presence of several peaks at chemical shifts, ranging from -84 to -98 p.p.m., can be attributed, at first, to different environments of the Si atoms in the parent chrysotile fibers. This contradicts the structural results of pure chrysotile, which has one Si site only, therefore, it must be related to the interactions of the impurities located between the layers of silicon in tetrahedral environment. Such an NMR spectrum bears some similarities to that of the clinoenstatite, MgSiO_3 (80). Partial leaching of chrysotile fibers, leading to an MLD of 63%, gives a strong peak at -110 p.p.m. in the NMR spectrum (Figure 4.15b). Such a peak is characteristic of the Si-O-Si assigned peak in silicates or quartz (80). The initial chrysotile peaks are still present, but much weaker in intensity, indicating incomplete removal of magnesium and ferromagnetic impurities.

At much higher MLD values (85 to 97%), i.e. in situations where the magnesium content is very low and the residue becomes very siliceous, the peak at -110 p.p.m. becomes extremely intense (Figure 4.15c). It is remarkable that the intense peak at -110 p.p.m. does not significantly change when zeolite particles of the ZSM-5 type are crystallized from such a similar Alix material (20). For MLD values close to 100%, a much cleaner spectrum is

obtained. The spectrum shows three peaks at about -93, -102 and -112 p.p.m. in the ratio of about 1:3:5, respectively. This can be attributed to three different local silicon environments of silica gel, the resulting product. Thus, the high intensity peak at -112 p.p.m. is assigned to the silicon atoms linked exclusively to other silicons via oxygen, while the peak at -102 p.p.m. is assigned to single hydroxyl silanol site $(\rightarrow\text{SiO})_3\text{SiOH}$; similarly, the low intensity peak at -93 p.p.m. is assigned to surface silicon atoms bonded to two silicon atoms via oxygen and two hydroxyl groups, $(\rightarrow\text{SiO})_2\text{Si}(\text{OH})_2$. These values are in reasonable qualitative agreement with the values obtained by Matiel et al. (81) for silica gel, by using ^{29}Si MAS technique.

4.7 Specific Surface Area

The specific surface area of chrysotile asbestos grade 7TF-12, one of the most "open" commercial grades with shortest fibril lengths, as determined by BET method, was in good agreement with the measured values determined by Fripiat et al. (69). The surface area measurement was obtained for the starting chrysotile specimens in the form in which they were received. The surface area results for the parent chrysotile asbestos and the leached asbestos materials are presented in Table 4.9. The BET surface areas of the acid-treated chrysotile reaction products

TABLE 4.9 Specific surface area of ALIX samples.

Nature of the acid	Leaching conditions used			ALIX	MLD	Surface area (m ² /g).
	Normality (N)	Leaching time	Temp. (°C)			
HCl				starting asbestos	0	49
	0.5	4.0hrs	80	076	14	52
	1.0	4.0hrs	80	077	27	71
	1.5	4.0hrs	80	067	55	167
	1.8	4.0hrs	80	068	80	227
	2.4	4.0hrs	80	061	92	302
	6.0	4.0hrs	80	075	98	423
H ₂ SO ₄	1.0	4.0hrs	80	113	37	118
	1.5	4.0hrs	80	114	60	211
	2.0	4.0hrs	80	115	68	257
	2.5	4.0hrs	80	116	88	349
	6.0	4.0hrs	80	120	99	483
HCl	2.4	0.5hrs	80	086	70	212
	2.4	1.5hrs	80	088	81	322
	3.0	7.0hrs	80	069	98	485
H ₂ SO ₄	2.4	0.5hrs	80	138	72	201
	2.4	3.0hrs	80	143	86	295
	2.4	7.0hrs	80	148	93	427
HCl	0.5	2 wks	R.T.	107	29	120
	2.4	2 wks	R.T.	109	92	440
	6.0	2 wks	R.T.	111	98	467

exhibited higher values than the starting chrysotile asbestos. In fact, the observed surface areas of the leached asbestos materials were strongly dependent on the leaching parameters used such as acid normality or reaction time (Table 4.9). In general, the surface areas of the Alix samples increased sharply with the acid normality of leaching solution, the reaction time and hence the resulting MLD. The variations of the BET specific surface area of the leached asbestos materials as a function of MLD is shown in Figure 4.16. From MLD=0 (original chrysotile fibers) to 55%, the surface area increases only from 49 to $140 \text{ m}^2 \text{ g}^{-1}$. This moderate increase is characteristic of relatively minor modifications in the crystalline size and fiber morphology, in agreement with electron microscopy and X-ray powder diffraction pattern.

The internal and external (voids between the fibrils) pores of chrysotile fibers contain appreciable amounts of amorphous materials such as organic solid matter. Convincing evidence for the presence of solid matter within the fibrils has been obtained by Bates et al. (82). Thus an assemblage of chrysotile fibrils like that depicted in Figure 2.2 have surface areas and porosities considerably smaller than would be expected from the geometry of the fibrils; this is better illustrated by the theoretical value computed by Neymann et al. (65) which is about twice larger than the observed value (see Table 4.10).

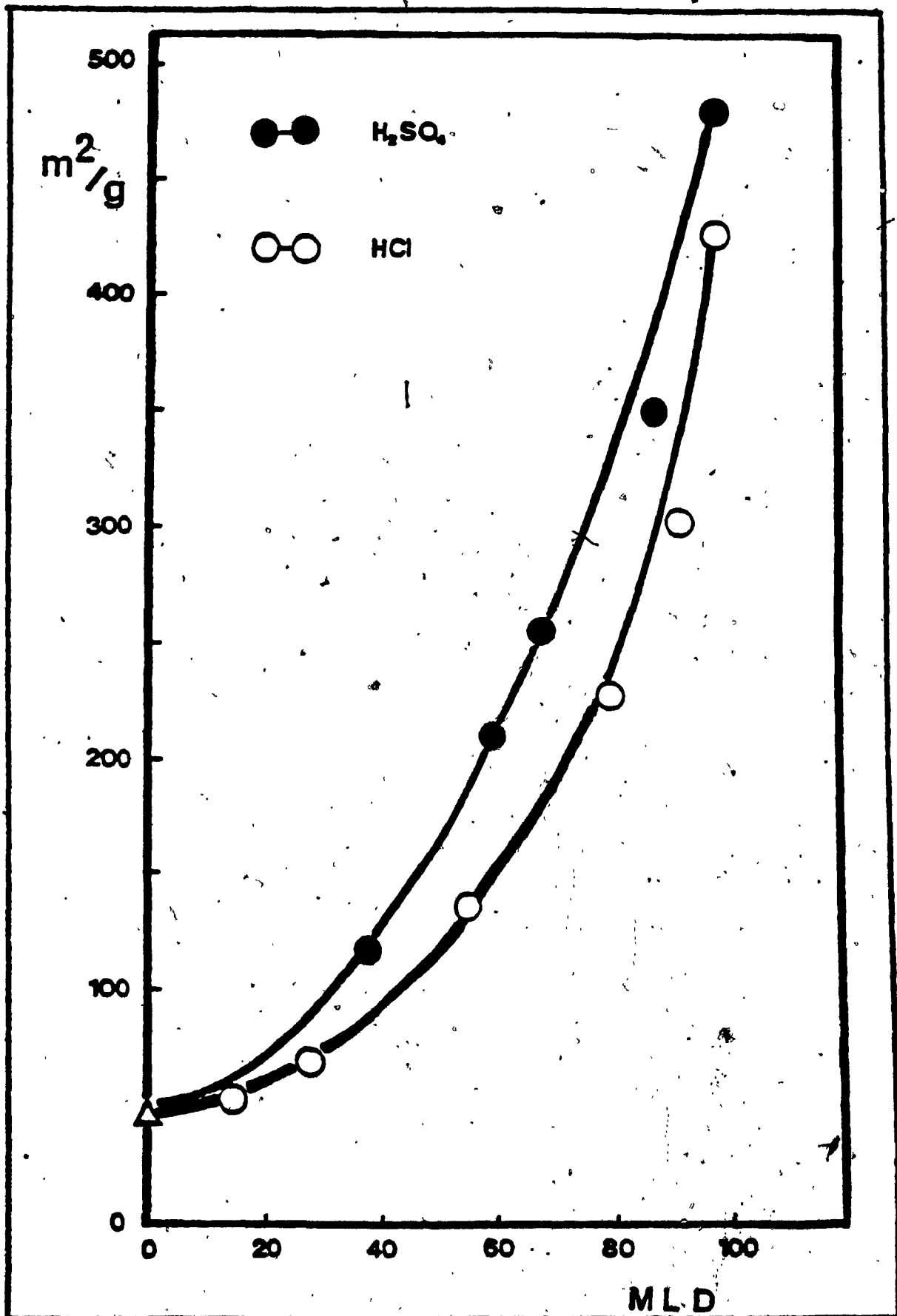


Figure 4.16: A plot of specific BET surface area of leached asbestos materials vs MLD.

The initial effect of the acid treatment of the fibers, particularly under rather mild leaching conditions, is to open up the filled or blocked pores and voids by the removal of the amorphous matter and the brucite impurity layer. The opening of the pores results in appreciable increase in the surface area of the fibers.

With the removal of free brucite impurity, organic matter and other amorphous materials, assumed to be filling some of the central pores and the voids between the fibrils of the parent chrysotile fibers, further reaction of the fibers with an acid results in continuing dissolution of magnesium ions. The acid by leaching out magnesium and metallic impurities such as iron creates random pores and small holes inside the fiber macrostructure. The chemical treatment of the acid also opens up the fiber bundles and splits them into thinner fibrils as observed in the SEM micrographs. All these chemical effects of the acid on the fibers, under mild to moderate leaching conditions, explain the increasing surface area of the leached asbestos material with increasing MLD. However, above MLD=55%, a sharp increase in surface area is observed such that at MLD equal or greater than 92% extremely very high surface area in the region of $400-500 \text{ m}^2 \text{ g}^{-1}$ is obtained. The leaching out of most or all of the Mg^{2+} ions leads to the formation of a very porous, highly divided phase consisting of some fragments of amorphous silica. The above observations corroborate the previous SEM observations,

since a decrease in particle size logically leads to an increase of the surface area. The unusually high BET specific surface area in excess of $400 \text{ m}^2 \text{ g}^{-1}$ leads one to suspect that considerable microporosity may be present at high MLD values.

4.8 External Surface Area

The external surface area of leached asbestos materials was obtained by filling up completely all the internal pores with benzene while leaving the external surface free for nitrogen adsorption. Furthermore, during the subsequent nitrogen adsorption BET determination benzene remained undesorbed because it was frozen inside the pores since the sample was immersed in liquid nitrogen.

The pores of chrysotile fibers consist of the external pores between the fibers and the internal pores (within the individual fibers), but there are twice as many external pores as the internal pores (83). As shown in Table 4.10, the external surface area of the parent chrysotile fibers obtained by our technique compared favourably with those obtained by Fripiat et al. (84). The geometrical surface area computed by Neumann et al. (65), assuming chrysotile was composed of hollow fibers arranged in hexagonal close packing, is rather higher than observed values; and this is attributed to the presence of amorphous material in the pores. As shown in Table 4.10,

TABLE 4.10: Computed and experimental surface areas of the chrysotile asbestos.

	External area (m^2/g)	Internal area (m^2/g)	Total area (m^2/g)
Present pore-filling method	30	19	49
Method of Fripiat et al. (84)	35	16	51
Theoretical value calculated by Neumann et al. (65)	69	35	104

TABLE 4.11: External surface area of the starting chrysotile asbestos and Alix samples.

MLD (%)	BET specific surface area				Benzene adsorbed (w/w) %
	Total (m^2/g)	External (m^2/g)	Internal (Total-External) (m^2/g)	(%)	
0	49	30	19	39	2.61
27	71	44	27	38	3.13
55	167	73	94	56	6.28
80	227	95	132	58	10.63
92	302	145	157	52	12.04
99	483	192	291	60	15.37

the geometrical and the observed external surface area of the starting chrysotile fibers is normally twice the internal surface area.

In Table 4.11, the contributions of the surface areas of the external and internal pores of the leached asbestos materials, as were obtained by the benzene pore filling and subsequent nitrogen adsorption BET method, are presented. At low MLD values, the external surface area was significantly larger than the internal surface area. As the MLD increases, the total surface area increases, but the ratio of the external to the internal surface decreases so that at MLD $\geq 55\%$ the external surface area becomes smaller than the internal surface area. Both the external and internal surface areas of the leached asbestos materials at high MLD values were several times larger than the values obtained for the starting chrysotile fibers. The results in Table 4.11 convincingly demonstrate that if the Alix material becomes more microporous at high MLD as suspected because of the unusually high surface area, then the microporosity is not confined to the internal pores but is also strongly associated with an appreciable amount of the external surface. The amount of adsorbed benzene in the internal pores, as was determined gravimetrically, increased with increasing MLD.

4.9 Pore Size Distribution

The pore size distribution was obtained as the plot of cumulative surface area versus mean pore radius. The pore size distribution curves of leached asbestos materials, as shown in Figure 4.17, are not distribution of all the pore radii in the solid, but only those within the range of validity of Pierce's method which extends down to only 15 Å and therefore excludes the pore radii and hence the surface area of micropores. In order to determine the surface area of micropores, the BET surface area had to be performed so as to obtain the total surface area of the leached asbestos materials. Since the pore size distribution method in the application of Pierce's model computed the surface area of macropores and mesopores, therefore the surface area of micropores has been extrapolated from the total surface area of Alix samples as given by the BET method. Thus, the difference between the BET surface area observed and the cumulative surface area of Alix samples as obtained from pore size distribution method gave the surface area of micropores. The BET surface areas, the surface area of micropores, being the difference between the BET and cumulative surface area, are tabulated in Table 4.12.

Figure 4.17 shows the macro and mesopores size distribution curves of Alix samples: each one has a single

TABLE 4.12 Cumulative surface area of the starting chrysotile asbestos and Alix samples from pore size distribution.

MLD (%)	BET area, S_{BET} (m^2/g)	Cumulative area, S_{Cum} (Surface area of macro and mesopores) (m^2/g)	Micropore area, $S_{BET} - S_{Cum}$ (m^2/g)	Mean pore radius of maximum peak * (Å)
0	49	51	0	26
27	71	53	18	25
55	167	58	109	24
80	227	52	175	22
98	423	29	394	21

* related to macro and mesopores only

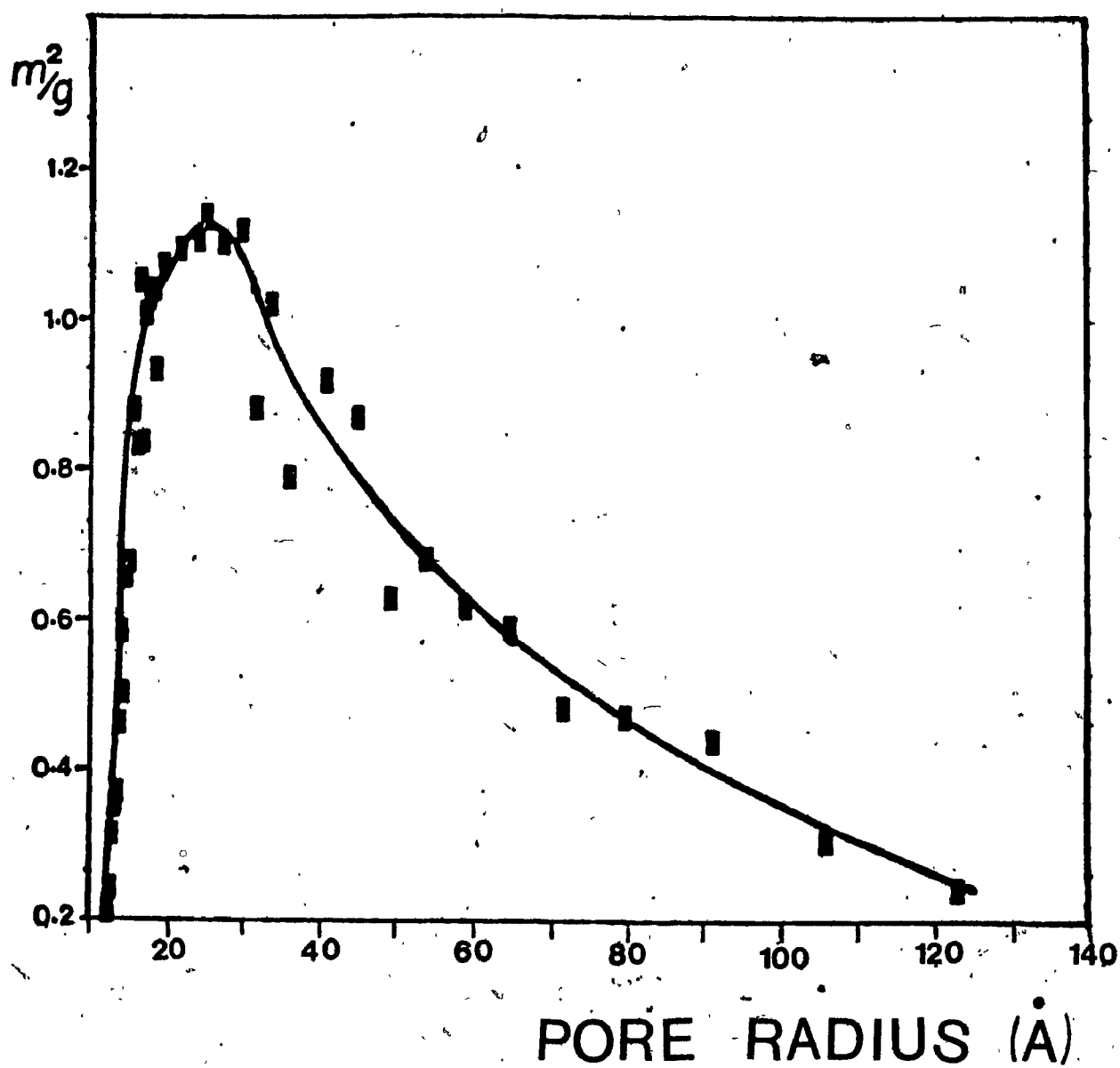


Figure 4.17a: Pore size distribution of Alix of MLD = 0%.

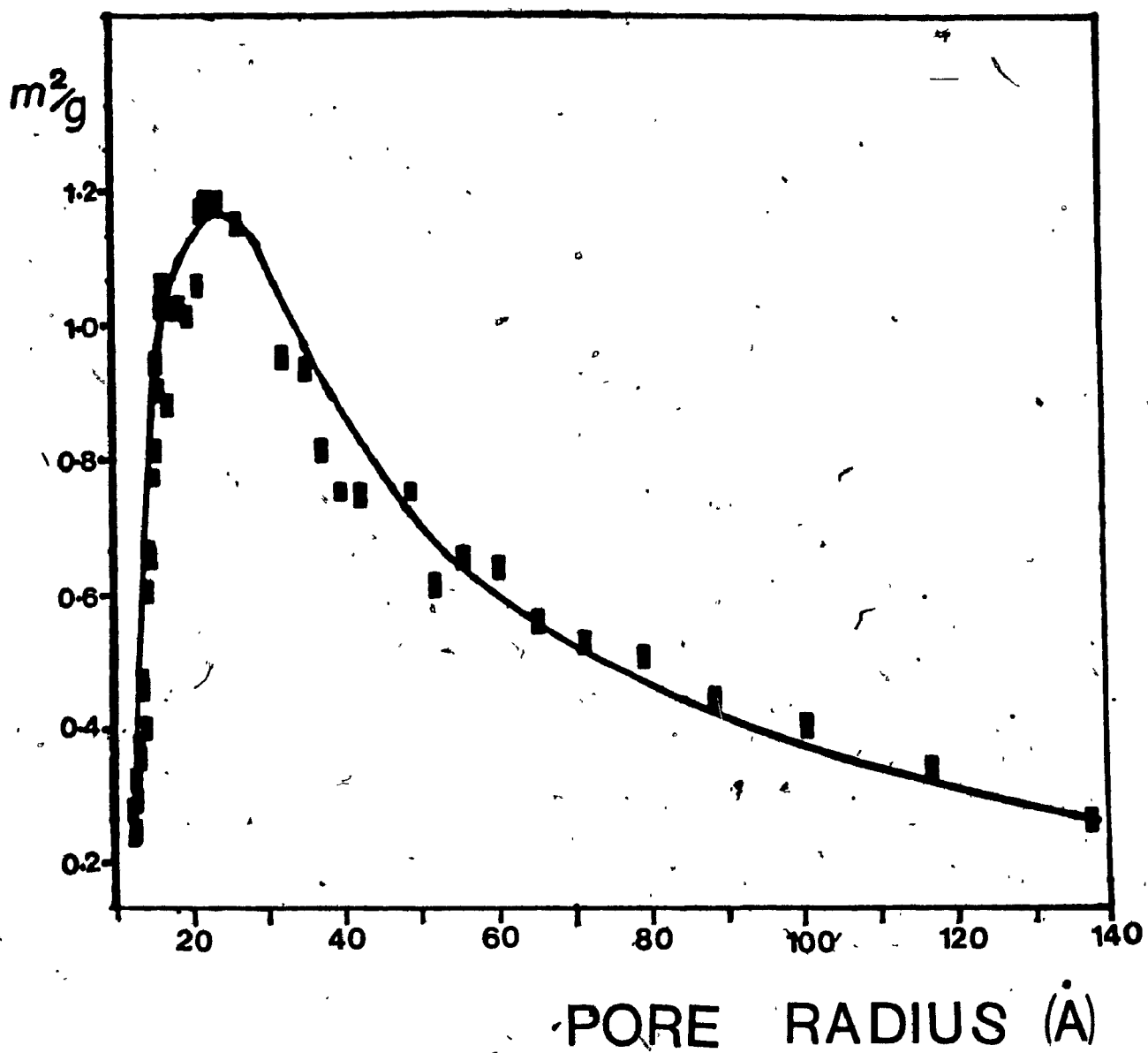


Figure 4.17b: Pore size distribution of Alix of MLD = 27%.

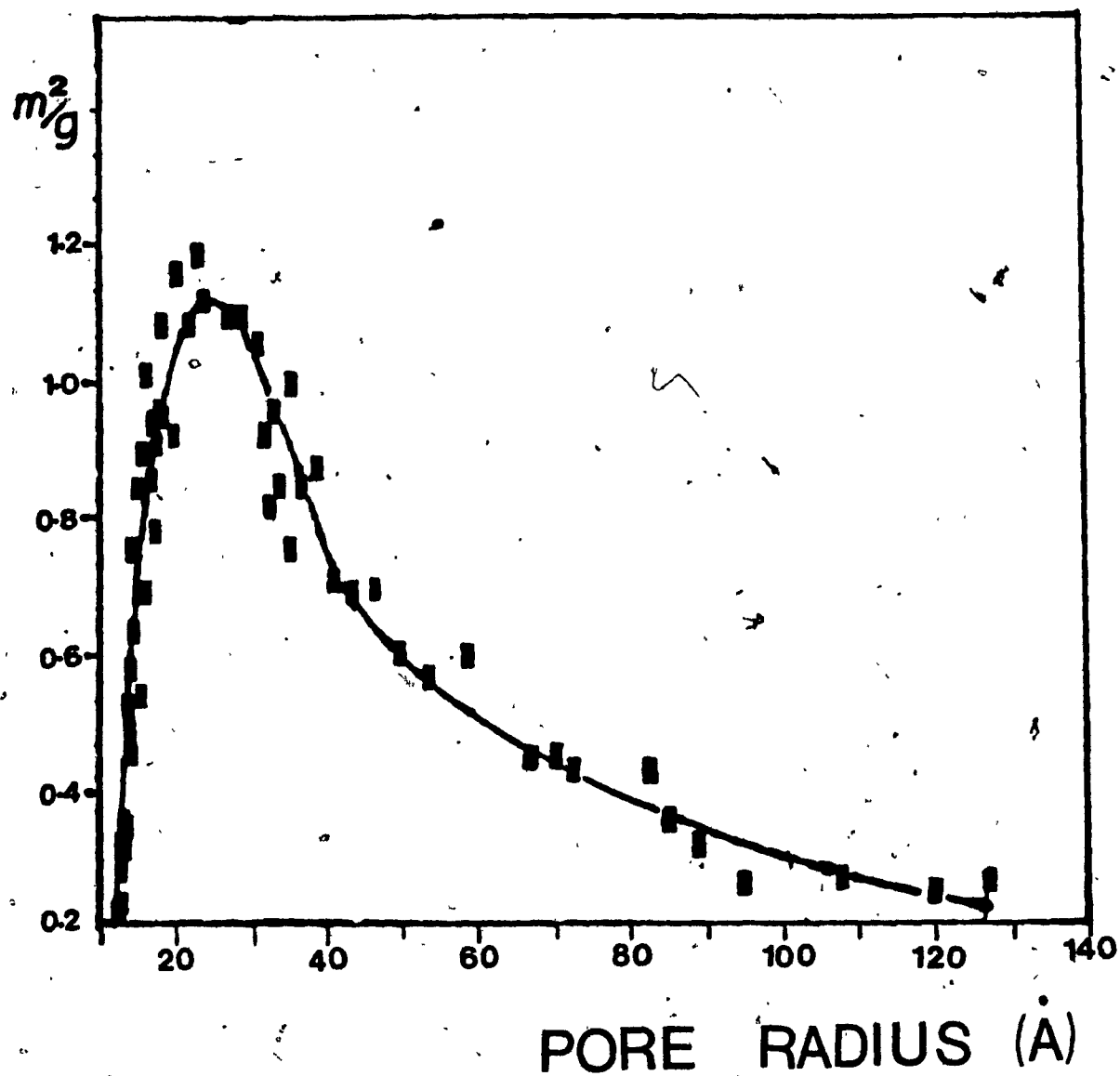


Figure 4.17c: Pore size distribution of Alix of MLD = 55%.

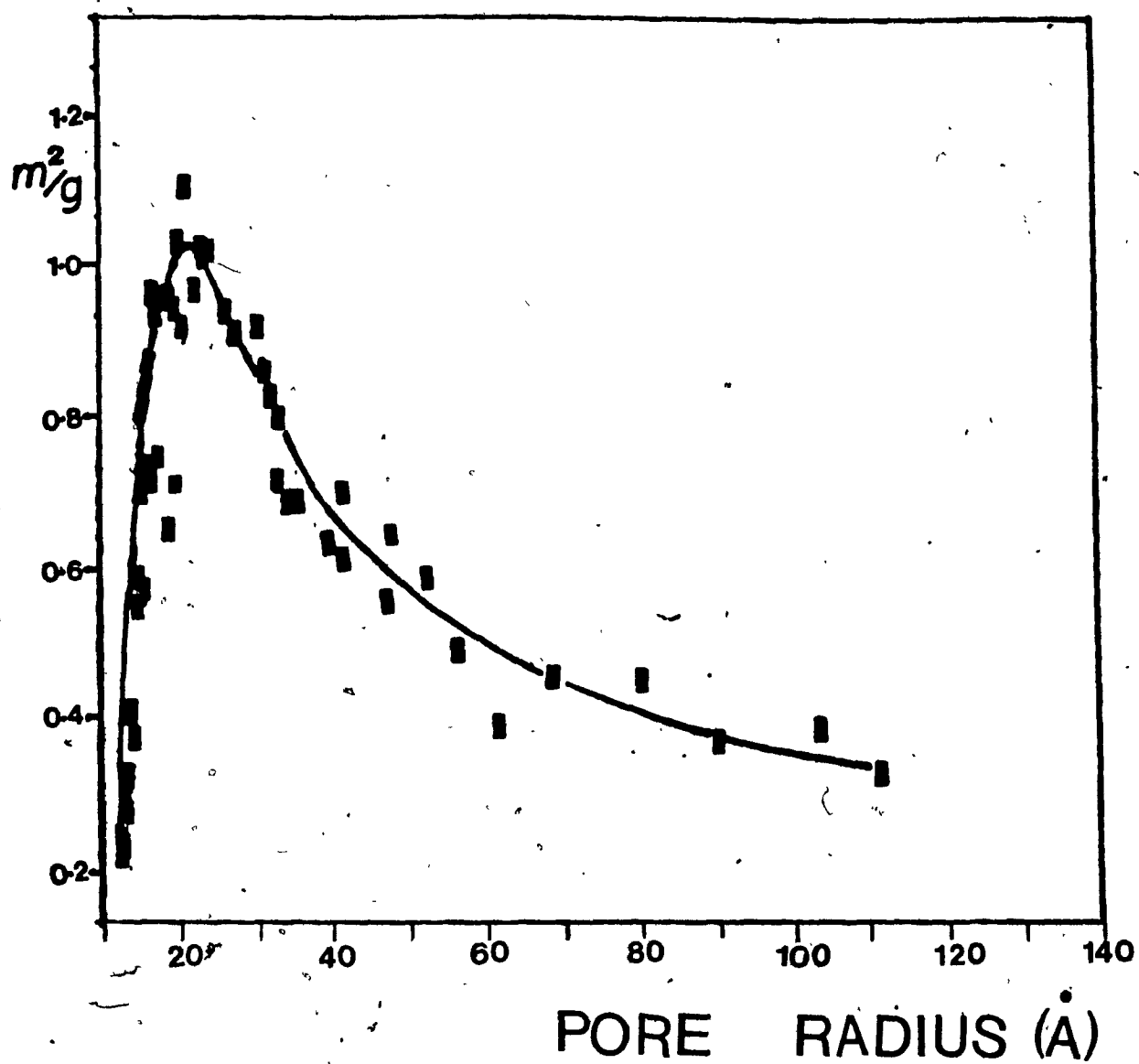


Figure 4.17d: Pore size distribution of Alix of MLD = 80%.

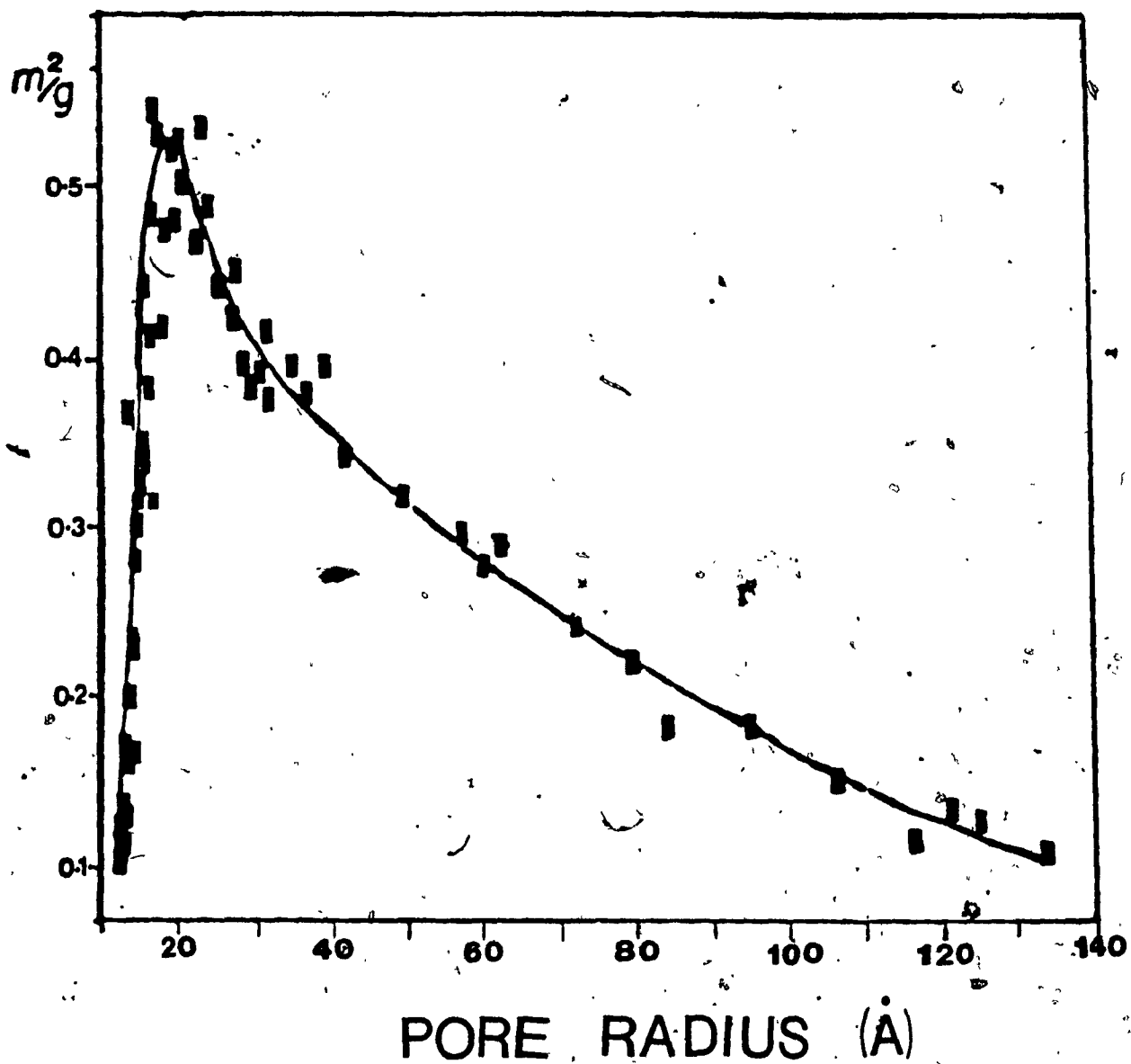


Figure 4.17e: Pore size distribution of Alix of MLD = 98%.

maximum, the position of the maximum and the mean pore radius appeared to be a function of MLD. As the MLD increased, the mean pore radius of the maximum peak decreased gradually. (Table 4.12) and a shift of the maximum peak towards the microporous region was observed. This phenomenon becomes more obvious from the surface area of micropores of Alix sample which increased dramatically with increasing MLD as shown in Table 4.12. Thus, as the MLD increases, the leached asbestos material becomes more microporous, the particle size decreases (as observed from SEM) and pores become narrower and narrower which consequently leads to decreasing mean pore radius of the maximum peak and a shifting of the pore size distribution curve towards the microporous region.

4.10 Density

Figure 4.18 reports the variation of the bulk density with the MLD (50,76). The removal of Mg up to an MLD=55% results in a decrease of the density from 2.5 g cm^{-3} to 2.4 g cm^{-3} , whereas further increase in MLD leads to a more dramatic decrease (2.4 g cm^{-3} at MLD=55% to 1.9 g cm^{-3} at MLD=98%). As the density is the ratio of the mass of the sample over its volume, removal of magnesium results in a decrease in the sample mass. As a consequence, no volume change would result in a rapid fall of the density, whereas a corresponding volume contraction could partly or

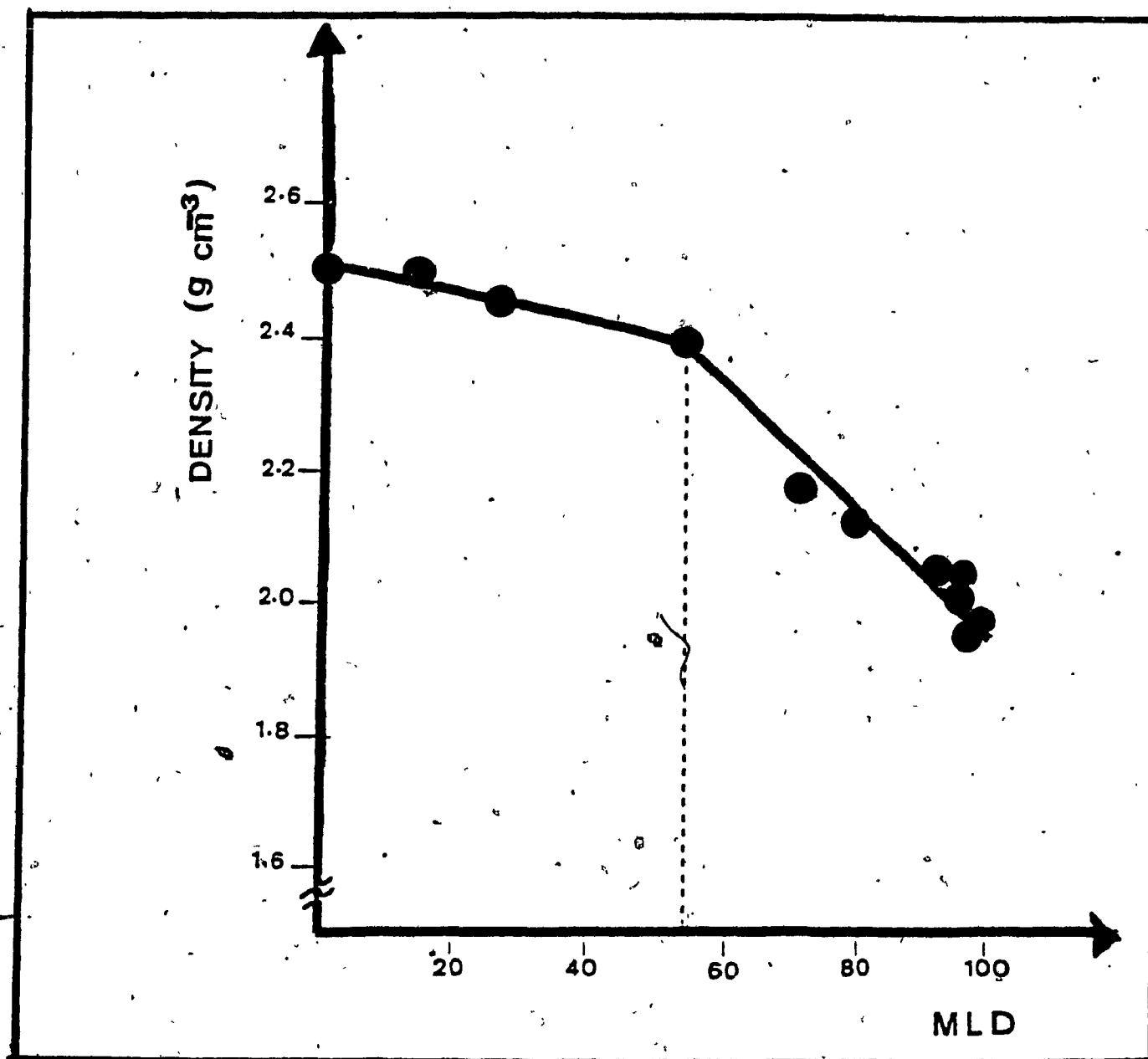


Figure 4.18: A plot of bulk density of Alix materials
vs MLD.

totally cancel the effect of loss of mass, i.e. results in a lower density decrease or none. Even an increase in density could be observed if a more efficient packing were obtained. As shown in Figure 4.18, a slow linear decrease in density is observed up to MLD=ca. 55%, i.e. the removal of just slightly more than half of the initial magnesium. Up to that point, SEM photographs show little fiber degradation (Figure 4.14a-c), such that, based on the density results, it is clear that magnesium leaching is not followed by a profound structural reorganization, only the release of some of the strain due to its large size, which partly offsets the volume vacated by magnesium.

The removal of the second half of the magnesium has a more drastic effect and leads to the collapse of the fibrous structure as shown by electron microscopy (Figure 4.14d-f). Amorphous silicon dioxide is produced, which is likely poorly organized, and therefore not well packed, as shown by the rapid decrease in density. At about 100% MLD, the density obtained of 1.9 g cm^{-3} is significantly lower than that reported (85) for various varieties of silica, such as cristobalite (2.32), vitreous lechatelierite (2.19), tridymite (2.26), and $\text{SiO}_2 \cdot \text{H}_2\text{O}$ opal (2.17-2.20), indicating a highly porous and hydrated material, $\text{SiO}_2 \cdot (0.5) \text{H}_2\text{O}$.

4.11 Adsorption of Water and n-hexane

The sorption capacities as well as the relative affinity index for the chrysotile asbestos and the Alix materials are shown in Table 4.13. The relative affinity index (RAI) is defined as the ratio of the volume of n-hexane over the volume of water sorptive capacities of the samples. Unleached chrysotile asbestos is highly hydrophilic, due to the sheet of hydroxyl groups covering the outer surface of each layer of the fibers. These hydroxyl groups form hydrogen bonding with adsorbed water molecules, making possible the adsorption of large amount of water, preferentially to hydrocarbons. However, in the case of silica, the reaction product at MLD close to 100%, this material is very hydrophobic and adsorbs large amount of n-hexane due to its porosity but still has some hydroxyls attached to the surface silicon atoms. As the leaching operation proceeds to higher MLD values, two phenomena are observed:

(a) The volume of sorbed water does not significantly change. The surface of the leached asbestos obviously becomes less hydrophilic but more surface becomes available with gradual removal of magnesium. The presence of many micropores of molecular dimensions particularly at high MLD values leads in principle to an increase in the adsorption of water molecules since they are small enough to enter the pores. As the MLD gradually increases, there

TABLE 4.13 Water and n-hexane sorptive capacities of the starting chrysotile asbestos and Alix samples.

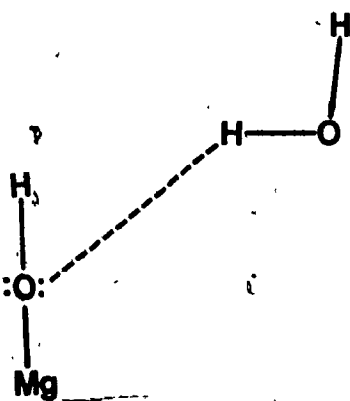
Leached Asbestos Material	MLD (%)	n-Hexane		H ₂ O (%wt/wt)**	RAI*
		(%wt/wt)	(%vol/wt)		
Chrysotile Asbestos	0	2.74	4.15	7.68	0.54
Alix 077	27	4.96	7.52	8.74	0.86
Alix 067	55	7.97	10.09	8.70	1.16
Alix 068	80	10.02	15.19	8.30	1.83
Alix 61	92	9.46	14.34	7.47	1.92
Alix 069	98	11.49	17.42	8.80	1.98

* RAI = n-hexane/H₂O (vol/vol) of relative adsorption affinity index.

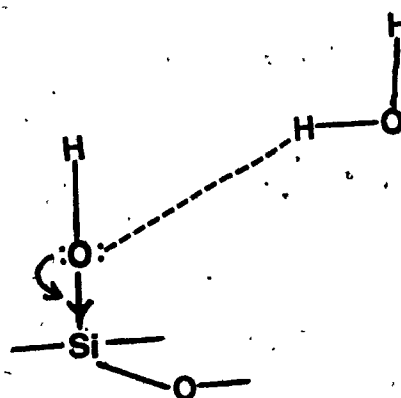
** For H₂O, the %wt/wt is equal to the %vol/wt as the density of H₂O is equal to 1.

are two opposing changes related to the adsorption of water which tend to balance each other. The increasing porosity of the solid surface offsets for the decreasing water affinity due to increasing hydrophobicity of the siliceous surface which leads to repulsion of water molecules. The net effect is that the water adsorbed remains almost constant with increasing MLD.

(b) The volume of sorbed n-hexane increases dramatically with the MLD and becomes significantly higher than that of the sorbed water at MLD higher than 55% due to the increased porosity and surface area available for adsorption. The surface of the silica formed, unlike that of the starting chrysotile asbestos, is highly hydrophobic according to schemes (a) and (b) shown below.



(a)



(b)

Pauling's electronegativity values are as follows:

Mg (1.31), Si (1.90).

As illustrated in scheme (a), the Mg atom is a very strong electron donor species, i.e. it is electropositive and makes the oxygen atom electron rich, thereby strongly enhancing its H-bond formation to water molecules. The silicon atom is electronegative and therefore has a tendency to attract lone pairs of electrons on oxygen atom as shown in scheme (b). This leaves less electrons available for H-bonding to water molecules, and results in some repulsion of water molecules. Thus H-bonding in scheme (a) is more favourable than are the interactions of silica with water molecules (see scheme (b)). On the other hand, the non-polar n-hexane molecules are readily adsorbed onto the apolar silica surface (physical adsorption with van der Waals type interactions).

As a consequence, the RAI, which gives a measure of the surface hydrophobicity of zeolite-like materials, particularly the ZSM-5 zeolites (86), increases with leaching. At the critical MLD value 55%, affinity for water and n-hexane are identical. The RAI is much higher than one when MLD exceeds 55%, i.e. the Alx surface hydrophobicity increases as the amount of magnesium in the sample decreases and finally a finely divided amorphous silica material is obtained, indicating preferential sorptive properties for hydrocarbons and potential

application in catalysts. The RAI values higher than one can be attributed to the more siliceous nature of the residue, which leads to a relatively higher affinity towards organic substances and to strong hydrophobic character. At a high MLD value, most of magnesium atoms are removed from the chrysotile and the silica surface of the residue is exposed, accounting for the increase in RAI. The non-polar organic n-hexane molecules can be strongly adsorbed on the surface of the amorphous silica which is not readily available to the highly polar water molecules, whereas the polar surface of unleached chrysotile and the Alix materials possessing low MLD values are hydrophilic and therefore have greater affinities for polar molecules such as water.

5 KINETIC AND THERMODYNAMIC STUDIES OF THE LEACHING PROCESS

Kinetic studies of chemical reactions are very important since they can be used to throw light on the general principles of reactivity and arrive at conclusive reaction mechanism. In a kinetic study of a reaction, there is no way of measuring the rate directly; normally, the concentration of a reactant or product is determined at various times. In particular, the initial slope, at $t=0$, gives the rate of reaction corresponding to the known concentrations with which the experiment was started. The initial rate method was used to determine the rate constant and derive the activation energy, since the concentration of the acid and the magnesium loss at the beginning were known. Thus the application of Arrhenius law to the dissolution of chrysotile in acidic media, activation energy was obtained. The Arrhenius rate constant equation:

$$\ln K = -E/RT + \text{const} \dots\dots\dots 5.1$$

may also be written as

$$K = Ae^{-E/RT} \dots\dots\dots 5.2$$

where K is the rate constant and E is the activation energy. A computer program for Langmuir type equation was used for better curve fitting; then

on differentiating the equation and extrapolating to $t=0$, the slope of the initial rate was obtained. The following Langmuir-type equation was used to express the dissolution of chrysotile (percentage loss of magnesium or MLD):

$$y = \frac{at}{b+t} \dots \dots \dots 5.3$$

The initial rate r_0 when t is close to zero is

$$r_0 = \lim_{t \rightarrow 0} r = \left(\frac{dy}{dt} \right)_{t=0} \dots \dots \dots 5.4$$

which gives

$$r_0 = K = a/b \dots \dots \dots 5.5$$

The rate curves of the chrysotile dissolution reaction were obtained by performing the experiment at three temperatures, viz., 25°C, 50°C and 80°C; the reaction time was varied while the concentration of the HCl acid solution was fixed. The results are shown in Tables 5.1, 5.2 and 5.3. The calculations obtained for the reciprocal of the absolute temperature and the corresponding initial rates are shown in Table 5.4. On plotting $\ln K$ against the reciprocal of the absolute temperature, according to Arrhenius equation, a straight line was obtained. Figure 5.1 shows the plot of $\ln K$ against $\frac{1}{T}$ for the dissolution of chrysotile in hydrochloric acid. From the slope, the apparent activation energy was calculated. The calculated apparent activation energy obtained was 20 K Cal.Mole⁻¹,

which is close to the value of $18 \text{ K Cal.Mole}^{-1}$ obtained by Bleiman and Mercier (87) and similar to that calculated for sheet silicates, such as kaolinite and montmorillonite.

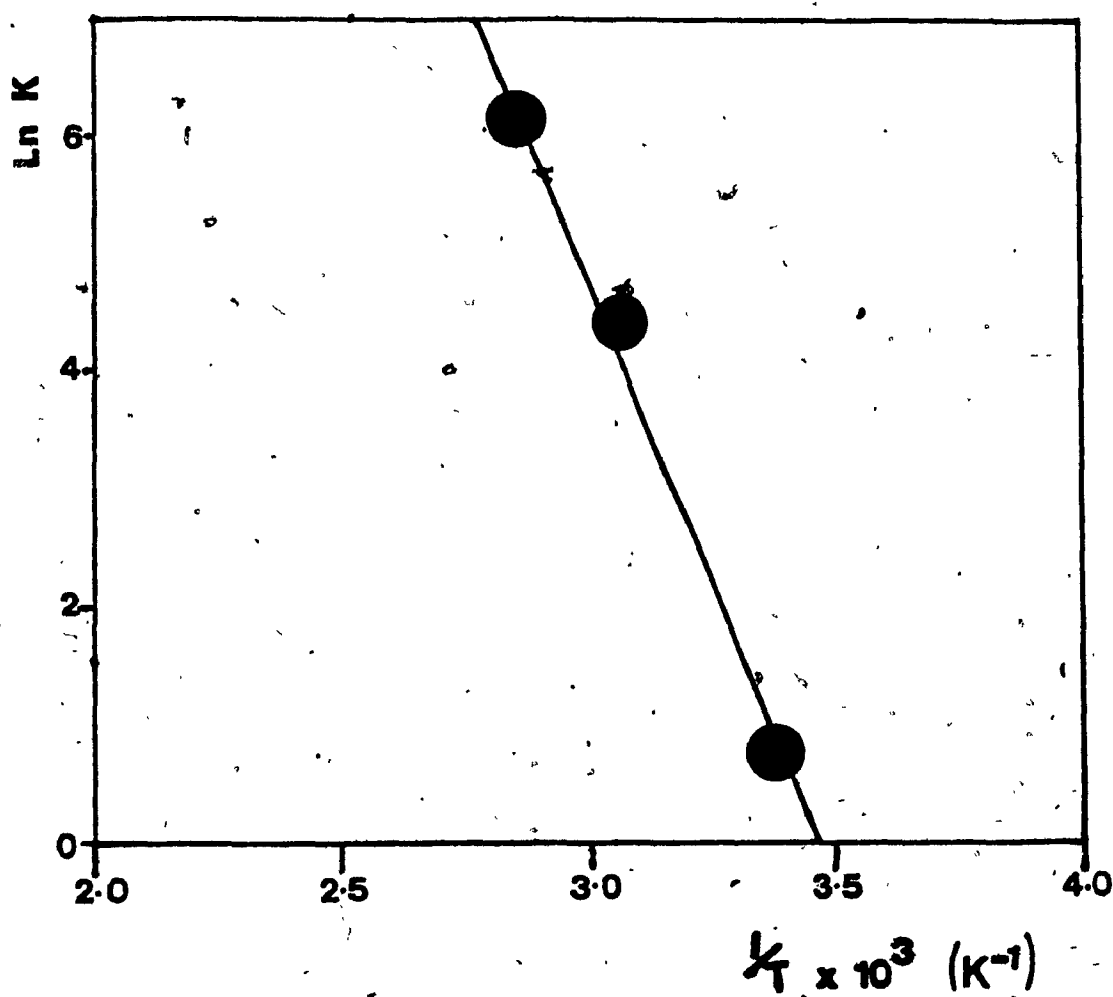


Figure 5.1: A plot of $\ln K$ against $\frac{1}{T}$ for the dissolution of chrysotile in acidic media. The slope is equal to $-E/R$, and leads to $E=20.0 \text{ K Cal. Mole}^{-1}$.

TABLE 5.1 Effects of the leaching time of HCl (2.4N) on the MLD at 25 °C.

$$Y = \frac{at}{(b+t)}$$

parameter a = 104.1534

b = 47.6238

Time (Hrs.)	MLD (%)	Y (func.)
0	0	0
12	26.8	20.962
24	36.2	34.900
36	43.2	44.838
48	51.8	52.282
60	57.0	58.065
72	61.3	62.886
96	69.2	69.617
120	72.8	74.562
144	77.9	78.268
192	84.3	83.454
240	87.7	86.908
312	91.8	90.361

The standard deviation of the function is 1.933

The estimated error of the function is 0.582

TABLE 5.2 Effects of the leaching time of HCl (2.4N) on the MLD at 50 °C.

$$Y = \frac{at}{(b+t)}$$

$$a = 105.6284$$

$$b = 1.2314$$

Time (Hrs.)	MLD (%)	Y (func.)
0	0	0
0.5	30.6	30.504
1.0	46.5	47.338
2.0	68.6	65.377
3.0	73.2	74.890
4.0	79.1	80.765
5.0	83.1	84.755
6.0	88.2	87.642
7.0	91.8	89.827

The standard deviation of the function is 1.622

The estimated error of the function is 0.613

TABLE 5.3 Effects of the leaching time of HCl (2.4N)
on the MLD at 80 °C.

$$Y = \frac{at}{(b+t)}$$

$$a = 97.5457$$

$$b = 0.2256$$

Time (Hrs.)	MLD (%)	Y (Func.)
0	0	0
0.5	70.6	67.219
1.0	76.6	79.591
1.5	80.9	84.793
2.0	85.2	87.658
2.5	92.8	89.472
3.0	93.0	90.724
4.0	91.6	92.338
4.5	92.1	92.889
5.0	93.0	93.335
6.0	95.2	94.011
7.0	95.7	94.500

The standard deviation of the function is 2.272

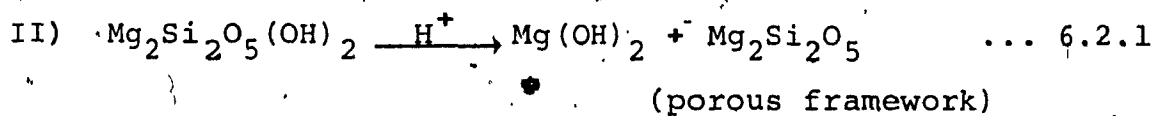
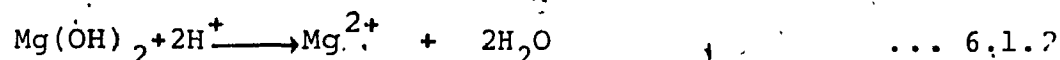
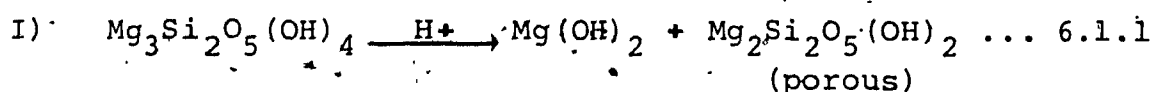
The estimated error of the function is 0.718

TABLE 5.4: The reciprocals of the absolute temperatures and the observed initial rate constants.

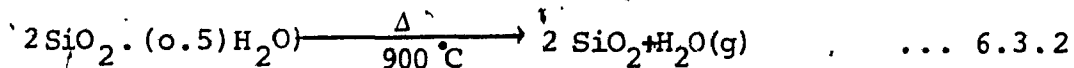
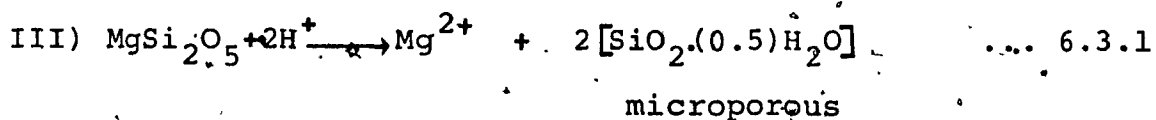
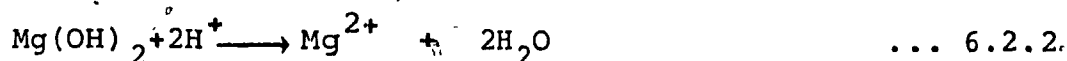
T (°C)	$\frac{1}{T}$ (K ⁻¹)	$r_0 = K$ (a/b)	$\ln(K)$
25	3.356×10^{-3}	2.187	0.78
50	3.096×10^{-3}	85.781	4.45
80	2.832×10^{-3}	432.410	6.07

6 A PROPOSED MECHANISM FOR THE CHRYSOTILE LEACHING IN THE PRESENCE OF ACIDS

A very interesting mechanism based on the crystal structure and stoichiometry of the parent chrysotile asbestos as well as the physico-chemical properties of the resulting leached asbestos materials is proposed in order to try to explain the results of chrysotile leaching in the presence of acids. This mechanism contains three main steps and two substeps as follows:



MLD=55-60%

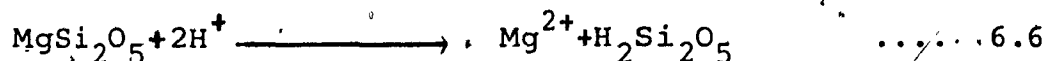
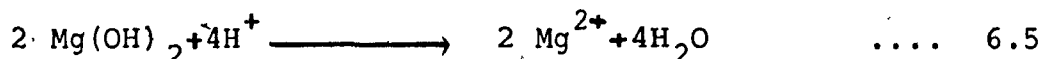
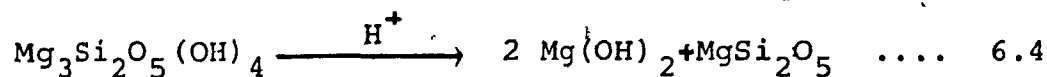


In the presence of H^+ ions, the rather detached and labile layers of $\text{Mg}(\text{OH})_2$, which are sandwiched between the silicate sheets of chrysotile fibers, are stripped away from the parent chrysotile asbestos. This is followed by the dissolution of the liberated $\text{Mg}(\text{OH})_2$ molecules into

Mg^{2+} ions. The residual chrysotile, although more porous and despite its loss of one-third of its Mg atoms, remains intact without any apparent structural change. The second major step involves the cleavage of all the structural hydroxyl groups with half of the "skeletal" Mg atoms which are linked to silicon via oxygen bridges. The reaction in step (II) leaves a very porous and siliceous residue which basically retains the fibrillar morphology of the parent chrysotile. However, this reaction is accompanied by the splitting of fiber into fibrils and moderate loss in the degree of crystallinity. The dissolution of $MgSi_2O_5$ in the last major step (III) requires an excess of H^+ ions and is a very slow and difficult reaction, and normally does not react unless severe leaching conditions are employed. The end product obtained at MLD 98% is a very microporous and amorphous material which was identified as hydrated silica gel of formula: $2 SiO_2 \cdot (0.5)H_2O$. On heating in air to higher temperatures, the chemisorbed water progressively decreased and became zero at 900 °C. The reaction in the last step is preceded by complete structural collapse and degradation of the fiber as was evidenced by several physico-chemical characterization techniques such as SEM, X-ray powder diffraction, ^{29}Si MAS NMR spectra and IR spectra, etc.

Our proposed mechanism is close to the one proposed by Pundsack and Reimschuessel (74). According to this

mechanism, the acid attack of chrysotile would take place in two dissolution steps, following a slow dissociation of chrysotile, as follows:



Pundsack and Reimschuessel also state that the resulting pH of an acid attack, when the amount of acid is less than that required for a total dissolution of chrysotile, would only be controlled by the Mg^{2+} ions leached out into the solution. However, another proposed mechanism put forward by Barbeau et al. (75,88), based on the resemblance in reactivity of chrysotile with that of forsterite and enstatite, is not consistent with our observed experimental results and therefore we have not accepted this mechanism.

7 CONCLUSIONS AND SUGGESTIONS FOR FUTURE RESEARCH

7.1 Conclusions

In the presence of strong mineral acids, the factors which governed the leaching of chrysotile asbestos fibers were respectively, the acid normality, the temperature and the duration of the operation. With weak organic acids, a two-step leaching process was necessary in order to refine the leaching and obtain a better control of magnesium removal. Alix materials of MLD ranging from 60 to 99% were very useful because from such leached asbestos materials very selective catalysts, adsorbents or ion-exchangers could be prepared. Organic acids acted more slowly in the removal of magnesium than mineral acids. The acid strength, and the nature of the organic acid involved in the second leaching step, played a big role in the removal of iron oxide impurities. Particularly, the chelating effect of EDTA is suggested for the very efficient elimination of the iron component from the leached chrysotile materials. The dissolution of chrysotile by acids resulted in a total maximum weight loss of 60%, the attainment of this value depended on the length of exposure, the nature, acid strength and concentration of the acid, and the temperature of the leaching solution.

The structural and chemical changes involved in the

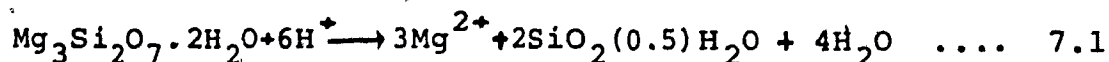
degradation of chrysotile asbestos by acids were determined with physico-chemical characterization techniques. The IR spectra of the leached asbestos materials showed that the intensity of O-H and Mg-O stretching vibrations gradually diminished and finally disappeared; in addition, progressive changes were observed in the silicate (Si-O) stretching vibrations, which suggested some disordering of the structure. The X-ray diffraction analysis showed that the external surface magnesium hydroxide (free brucite) layer was removed very rapidly and that the crystalline structure of chrysotile was gradually destroyed by an acid. In fact, the degree of crystallinity decreased linearly with increasing MLD.

The weakest points for an acid attack in the chrysotile structure, after dissolution of free brucite and amorphous impurities, are probably the brucite-like $\text{Mg}(\text{OH})_2$ freely sandwiched between the silicate sheets of chrysotile fibers (IR observations). The main structural changes occur at the $\text{MLD}=55\text{-}60\%$, called the "critical MLD value", when slightly more than half of the total Mg has been removed. Below this value, the leached materials remain fibrous and physical changes are fairly minor. The loss in chrysotile crystallinity is directly proportional to the increase in the MLD, whereas the specific surface area (BET) gradually increases from 50 to around $140 \text{ m}^2 \text{ g}^{-1}$. These gradual variations are also observed in the density.

Under the critical value, the Alix materials remain hydrophilic (they absorb more water than n-hexane). Above the critical MLD value, in morphology, as well as in porosity (high surface area and low density), are observed. The collapse of the fibrous texture and the rather rapid morphological degradation (particularly, drastic changes in length) are accompanied by a more rapid loss in chrysotile crystallinity, a rather sharp increase in the surface area and a dramatic drop of the bulk density. The high MLD Alix materials tend to have the characteristics of very porous (high surface area and low density) and hydrophobic silica. However, solid state NMR shows that the Mg, which remains in very small amount at very high MLD, is bound to the silica network, i.e. it is skeletal Mg; this detail is very important in order to explain the peculiar catalytic behaviour of the chrysozeolites at high MLD values. No ZSM-5 zeolite containing the same amount of Mg can reproduce such interesting catalytic properties (20).

The end product, obtained with an MLD=98-100%, exhibits properties which are very close to those of a highly siliceous ZSM-5 zeolite or corresponding silicalite: specific surface area = $500 \text{ m}^2 \text{ g}^{-1}$, density = 1.9 g cm^{-3} , adsorption of hexane = 18 vol.% and RAI = 2. However, contrary to zeolites and silicalites, the Alix material is amorphous. Alix free of magnesium (MLD=100%) consists of hydrated amorphous silica, $\text{SiO}_2 \cdot (0.5)\text{H}_2\text{O}$. The

overall acid leaching equation is:



7.2 Suggestions for Further Research Work

In this work, through the use of atomic absorption spectrophotometer for elemental analysis, it was possible only to determine the total iron content of the parent chrysotile asbestos and the resulting leached asbestos materials. It would be more useful to have a detailed knowledge of each of the three iron oxide phases. It is therefore suggested that further studies be carried out with Mössbauer spectroscopy to determine quantitatively the FeO, Fe₂O₃ and Fe₃O₄ contents, respectively. The information obtained on the magnetite (Fe₃O₄) content is particularly very useful, because it is the most undesirable impurity and its high magnitude can greatly limit the range of applications of leached asbestos materials. From such studies some knowledge can be gained on the leaching effects of each of the iron oxide phases by mineral acids and organic acids, particularly EDTA and oxalic acid. It is suspected that some iron oxides are selectively leached out to a greater degree than others; obviously, the magnetite is the most difficult to remove.

It is also recommended that future research work to be carried out should include particle size measurements

and thermal analysis." A thermogravimetric analysis is needed to determine the brucite impurity content and to follow its loss during the leaching process.

The most important question of this research that should be addressed is: "How can the physico-chemical properties of the leached asbestos materials affect the catalytic, adsorptive or ion-exchange properties of the chrysozeolites which are synthesized from these Alix materials?" It will also be useful to find out whether there is any relationship between the degree of crystallinity of the leached asbestos materials and the resulting chrysozeolites synthesized. In order to ensure the production of the highest efficiency chrysozeolites, which have found a broad spectrum of applications as catalysts (or catalyst supports) and adsorbents (7,14), a current research program is in progress to better understand the further changes in their physico-chemical characteristics when the leached asbestos materials are submitted to various hydrothermal conditions for the synthesis of zeolites with various particle sizes and structures. It is worth noting that the chrysozeolites are materials which do not present any cytotoxicity, as recently evidenced by a systematic investigation on hemolytic and macrophage damage activity (14); this is not the case for the parent chrysotile asbestos. Therefore, chrysozeolites provide new safe applications for asbestos,

a material definitely carcinogenic, although its useful mechanical and/or thermal properties are sometimes very hard to find in synthetic substitutes.

REFERENCES

1. R. Gaze, "The Physical and Molecular Structure of Asbestos", Annals of the New York Academy of Sciences, 132, 23- (1965).
2. M. Ross, Definitions for Asbestos and Other Health-Related Silicates, ASTM, B. Levadie, Ed., 1984, p. 51-104.
3. T.F. Bates and B. Nagy, Am. Mineralogist, 37, 1055 (1952).
4. M.S. Badollet, Encyclopedia Chemical Technology, 2, 734. (1963).
5. M.S. Badollet, Environ. Res., 2, 166 (1969).
6. A. Hiscock, Royal Inst. Chem., London Lectures, Monographs (1965).
7. R. Le Van Mao and P.H. Bird, U.S. Pat. 4511667, April 16, 1985.
8. R. Le Van Mao, U.S. Pat. 4615995, October 7, 1986.
9. R. Le Van Mao, P. Lévesque, B. Sjiariel and P.H. Bird, Can. J. Chemistry. 63, 3464 (1985).
10. R. Le Van Mao, P. Lévesque, B. Sjiariel and N.T. Do., Can. J. Chem. Eng. 64, 462 (1986).
11. R. Le Van Mao, T. Centazao, P. Lévesque, B. Sjiariel, G.P. McLaughlin and L.H. Dao, 10th Can. Symp. on Catalysis, Kingston (Canada), 298, 1986.
12. R. Le Van Mao, P. Lévesque, L. Dufresne, G.P. McLaughlin, T.N. Do and P. Kipkemboi, Interface, March-April 1987, 25.

13. P. Lévesque and R. Le Van Mao, 10th Can. Symp. on Catalysis, Kingston (Canada), 316, 1986.
14. R. Le Van Mao, G.P. McLaughlin, P. Lévesque and J. Dunningan, "Method for Enhancing the Water-Retention Capacity in Soils", U.S. Pat. Application, May 1987.
15. S.L. Meisel et al., Chem. Tech., 6, 86 (1976).
16. C.D. Chang et al., Ind. Eng. Chem. Process Des. Dev. 17, 255 (1978).
17. E.G. Derouane, "Zeolites, Science and Technology", Lisbon, 1983, 515.
18. D.W. Breck, "Zeolites Molecular Sieves", J. Wiley and Sons, New York (1974).
19. R. Le Van Mao, P. Lévesque, G.P. McLaughlin and L. Dufresne, "Chrysozeolites: Nouveaux Matériaux pour la Catalyse Hétérogène et l'Agriculture", Entr. Centre Jacques Cartier, Lyon (France), June 25, 1987.
20. P. Lévesque, Ph.D. Thesis, Concordia University, Montreal, (Canada), September 4, 1987.
21. Bragg et al., Z. Krist, 76, 201 (1930).
22. B. Warren and K.W. Herring, Phys. Rev., 59, 925 (1941).
23. G.S. Rajhans and J.L. Sullivan, "Asbestos Sampling and Analysis", Ann Arbor Science Publishers Inc., Ann Arbor, Michigan (1981). p. 11.
24. K. Yada, Acta Cryst., A27, 659 (1971).
25. H. Berger, "Asbestos Fundamentals, Origin, Properties, Mining, Processing and Utilization", Chemical Publishing Comp. Inc. (1963), p. 48.

26. S. Speil and J.P. Leineweber, Environ. Res., 2, 166 (1969).
27. F.J. Wicks, "Short Course in Mineralogical Techniques of Asbestos Determination", R.L. Ledoux, Ed., Quebec (1979), p. 1-34.
28. A.A. Hodgson, "Asbestos: Properties, Applications and Hazards", vol. 1, L. Michaels and S.S. Chissick, Eds., John Wiley and Sons, (1979), p. 67-114.
29. F.L. Pundsack, J. Phys. Chem., 59, 892 (1955).
30. "Testing Procedure for Chrysotile Asbestos Fibers", Quebec, Asbestos Mining Assn., 2nd ed., (1966).
31. I.J. Selikoff and D.H. Lee, "Asbestos and Disease", New York: Academic Press Inc. (1978).
32. R.E. Sturgeon, Anal. Chem., 49, 1255A (1977).
33. W. Slavin, Anal. Chem., 54, 685A (1982).
34. J.W. Robinson, Anal. Chem., 32, 17A (1960).
35. H. Kahn, Chem. Edu., 43, A7 (1966).
36. J.C. Van Loon, "Analytical Atomic Absorption Spectroscopy Selected Methods", (Academic Press, 1980), p. 5.
37. L.R. Morris, Spectrochim. Acta, 35B, 687 (1980).
38. M.E. Pillow, Spectrochim. Acta, 36B, 821 (1981).
39. A. Walsh, Pure and Appl. Chem., 49, 1621 (1977).
40. R.D. Dresser et al., J. Chem. Edu., 52, A403 (1975).

41. J.V. Crable, Am. Ind. Hyg. Ass. J., 27, 383 (1966).
42. H. Hayashi, Ind. Hlth., 11, 225 (1973).
43. B.A. Lange et al., Anal. Chem., 51, 520 (1979).
44. A.R. West, Solid State Chemistry and its Applications, (John Wiley and Sons, 1984), p. 115.
45. D.A. Skoog, Principles of Instrumental Analysis, 3rd edition. (Saunders College Publishing, 1985), p. 464.
46. G.S. Rajhans and J.L. Sullivan, "Asbestos Sampling and Analysis", Ann Arbor Science Publishers Inc., Ann Arbor, Michigan (1981), p. 185-231.
47. A.P. Middleton, "Asbestos: Properties, Applications and Hazards", L. Michaels and S.S. Chissick, Eds., John Wiley and Sons, (1979), p. 247-277.
48. Annual Book of ASTM Standards, Section 5, Petroleum Products and Lubricants (1987), p. 653-660.
49. S.B. Kulkarani et al., Zeolites, 2, 313 (1982).
50. A. Vaillancourt, M.Sc. Thesis, Concordia University, Montreal, to be submitted.
51. J.P. Coats, "The Infra Red Analysis of Quartz and Asbestos", Perkin-Elmer, Beaconsfield, Bucks (1977).
52. J.M. Hunt et al., "Infra Red Absorption Spectra of Minerals and Other Inorganic Compounds", Anal. Chem., 22, 1478 (1950).
53. G.W. Brindley and J. Zussman, "Infra Red Absorption Data for Serpentine Minerals", Am. Min., 44, 185 (1959).
54. J.P. Coates, "IR Analysis of Toxic Dusts, Analysis of Collected Samples of Quartz and Asbestos, Part I", Am. Lab., Nov. 1977, p. 105-111.

55. I.A. Gadsen et al., "Determination of Chrysotile in Airborne Asbestos by an Infrared Spectrometric Technique." *Atm. Environ.*, 4, 667 (1970).
56. R.P. Bagioni, *Environ. Sci. Tech.* 9, 262 (1975).
57. Anderson and Boudart, Eds., "Catalysis: Science and Technology", vol. 7, Springer-Verlag, Berlin, Heidelberg (1985), p. 53-149.
58. J. Schaefer and E. Stejskal, *J. Am. Chem. Soc.*, 98, 1031 (1976).
59. B. Shapiro, Ed., "Heterogeneous Catalysis", ACS Symp. Ser., 288, 1984. p. 347-379.
60. G. Stucky and F. Dwyer, Eds., "Intrazeolite Chemistry", ACS Symp. Ser., 218, 1983, p. 159-177.
61. G.C. Gerstein, *Anal. Chem.*, 55 (1983), 781A.
62. S. Brunauer, P.H. Emmett and E. Teller, *J. Am. Chem. Soc.*, 60, 309 (1933).
63. A.J. Lecloux, "Catalysis: Science and Technology", vol. 2, Anderson and Boudart, Eds., Springer-Verlag, Berlin (1981), p. 171-230.
64. S.J. Gregg and K.S. Sing, "Adsorption, Surface Area and Porosity", Academic Press Inc., London (1982), p. 41-105.
65. A.W. Naumann and W.H. Dresher, *Am. Mineral.*, 51, 711 (1966).
66. J.R. Anderson and K.C. Pratt, "Introduction to Characterization and Testing of Catalysts", Academic Press, Harcourt Brace Jovanovich Publishers (Australia), (1985), p. 2-43.
67. M. Niwa et al., *J. Catal.*, 100, 264 (1986).

68. B. Lippens and J. deBoer, J. Catal., 4, 319 (1965).
69. J. Fripiat, J. Chaussidon and A. Jelli, "Chimie-Physique des Phénomènes de Surface", Masson et Cie., Paris (1971).
70. S.J. Gregg and K.S. Sing, "Adsorption, Surface Area and Porosity", Academic Press Inc., London (1982), p. 111-190.
71. C. Pierce, J. Phys. Chem., 57, 149 (1953).
72. R. Le Van Mao, React. Kinet. Catal. Lett., 12, 69 (1979).
73. R. Le Van Mao et al., React. Kinet. Catal. Lett., 15, 293 (1980).
74. F. Pundsack and G. Reimschuessel, J. Phys. Chem., 60, 1218 (1956).
75. C. Barbeau, "Short Course in Mineralogical Techniques of Asbestos Determination", R.L. Ledoux, Ed., Quebec (1979), p. 197-212.
76. R. Le Van Mao, P. Kipkemboi, A. Vaillancourt, P. Lévesque and G. Dénès, Zeolites and Can. J. Chem., (1987), submitted.
77. ASTM 14-293, from Neumann and Bergstol, Mineral. Museum, Oslo, Norway (sample from Langban, Sweden).
78. J.S. Harington, Ann. N.Y. Acad. Sci., 132, 31 (1965).
79. R.O. Kagel, "Infrared Spectra of Inorganic Compounds", Academic Press, New York, p. 211.
80. E. Oldfield and E.J. Kirkpatrick, Science, 227, 4694 (1985).
81. D. Sindorf and G. Macial, J. Am. Chem. Soc., 105, 1487 (1983).

82. F. Bates and J. Comer, Clay Minerals, Proc. Nat'l. Conf., Clay and Clay Minerals, 6, 237 (1959).
 83. F.J. Pundsack, J. Phys. Chem., 65, 30 (1961).
 84. J.J. Fripiat and M.D. Faille, Clays and Clay Minerals, Proceedings of the 15th Conference, Pittsburgh, Pennsylvania Pergamon Press, Oxford and New York, 1967, p. 305-320.
 85. "CRC Handbook of Chemistry and Physics", 61st edition, R.C. Weast, Ed., CRC Press, Boca Raton, Florida (United States), 1980-1981, p. B-143.
 86. R. Le Van Mao, V. Bagaini, G. Leofante and R. Fois, J. Catal., 81, 418 (1983).
 87. C. Bleiman and J.P. Mercier, Bull. Soc. Chim., 3, 529 (1975).
 88. C. Barbeau, J. Roy and M. Dupuis, 3rd International Conference on Asbestos Minerals, Quebec (1975).
-

APPENDIX A: A program used to compute the
specific BET surface area of Alix
samples.


```

10 CLS
20 DIM V(6),LVL1(10),LVL2(10),LVL3(10),LVL4(10)
30 DIM P1(10),P2(10),P3(10),P4(10),X(10),Y(10),FD(40)
40 CLEAR
50 DATA 0,13.32,32.2,59.61,93.23,136.43
60 REM read in the standard volumes
70 FOR I=1 TO 6
80 READ V(I)
90 NEXT I
100 INPUT " Sample name : ";SAMPLE$
110 PRINT " _____ "
120 LPRINT " Sample name : ";SAMPLE$
130 LPRINT " _____ "
140 REM input the experimental data
150 INPUT " No. of equilibrium in step 1 : ";NEP1
160 INPUT " The equilibrium temperature in step 1 : TC1
170 PRINT " Enter the levels and equilibrium pressures in step 1"
180 PRINT
190 FOR I = 1 TO NEP1
200 INPUT LVL1(I),P1(I)
210 NEXT I
220 PRINT " _____ "
230 INPUT " No. of equilibrium in step 2 ";TC2
240 INPUT " The equilibrium temperature in step 2 : ";TC2
250 PRINT " Enter the levels and equilibrium pressures in step 2"
260 PRINT
270 FOR I = 1 TO NEP2
280 INPUT LVL2(I),P2(I)
290 NEXT I
300 PRINT " _____ "
310 INPUT " No. equilibrium in step 3 : ";NEP3
320 INPUT " The equilibrium temperature in step 3 : ";TC3
330 PRINT " Enter the levels and equilibrium pressures in step 3"
340 PRINT
350 FOR I = 1 TO NEP3
360 INPUT LVL3(I),P3(I)
370 NEXT I
380 PRINT " _____ "
390 INPUT " No. of equilibrium in step 4 : ";NEP4
400 INPUT " The equilibrium temperature in step 4 : ";TC4
410 PRINT " Enter the levels and equilibrium pressures in step 4"
420 PRINT
430 FOR I = 1 TO NEP4
440 INPUT LVL4(I),P4(I)
450 NEXT I
460 PRINT " _____ "
470 PRINT : INPUT " The weight of sample : ";W
480 REM calculate the dead volume
490 SUM = 0
500 FOR I = 1 TO (NEP1-1)
510 V1 = V(LVL1(I))
520 V2 = V(LVL1(I+1))
530 V3 = ((V2 * P1(I+1)) - (V1 * P1(I)))/(P1(I) - P1(I+1))

```

```

540 SUM = SUM + V3
550 NEXT I
560 DEAD = SUM / (NEP1-1)
570 LPRINT : LPRINT " Dead volume : ";DEAD;"cc."
580 REM calculate the total volume of Helium
590 SUM = 0
600 FOR I = 1 TO NEP1
610 V1 = V(LVL1(I)) + DEAD
620 SUM = SUM + (V1*P1(I)*273.15/((TC1+273.15)*760))
630 NEXT I
640 HE = SUM / NEP1
650 LPRINT : LPRINT " Total volume of He : ";HE;"cc."
660 REM calculate the free space
670 SUM = 0
680 FOR I = 1 TO NEP2
690 V1 = V(LVL2(I)) + DEAD
700 V2 = HE - (V1*P2(I)*273.15/((TC2+273.15)*760))
710 FREE = V2 / P2(I)
720 LPRINT : LPRINT " Free space ";I;" : ";FREE
730 SUM = SUM + FREE
740 NEXT I
750 AVE = SUM / NEP2
760 LPRINT : LPRINT " Average free volumes : ";AVE
770 REM calculate volume absorbing gas introduced
780 SUM = 0
790 FOR I = 1 TO NEP3
800 V1 = V(LVL3(I)) + DEAD
810 SUM = SUM + (V1*P3(I)*273.15/((TC3+273.15)*760))
820 NEXT I
830 N2 = SUM / NEP3
840 LPRINT : LPRINT " Volume of N2 introduced :";N2;"cc."
850 REM calculate the added volumes of N2 at various pressures
860 LPRINT : LPRINT " Vol. ads., "P. relative", "P. equil.", "T. equil."
870 LPRINT " _____, _____, _____, _____"
880 PO = 10-2.8806618#
890 FOR I = 1 TO NEP4
900 V1 = V(LVL4(I)) + DEAD
910 V2 = V1 * P4(I)*273.15/((TC4+273.15)*760)
920 V3 = P4(I) * AVE
930 VADD = N2 - V2 - V3
940 X(I) = P4(I) / PO
950 Y(I) = P4(I) / (VADD * (PO-P4(I)))
960 LPRINT : LPRINT VADD,X(I),P4(I),TC4
970 NEXT I
980 REM Calculate the slope and intercept by least square
990 SX = 0
1000 SY = 0
1010 SY = 0
1020 SXX = 0
1030 SYY = 0
1040 FOR I = 1 TO NEP4
1050 SX = SX + X(I)
1060 SY = SY + Y(I)

```

```

1070   SXX = SXX + X(I)*X(I)
1080   SXY = SXY + X(I)*Y(I)
1090   SYX = SYX + Y(I)*Y(I)
1100   NEXT I
1110   ITC = ((SXX * SY) - (SXY * SX)) / ((NEP4 * SXX) - (SX * SX))
1120   LPRINT : LPRINT : LPRINT " Intercept : ";ITC
1130   SLP = ((NEP4 * SXY) - (SX * SY)) / ((NEP4 * SXX) - (SX * SX))
1140   LPRINT : LPRINT " Slope
1150   VM = 1 / (SLP + ITC)
1160   C = (SLP / ITC) + 1
1170   REM Calculate the surface area
1180   SA = VM * (6.023E+23) * (9.999999E-21) / (22414 * W)
1190   REM Calculate the correlation coefficient (r)
1200   CXY = 0
1210   XVARI = 0
1220   YVARI = 0
1230   FX = 0
1240   XAVE = SX / NEP4
1250   YAVE = SY / NEP4
1260   FOR I = 1 TO NEP4
1270     CXY = CXY + (X(I) - XAVE) * (Y(I) - YAVE)
1280     XVARI = XVARI + (X(I) - XAVE) ^ 2
1290     YVARI = YVARI + (Y(I) - YAVE) ^ 2
1300     FX = FX + X(I)*Y(I)
1310   NEXT I
1320   R = ABS(CXY) / SQR(YVARI * XVARI)
1330   LPRINT : LPRINT " Correlation coefficient r : ";R
1340   REM Calculate standard deviation
1350   MEAN = FX / SY
1360   DEVI = ABS((SY - SY ^ 2 / NEP4) / (NEP4 - 1))
1370   STDEV = SQR(DEVI)
1380   LPRINT : LPRINT " Standard deviation : ";STDEV
1390   REM Calculate the surface error
1400   FOR J = 1 TO 10
1410     READ FD(J)
1420   NEXT J
1430   DATA 12.706,4.303,3.182,2.776,2.571,2.447,2.365,2.306,2.262,
1440   DATA 2.201,2.179,2.16,2.145,2.131,2.12,2.11,2.101,2.093,2.086
1450   DATA 2.074,2.069,2.064,2.06,2.056,2.052,2.048,2.045,2.042
1460   CORR = ABS(1 - R*R)
1470   ERROR1 = FD(NEP4-2) * SQR(CORR) * STDEV
1480   LPRINT : LPRINT " Error on the intercept : ";ERROR1
1490   XM1 = 1 / (SLP + ITC + ERROR1)
1500   XM2 = 1 / (SLP + ITC - ERROR1)
1510   XM12 = ABS(XM1 - XM2) / VM
1520   ERROR2 = SA * XM12
1530   LPRINT : LPRINT " Monolayer volume : ";VM;"cc."
1540   LPRINT : LPRINT " Parameters C per BET : ";C
1550   LPRINT
1560   LPRINT : LPRINT : LPRINT " SPEC. AREA (m^2/g. ads.) : ";SA
1570   LPRINT : LPRINT " ERROR (+/-) : ";ERROR2
1580   END

```

APPENDIX B: A program used to compute the pore size
distribution of Alix samples.

```

0 REM
10 REM
20 INPUT " Sample name : ";NAM$
30 PRINT "
40 INPUT " Weight of sample : ";W
50 INPUT " Enter equilibrium temperature : ";RT
60 INPUT " Enter number of data point : ";N
65 INPUT " DEAD VOLUME : (=0 IF NO)";DV
70 DIM P(N),V(N),B(N,5),A(N,17),FX1(10),FX2(10),PO(N),PI2(N)
80 REM
90 FOR I = 1 TO 7
100 READ FX1(I)
110 NEXT I
120 DATA -9.150241E-3,174.645,-3843.314,46907.4,-304972.2
121 FOR I = 1 TO 9
123 READ PX2(I)
125 NEXT I
130 DATA 5.934531,-24.01543,147.535,-294.9527,141.7335
135 DATA -455.7216,284.1504
140 REM
150 PRINT " Enter your data please ! (Pressures,Volumes)"
160 FOR I = 1 TO N
170 READ P(I),V(I)
180 NEXT I
190 REM
191 FOR I=1 TO N
192 IF I=1 THEN V(I)=V(I) + DV
194 IF I>1 THEN V(I) = V(I) + 5.65 + DV
195 NEXT I
200 FOR I = 1 TO N
220 B(I,1) = P(I)/760
230 B(I,2) = (LOG(10)*4.15)/LOG(760/P(I))
235 NEXT I
237 FOR I = 1 TO N-1
240 IF B(I+1,1) <= .2 THEN GOSUB 1000 ELSE GOSUB 2000
270 B(I,3) = SUM
280 B(I,4) = B(I,2) + B(I,3)
290 TE = 273.15 / (273.15 + RT)
291 B(I,5) = TE * (V(I)*B(I,1)-V(I+1)*B(I+1,1))
300 NEXT I
310 L = 0
320 FOR I = 1 TO N
330 IF B(I,4) = 150 AND B(I,4) >= 10 THEN 340 ELSE 400
340 L = L + 1
350 A(L,1) = B(I,1)
360 A(L,2) = B(I,2)
370 A(L,4) = B(I,3)
380 A(L,6) = B(I,4)
390 A(L,8) = B(I,5)
400 NEXT I
410 REM
420 SA = 0
430 FOR I = 1 TO L-1

```

```

440      P12(I) = (A(I,1)+A(I+1,1))/2
450      A(I,3) = (A(I,2) + A(I+1,2))/2
460      A(I,5) = A(I,4) - A(I+1,4)
470      A(I,7) = (A(I,6) + A(I+1,6))/2
480      A(I,9) = A(I,8)
490      A(I,10) = .064 * A(I,5)
500      A(I,11) = A(I,10) * A(I-1,17)
510      A(I,12) = A(I,9) - A(I,11)
520      A(I,13) = A(I,7) ^ 2 / A(I,3) ^ 2
521      A(I,13) = A(I,13) * .148
530      A(I,14) = A(I,13) * A(I,12)
540      A(I,15) = 31.2 / A(I,7)
550      A(I,16) = A(I,15) * A(I,14)/W
560      SA = SA + A(I,16)
570      A(I,17) = SA
572      RAD I = RAD I + (A(I,7) * A(I,16)
580      NEXT I
582      RAD I = RAD I /SA
590      REM
600      LPRINT " Sample : ";NAM$
610      LPRINT "
620      LPRINT
630      LPRINT "      Weight of sample:(g) : ";W
640      LPRINT "      Equilibrium temperature (degree C) : ";RT
641      LPRINT "      DEAD VOLUME DV : "; DV
650      LPRINT
660      LPRINT " Radius (A)","Area (m 2/g)". "Total Area". "Percentages"
670      LPRINT "
680      LL = 0
690      FOR I = 1 TO L - 1
700          IF A(I,16) > 0 THEN 710 ELSE 730
710          FINA = A(I,17)
720          LL = LL + 1
730      NEXT I
740      FOR I' = 1 TO LL
750          PC(I) = A(I,16)/FINA * 100
760          LPRINT A(I,7),A(I,16),A(I,17),PC(I)
770      NEXT I
780      LPRINT "
782      LPRINT:LPRINT
786      LPRINT "Average pore radius (A): ";RAD I
790      END
800      DATA 758,95.5,753,94.8,751,94.3,741,93.2,732,91.9,722,90.4,712,89,
801,87.3,6,91,85.6,680,83.9,666,82.2,654,80.3,643,78.5,630,76.8,618,
802,75.1,605,73.6,591,73,57,2,72.8,555,72.4,543,72.1,530,71.8,514,71.6,501,
803,71.4,486,71.1,475,70.8,462,70.4,4,48,70.1,437
810      DATA 69.4,426,68.9,414,68.2,403,67.6,394,66.9,384,66.2,373,65.6,
811,364,64.9,356,64.2,346,63.5,339,62.9,331,62.3,323,61.7,315,61.1,307,
812,60.5,301,59.8,292,59.2,28,5,58.6,277,58,269,57.3,263,56.6,256,56,248,
813,55.4,244,54.6,235,54,229,53.3,225,52.6
820      DATA 218,52,212,51.3,206,50.6,200,50,195,49.4,189,48.8,184,48.1,
821,179,47.5,174,46.9,169,46.3,164,45.7,159,45,155,44.5,150,44,145,43.4,
822,142,42.8,138,42.3,134,41.8

```

```
1000 REM -----Relative pressure is less than .2-----
1010 SUM = 0
1020 FOR J = 1 TO 7
1030     SUM = SUM + (FXI(J) + B(I,1) ^ (J-1))
1040     NEXT J
1050 RETURN
2000 REM -----Relative pressure is greater than .2-----
2010 SUM = 0
2020 FOR J = 1 TO 9
2030     SUM = SUM + (FX2(J) * B(I,1) ^ (J-1))
2040     NEXT J
2050 RETURN
```